“Enhancement of mixing characteristics of passive T-type micromixer through geometry optimization”

Enhancement of mixing characteristics of passive T-type micromixer through geometry optimization

A Dissertation
Submitted in partial fulfillment of the requirements for
the award of the Degree of

DOCTOR OF PHILOSOPHY

in

MECHANICAL ENGINEERING

by

R SHASIDHAR

(Roll No.: 718024)

Under the Supervision of

Dr. V. R. K. Raju
Professor

Mechanical Engineering Department

DEPARTEMENT OF MECHANICAL ENGINEERING
NATIONAL INSTITUTE OF TECHNOLOGY,
WARANGAL (TS), INDIA−506004,

August, 2023

Enhancement of mixing characteristics of passive T-type micromixer through geometry optimization

A Dissertation
Submitted in partial fulfillment of the requirements for
the award of the Degree of

DOCTOR OF PHILOSOPHY

in

MECHANICAL ENGINEERING

by

R SHASIDHAR

(Roll No.: 718024)

Under the Supervision of

Dr. V. R. K. Raju
Professor

Mechanical Engineering Department

DEPARTEMENT OF MECHANICAL ENGINEERING
NATIONAL INSTITUTE OF TECHNOLOGY,
WARANGAL (TS), INDIA−506004,

August, 2023

राष्ट्रीय प्रौद्योगिकी संस्थान वारंगल National Institute of Technology Warangal

Department of Mechanical Engineering

CERTIFICATE

This is to certify that the dissertation work entitled — **ENHANCEMENT OF MIXING CHARACTERISTICS OF PASSIVE T-TYPE MICROMIXER THROUGH GEOMETRY OPTIMIZATION**, which is being submitted by **Mr. R SHASIDHAR (**Roll No. 718024), is a bonafide work submitted to the Department of Mechanical Engineering, National Institute of Technology, Warangal in partial fulfillment of the requirement for the award of the degree of **Doctor of Philosophy in Mechanical Engineering.**

To the best of our knowledge, the work incorporated in this thesis has not been submitted elsewhere for the award of any degree.

Dr. V. R. K. RAJU
Supervisor
Department of
Mechanical Engineering
National Institute of
Technology
Warangal- 506004

Prof. V. Suresh Babu
Head of the Department
Department of Mechanical
Engineering
National Institute of
Technology
Warangal-506004

DECLARATION

This is to certify that the work presented in the thesis entitled, **"ENHANCEMENT OF MIXING CHARACTERISTICS OF PASSIVE T-TYPE MICROMIXER THROUGH GEOMETRY OPTIMIZATION"** is a bonafide work done by me under the supervision of Dr. V. R. K. Raju, Professor, Department of Mechanical Engineering, NIT Warangal, India and was not submitted elsewhere for the award of any degree.

I declare that this written submission represents my ideas in my own words and where others' ideas or words have been included, I have adequately cited and referenced the original sources. I also declare that I have adhered to all principles of academic honesty and integrity and have not misrepresented or fabricated or falsified any idea / data / fact / source in my submission. I understand that any violation of the above will be a cause for disciplinary action by the Institute and can also evoke penal action from the sources which have thus not been properly cited or from whom proper permission has not been taken when needed.

R Shasidhar

(Roll No.: 718024)

Date:

Dedicated to

My Parents (Shri. R Narsimha chary & Smt. R Bhagyavathi)

ACKNOWLEDGMENT

Foremost, I Praise God for the opportunity of Ph.D. I am indebted forever to my supervisor **Dr. V. R. K. Raju** for his utmost care, unceasing support, and patient guidance throughout the course of this research. Whenever it necessitates for technical discussions or implementing research ideas or document corrections, numerous times he sat with me for many hours together late up to night neglecting meals which inspired me for life to treasure research and hard work more than anything.

I express my sincere thanks to Director of NIT Warangal, **Prof. Bidyadhar Subudhi** for providing all academic and administrative help during the course of my work.

I like to extend my sincere thanks to **Prof. V. Suresh babu**, Chairman (Doctoral Scrutiny Committee), Head of the Mechanical Engineering Department and to the members of DSC, **Dr. V. P. Chandramohan**, Professor, Department of Mechanical Engineering, **Dr. D. Jaya Krishna**, Professor, Department of Mechanical Engineering, and **Dr. Benerji Babu**, Associate Professor, Department of Mathematics, for all the support bestowed on me by suggesting and verifying the research work.

I am grateful for the moral support and help from my teachers and friends throughout this research journey. Particularly, **Shri. G.R.K. Gupta**, Associate Professor, Department of Mechanical Engineering, for his continuous moral support, **Dr. M. Raja Vishwanathan**, Assistant Professor, Department of H&SS, for all his assistance and encouragement. I am grateful to **Dr. D. Jaya Krishna** for his technical insights and advice. I thank my co-scholars: **Dr. S.V.B. Vivekanand, S. Chandrasekhar**, **K. Siva Prasad, Manoj kumar**. I particularly thank K. Siva Prasad for his valuable company and timely assistance, S. Chandrasekhar for all the help and Manoj kumar for support which was very helpful during stressful times of research, I will long cherish the joyful and humorous times spent at coffee day.

I could not have completed my doctoral study without the patience and love of my parents, my wonderful uncle and my beloved sister.

(**R SHASIDHAR**)

ABSTRACT

Passive micromixers play a crucial role in chemical, biomedical, and bio-chemical analyses on micro total analysis systems (μTAS) or Lab-on-chips. However, at very low Reynolds numbers, the mixing performance of passive mixers is poor due to the laminar nature of liquid flows. In this thesis, various novel designs of passive mixers were investigated to improve mixing at low Reynolds numbers. The focus was on serpentine square-wave type mixers and T-mixers, which are commonly used in microfluidic applications. Additionally, obstacle geometry in T-T mixers and the effect of in-step configurations in T-mixers were explored for enhanced mixing.

The study revealed that the serpentine type passive mixer with convergent-divergent passages showed significant improvement in mixing performance compared to the serpentine square-wave type mixer at low Reynolds numbers. The varying cross-section of channels in the serpentine type mixer facilitated better stretching and folding of samples, leading to improved mixing.

For T-mixers, a shape optimization technique using Bernstein polynomials was employed to optimize the geometrical shape and improve mixing performance. The results demonstrated nearly threefold improvement in mixing by optimizing the wall profile of the T-mixer while maintaining ease of fabrication. The optimized shape exhibited a reduced channel thickness, resulting in enhanced mixing compared to conventional T-mixers.

Numerical simulations were conducted to optimize obstacle geometry in T-T mixers. Cylindrical and prismatic obstacles were considered, and their pitch and geometrical parameters were optimized for improved mixing. The optimized cylindrical obstacle configuration showed symmetrical recirculation zones and achieved higher mixing qualities at Reynolds numbers above 30. However, it also resulted in increased pressure drop. Prismatic obstacles achieved better mixing at higher Reynolds numbers but exhibited asymmetric recirculation zones and increased pressure drop.

The insertion of in-step configurations in T-mixers significantly increased mixing quality. Optimization of the in-step geometry using the Nelder-Mead algorithm revealed that the width and pitch of the in-step influenced the mixing performance. At different Reynolds numbers, varying optimal values for width and pitch were observed, with the highest mixing quality achieved at smaller widths and pitches at lower Reynolds numbers. The pressure drop also increased with larger widths and pitches.

In conclusion, this thesis explores different strategies to improve mixing in passive micromixers. The findings provide valuable insights into optimizing the geometrical shapes of mixers, obstacle configurations, and the inclusion of in-step structures. These advancements contribute to the development of efficient and cost-effective passive micromixers for various microfluidic applications.

Keywords: Circumferential in-step, Cylindrical elements, Prismatic elements, Micromixing, Mixing quality, Passive micromixers, T-mixer, T-T mixer.

CONTENTS

LIST OF FIGURES

LIST OF TABLES

NOMENCLATURE

A	area of cross-section (m^2)
D	Diffusion co-efficient (m^2/sec)
D_h	hydraulic diameter (m)
h	channel height (m)
m	mass flow rate of species
MI	Mixing Index
P	perimeter of cross-section (m)
Pe	*Peclet* number(-)
r	hydraulic radius of microchannel (m)
Re	*Reynolds* number(-)
S	*Swirl* number
t	residence time (s)
V	velocity (m/s)
V_z	axial velocity (m/s)
V_θ	tangential velocity (m/s)
$\dot{V}$	Total volume of micromixer

Greek letters

α	mixing quality
ω	frequency (rad/s)
μ	dynamic viscosity (Pas)
ρ	density (kg/m^3)
ε	energy dissipation
Δp	pressure drop (kPa)

Subscripts

avg	average
h	hydraulic
z	axial direction
θ	tangential direction

CHAPTER 1

INTRODUCTION AND LITERATURE SURVEY

1.1 Origin and importance of micromixers

Micromixers play a crucial role in various microfluidic applications, such as analytical, sensing, detection, and chemical reaction systems. These devices are considered essential components in the field of microfluidics, which originated from the concept of miniaturization borrowed from micro-electro-mechanical systems (MEMS). By applying this concept to the fields of biomedical, bio-chemical, and chemical processing, microfluidics has evolved and given rise to revolutionary devices.

Micromixers are tiny systems for mixing small volumes of fluids, which have become essential in biomedical, chemical, and biochemical analyses. They are made up of micro-structures such as fluid channels with dimensions ranging from sub-millimeter to micrometer scale. Compared to conventional batch reactors, micromixers consume less reagents, have a high surface-to-volume ratio, and are safer for carrying out explosive reactions[1]. They are also portable, easy to integrate with lab-on-chips or micro total analysis systems, and can provide rapid analysis with shorter operation time[2]. Micromixers are classified into active and passive types, with passive mixers being easier to fabricate, operate, and maintain than active mixers. Passive mixers are designed to induce stretching, folding, splitting, and recombining of fluids to increase the interfacial area and enhance mixing[3]. Therefore, this research focuses on the design and study of simple structured passive micromixers due to their robustness, stability, and cost-effectiveness.

Passive micromixers do not require an external energy source or moving parts to induce mixing. Instead, they rely on the design of the mixing channel to promote fluid mixing through hydrodynamic phenomena. The geometry of the mixing channel is carefully designed to induce chaotic advection, which leads to high mixing efficiency. The most commonly used geometries are serpentine, zigzag, and staggered herringbone mixers. In these mixers, the fluids are forced to undergo repeated folding and stretching motions, resulting in efficient mixing with low energy consumption.

Passive micromixers have several advantages over active mixers. First, they are easier to integrate into complex microenvironments due to their simple structure and lack of moving parts. Second, they are cheaper to fabricate since they do not require external energy sources or complex fabrication processes. Third, they are more stable and robust than active mixers, which can be sensitive to external disturbances. Finally, they are easier to operate and maintain since they do not require complicated control systems.

Passive micromixers have found a wide range of applications in various fields such as chemical synthesis, biochemical assays, drug discovery, and microfluidic diagnostics. They have been used for mixing multiple reagents, carrying out enzymatic reactions, synthesizing nanoparticles, and separating particles. In addition, they have been integrated with other microfluidic components such as microreactors, microfluidic pumps, and microvalves to create complex microfluidic systems for various applications.

In conclusion, passive micromixers are essential components of microfluidic systems and have several advantages over active mixers. They have found numerous applications in various fields and offer great potential for further development. Therefore, research on passive micromixers is expected to continue to grow in the future.

1.2 Applications of micromixers

Micromixers have immense potential and have been extensively utilized in various microfluidic applications. These applications range from bio-medical and bio-chemical engineering, where they are employed in lab-on-chips or μTAS for protein folding studies, DNA micro-arrays[4], enzyme assays[5], drug screening[6], cell separation[7], cell lysis[8], circulating tumor cell detection[9], sample concentration[10], and biological agent detection[11]. In chemical engineering, micromixers are used for organic synthesis[12], crystallization[13], polymerization[14], extraction[15], and chemical reaction kinetic studies[16]. They are also commonly utilized in microreactors for the synthesis of biodiesel[17]. Overall, micromixers offer numerous advantages and have proven to be an essential tool in various important fields of engineering.

The advantages of micromixers in bio-medical and bio-chemical engineering are manifold. They offer a high degree of mixing efficiency, which is critical for many biological and chemical reactions. Micromixers are capable of achieving rapid mixing at low Reynolds numbers, resulting in improved reaction rates and reduced reaction times. Additionally, the

small size of micromixers allows for a reduced amount of reagents and samples required, resulting in cost and time savings.

In chemical engineering, micromixers have become an indispensable tool for optimizing chemical reactions. They provide precise control over reaction parameters such as mixing rates, temperature, and residence time, resulting in improved reaction yields and selectivity. Micromixers also facilitate the scale-up of chemical reactions from laboratory to industrial-scale, resulting in significant cost savings and increased efficiency.

The use of micromixers in microreactors for biodiesel synthesis is a particularly exciting application. Biodiesel synthesis typically requires the use of large volumes of organic solvents, resulting in significant environmental impact. The use of micromixers in microreactors allows for a significant reduction in the volume of solvents required, resulting in a more sustainable and environmentally friendly process.

Overall, the potential of micromixers in various engineering fields is immense, and their continued development and application will undoubtedly lead to many exciting innovations and advancements in the future.

1.2.1 Sample Concentration

Passive serpentine micromixers are used in a microfluidic network [18] (Fig. 1.1) to generate concentration gradients in a solution or transfer these gradients onto a surface for the applications of haptotaxis (movement of cell in a gradient), chemotaxis (movement of organism in reaction to chemical stimulus) and analysis of cell-surface interactions. Compared to other methods such as retarded diffusion or self-assembled monolayers (SAMs), it is easier to fabricate complex shaped gradients using micromixers network as well as easier to achieve the resolution of microns which is essential for many biological processes. Similarly, a passive type unbalanced split and cross-collision type micromixer [19], series of split and recombine type micromixers [20] and an inclined single surface grooved micromixer [21] are employed in different gradient generation and sample concentration applications.

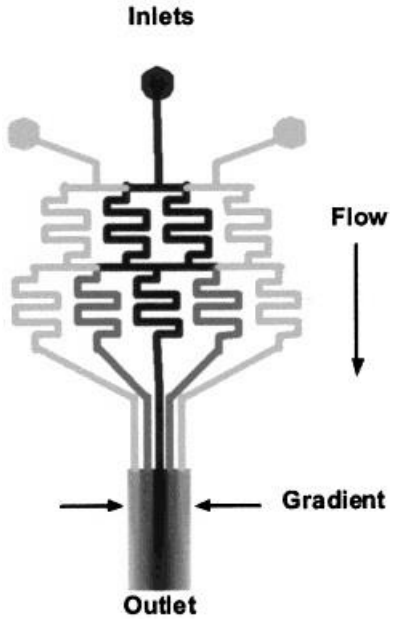

Fig. 1.1 Schematic of gradient generator with serpentine micromixers (Jeon et al. [18])

1.2.2 Circulating Tumor cell detection

Micromixers are utilized in Lab-on-chips for circulating tumor cell detection which is very crucial in the treatment of cancer patients. The size of white blood cells (WBC) is of the same order of circulating tumor cells (CTC) and hence difficult to be separated from blood for analysis. A passive vortex micromixer is employed [9] (Fig. 1.2) to mix and coat CTC with 3 µm beads and thus increase the size of CTC and separate them from the blood sample. Chaotic type micromixer [22] and staggered herringbone mixer with larger width grooves [23] are utilized in similar studies of capturing circulating tumor cells.

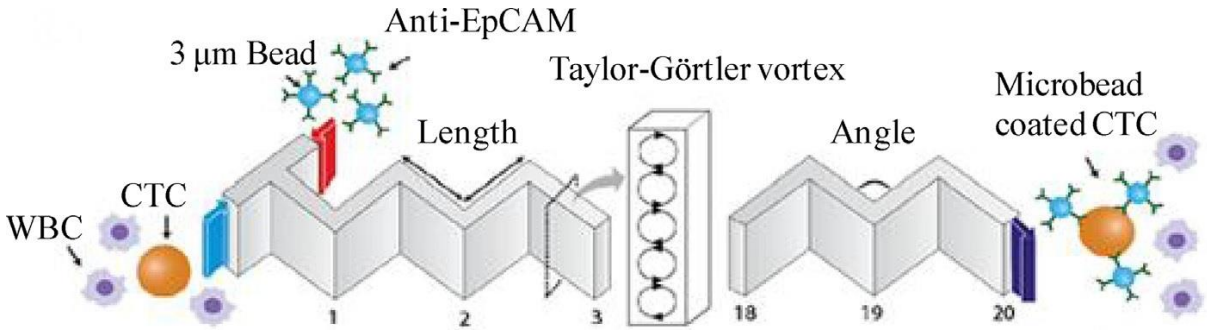

Fig. 1.2 Schematic of passive micromixer to separate circulating tumor cells (Lin et al. [9])

1.2.3 Biological agent detection

Micromixers are proven to be highly effective when employed in the applications of biological agent (used in bioterrorism) detection. A serpentine type micromixer with micropillars (Fig. 1.3) has been employed in the biobarcode assay [24] in order to mix the

targeted pathogens with particle probes and later separate them in magnetic chamber and analyze them in the μCE (micro Capillary Electrophoresis) channel. In contrast to conventional lateral flow screening assay the biobarcode assay possesses high sensitivity and multiplexity. In similar studies, a four-membrane air chamber type micromixer is utilized in the application of rapid diagnosis of dengue virus [25] and a Y-injection mixer with Dean's vortex structures and chaotic generation obstacles [26] is employed for determining minimum amount of free chlorine required for removing pathogens in food processing industry applications.

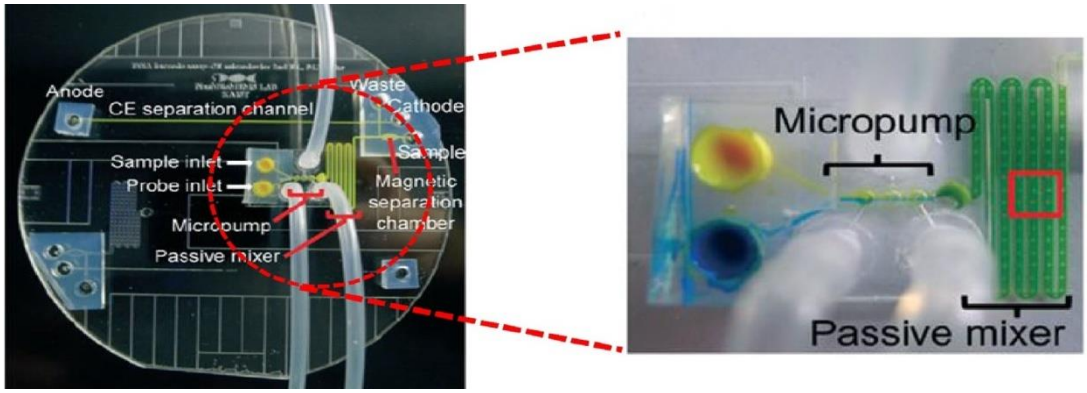

Fig. 1.3 Bio-barcode assay for biological agent detection (Cho et al. [24])

1.2.4 Chemical synthesis

Micromixers are employed widely in chemical synthesis due to the advantages of high selectivity and yield in the synthesis process as well as better thermal management. A multi-inlet vortex micromixer is employed (Fig. 1.4) [27] in the synthesis of molybdenum sulfide (MoS_2) nanoparticles. The degree of mixing could be controlled by the device by manipulating inlet flow rates such that a desired size of nanoparticles is obtained at the outlet. Similarly, a static split and recombine type micromixer [28] is used in the synthesis of ZnO nanoparticles and a T-type micromixer [29] is employed in the synthesis of NiO nanoparticles.

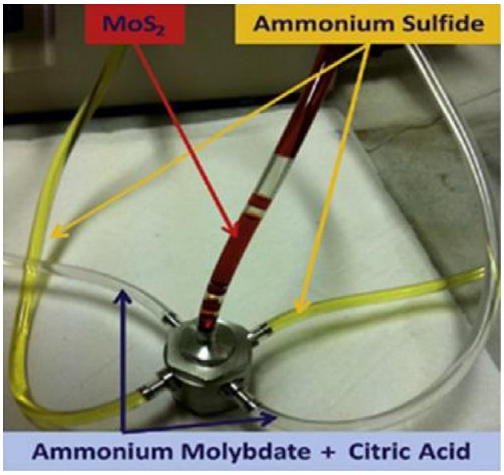

Fig. 1.4 Multi-inlet vortex micromixer for MoS_2 nanoparticles synthesis (Bensaid et al. [27])

1.2.5 Polymerization

Mixing plays a very crucial role in the process of polymerization in determining the properties of final product. A multi-layered laminar micromixer is utilized (Fig. 1.5) [30] in polymerization of amino acid *N-carboxyanhydride*. It is found that compared to conventional batch-wise systems, a strict control of polymerization reactions is possible with microreaction systems and therefore a better control over average molecular weight and molecular weight distribution is possible. Moreover, the control of molecular weight is achieved simply by varying the flow rate in the microreactor. In other studies, a caterpillar SAR (split-and-recombine) micromixer is used in the synthesis of defined PMSSQ (Poly(methylsilsesquioxane)) [31] and a high pressure slit inter digital micromixer (HP-IMM) combined with T-micromixer are utilized in synthesis of end-functionalized polystyrenes [32].

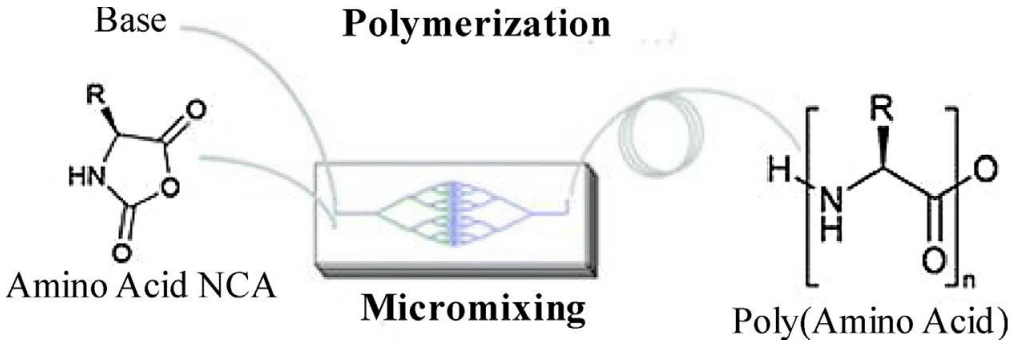

Fig. 1.5 Micromixer employed in a polymerization process (Honda et al. [30])

1.2.6 DNA Analysis

Micromixers play a crucial role in the field of biomedical engineering to carry out integrated processes of bio-reaction and analysis in a single continuous system. For example in the application of DNA analysis [33], mixing of DNA and restriction enzyme is carried out

through electro-osmosis in a T-micromixer (Fig. 1.6) and a serpentine channel is employed in the downstream for digestion reaction of DNA and afterwards passes through CE (Capillary Electrophoresis) channel for the DNA analysis. Similarly different passive type micromixers such as labyrinth SAM (Split and Merge) micromixer [34] and zigzag type micromixers [35][36] are employed for DNA digestion reactions.

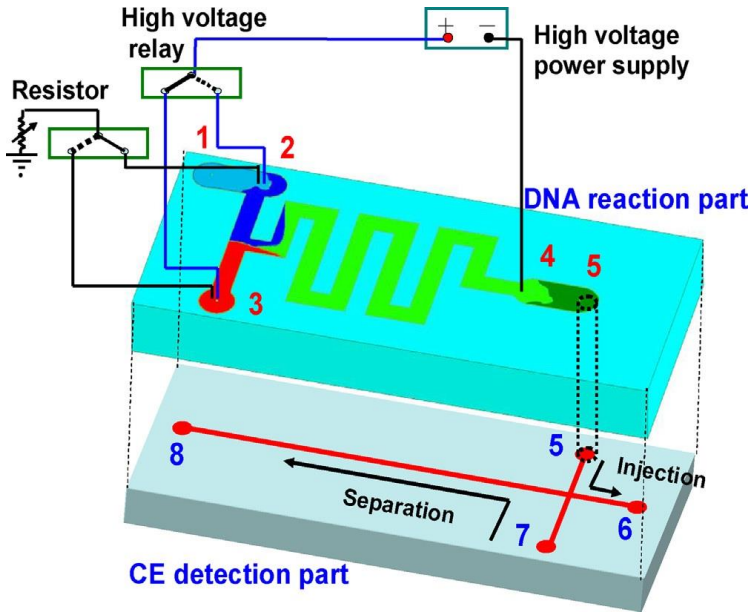

Fig. 1.6 Schematic of T-mixer for DNA digestion and restriction (Lin et al. [33])

1.3 Fabrication techniques

Most of the fabrication techniques employed in fabricating micromixers are evolved from the silicon-based fabricating methods developed for MEMS (Micro-electromechanical systems). Apart from these already available silicon-based fabrication methods, many other fabrication techniques are developed over the past decade to suit the particular needs of micromixer functionality. The classification (Fig. 1.7) shows various fabrication techniques that are available for manufacturing micromixers and other micro-structured devices. Broadly the fabrication techniques can be classified into i) Silicon-based techniques ii) Polymeric-based techniques and iii) Metallic-based techniques. Nguyen et al. [37]presented a very detailed study on each of these fabrication methods. Generally, many techniques from different methods are combined in fabricating different microfluidic devices based on their functional requirements. On a brief note, some of these methods are briefly explained below mainly focusing on their ability to fabricate different features of microchannels (like high aspect ratio channels) precision of channel dimensions, chemical and bio compatibility, erosion, cost effectiveness,

access and fast prototyping. For more detailed review of fabrication techniques Qin et al. [38] can be referred.

1.3.1 *Silicon-based techniques*

In Silicon-based techniques, silicon may be directly used as substrate material or oxides of silicon layers are deposited on other substrates as sacrificial layers to etch the microchannels. Some of the most widely used techniques are 1) Anisotropic wet chemical etching of silicon, 2) Dry etching of silicon and 3) Wet chemical etching of glass. The merits of anisotropic wet chemical etching of silicon are obtaining high precision and less corrosive surfaces whereas the demerits are costly equipment and clean room requirement for processing. The advantages of dry etching are better resolution and high aspect ratios while the disadvantages are slow-etch rates and trenches formed on substrate due to reflected ions. The advantages of glass are resistance to highly corrosive chemicals, biocompatibility whereas the main limitation is that the structural precision is low compared to silicon.

1.3.2 *Polymeric-based techniques*

Micromixers fabricated in silicon have the limitations of higher costs and less biocompatibility. Polymers are low cost and very bio-compatible devices. Polymers are also suitable for bulk and surface micromachining. However, most of polymers are self-fluorescent for low excitation wavelengths which affects the sensitivity of analysis in specific applications. They are also poorly resistant to chemical solvents involved in the applications of drug discovery and other chemical industry applications. The surface properties of polymer are not favorable for electro-osmotic applications where the material of glass suits very well. The different materials and important methods in Polymeric-based techniques are 1) PMMA (Polymethylmethacrylate) resist, 2) SU-8 resist, 3) Injection molding, 4) Hot embossing, 5) Soft lithography and 6) Laser machining. PMMA resist allows higher structural heights and higher aspect ratios. However, fabricating structures on PMMA require X-ray form synchrotron facility which is expensive and limited to access. The advantage in employing SU-8 resist is that the structuring of SU-8 can be worked with inexpensive UV light source in contrast to X-ray source utilized for PMMA. The limitations are difficulty in removal of SU-8 film and forming three-dimensional structures is relatively complicated. Soft lithography in PDMS (Polydimethylsiloxane) is predominantly utilized in fabricating various lab-scale microfluidic devices for research due to its rapid prototyping nature. The PDMS used in soft lithography has the advantages of low cost, less toxicity, optical transparency and low self-fluorescence. The limitations of PDMS are swelling, shrinkage and elastic deformation. Its elastic

deformation allows only low aspect ratio (0.2 to 2) structures. Though laser machining is capable of fabricating three-dimensional structures and fast prototyping, mass fabrication is not achievable due to longer processing times. The processing costs are also very expensive.

1.3.3 *Metal-based techniques*

The compatibility of metals with silicon-based techniques allow fabrication of metallic microstructures using standard photolithography. The important methods in metal-based techniques are 1) Isotropic wet chemical etching of metal foils, 2) LIGA process and 3) Micro-electro-discharge machining (μ-EDM). Wet chemical etching of metal foils allow mass fabrication with reasonable costs and reliability. However, the isotropic nature of etching allows only smaller aspect ratios. LIGA process is a combination of fabrication techniques of lithography, electroforming and molding (Lithographie, Galvanoformung, Abformung is the German Acronym). The merits of LIGA are ultra precision, high surface quality and high aspect ratio structures. However, X-ray lithography with synchrotron radiation is very expensive and not practical for mass fabrication of micromixers. The advantages of μ-EDM are fabrication of highly complex geometries, and higher structural flexibility to fabricate three-dimensional structures. The main disadvantage is the very high local temperatures up to 10000 ^{0}C generated on workpiece, and hence electro-polishing is required to remove heat-affected zone.

Overall, from the above study of fabrication standpoint view of micromixers, the following conclusions can be drawn. Though silicon-based fabrication is well established to manufacture the geometry of choice, it has its own limitations of costly equipment, clean room facility requirement, bio-compatibility and other issues. While the polymeric-based techniques offer inexpensive mass fabrication for specific applications (analytical chemistry and drug delivery), they turn out to be unsuitable for drug discovery and electro-osmotic applications due to poor chemical resistance and poor surface charge density respectively. In metal-based techniques, though LIGA process can deliver ultra precision and high aspect ratio microstructures, the required X-ray lithography with synchrotron radiation is not economical for mass fabrication. Considering various benefits of micromixers and the constraints in fabrication in terms of cost, access to equipment and reliability it is difficult to implement complex micromixer designs for wide range of applications particularly in developing countries. Therefore, it is vital to design and develop simple structured efficient passive micromixers for widespread implementation to reap their benefits in various scientific applications.

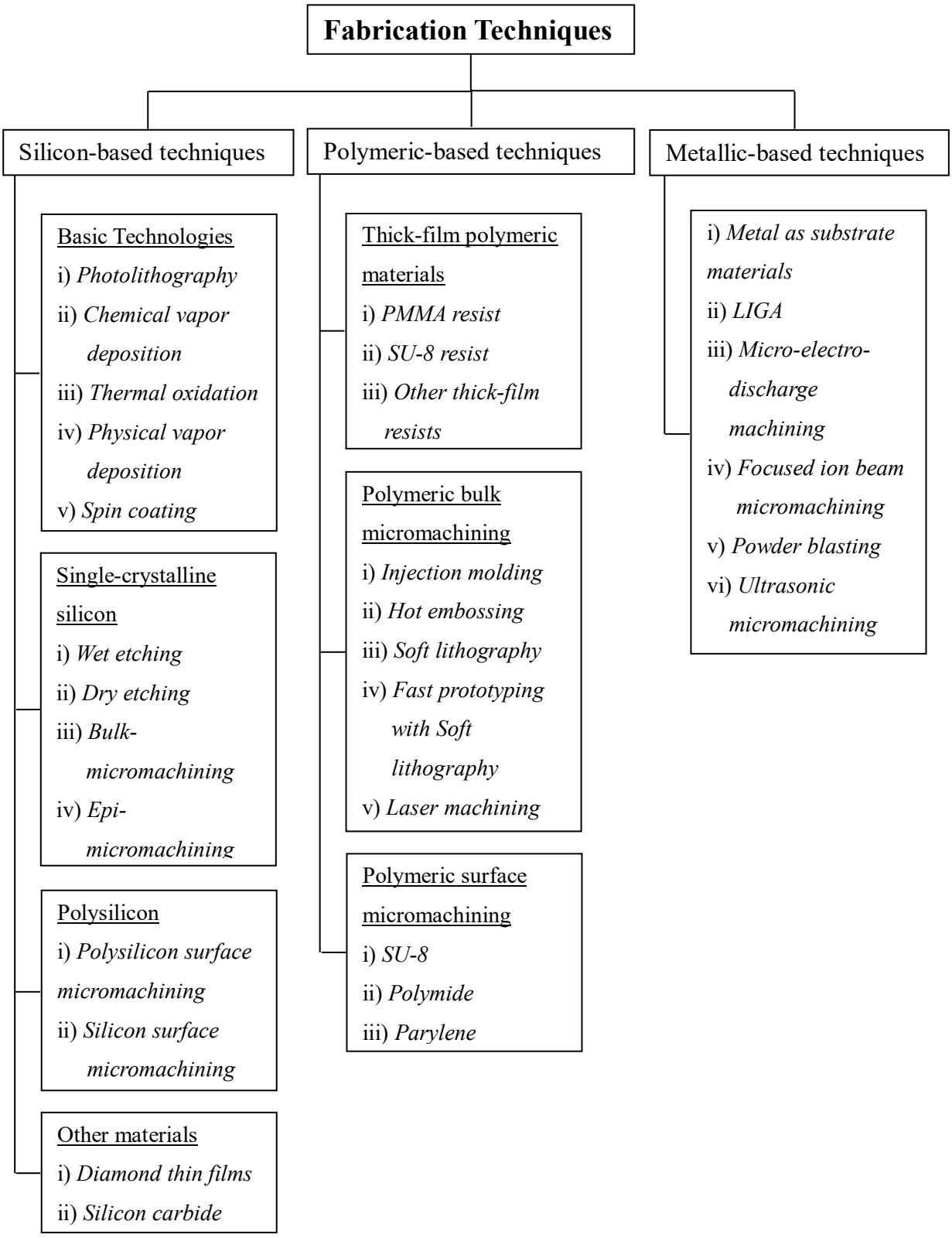

Fig. 1.7 Classification depicting different micro-fabrication techniques

1.4 Geometry optimization of Micromixers

Geometry optimization plays a critical role in micromixing, which refers to the process of achieving efficient mixing at the microscale. Micromixing is important in a wide range of applications, including chemical synthesis, pharmaceutical manufacturing, microfluidic devices, and lab-on-a-chip systems, where precise control over mixing at small length scales is crucial.

Geometry optimization in micromixing involves designing and optimizing the geometry of microscale devices or structures, such as microchannels, micromixers, and microreactors, to enhance mixing performance. Here are some key reasons why geometry optimization is important in micromixing:

- Enhances Mixing Efficiency: The geometry of microscale devices can significantly influence the efficiency of mixing. Optimizing the geometry, such as the shape, size, and arrangement of microchannels or other mixing elements, can enhance the mixing performance by promoting fluid deformation, stretching, and folding, leading to increased interfacial contact and enhanced mixing efficiency. Geometry optimization can help achieve desired mixing characteristics, such as reduced mixing time, improved uniformity, and increased reaction rates, which are crucial for many microscale applications.
- Enables Tailored Mixing: Different micromixing applications require specific mixing characteristics, such as laminar or turbulent flow, plug flow, or chaotic flow. Geometry optimization allows for tailoring the mixing characteristics by designing microscale devices with desired geometries, such as serpentine, split-and-recombine, or T-shaped channels, which can result in specific flow patterns and mixing behaviors. This allows for customization of micromixing systems to achieve optimal performance for a given application.
- Overcomes Diffusion Limitations: At the microscale, diffusion becomes dominant over convection due to reduced length scales, resulting in slower mixing compared to macroscale mixing. Geometry optimization can help overcome these diffusion limitations by creating complex and tortuous flow paths, increasing the contact area between different fluids, and promoting chaotic advection, which can enhance mixing efficiency and overcome diffusion limitations. Optimized geometries can also minimize the dead zones or stagnant regions that can hinder mixing in microscale devices.

- Enables Scalability and Miniaturization: Micromixing is often employed in microfluidic devices and lab-on-a-chip systems, where miniaturization and scalability are critical. Geometry optimization allows for designing compact and integrated micromixers with small footprint, low sample volumes, and reduced reagent consumption. Optimized geometries can also facilitate scaling up of micromixing processes by maintaining consistent mixing performance across different device sizes and flow rates.
- Improves Process Control and Reproducibility: Geometry optimization in micromixing enables better control over the mixing process, which is essential for reproducibility and consistency in microscale applications. Optimized geometries can result in predictable and repeatable mixing behavior, allowing for precise control of mixing parameters, such as flow rates, fluid properties, and residence times. This can improve process control, reduce variability, and enhance the reproducibility of micromixing processes.

In conclusion, geometry optimization plays a crucial role in micromixing by enhancing mixing efficiency, enabling tailored mixing, overcoming diffusion limitations, enabling scalability and miniaturization, and improving process control and reproducibility. It is a critical design parameter in microscale devices and systems, allowing for efficient and controlled mixing, which is vital for various microscale applications.

1.5 Literature Review

Voluminous research in the field of micromixing is dedicated to design, development and optimization of passive micromixers. The driving factor for the extensive research on passive micromixers is their high suitability and reliability for vital applications of biomedical and biochemical analyses (carried out in a complex microfluidic environment where integrating an active mixer can further complicate handling and operation of lab-on-chip) as well as cost effectiveness as compared to active mixers. Passive mixers also play a dominant role in the applications of chemical processing field [12]. However, the challenge that is mainly concerning in the design of passive mixers is the absence of turbulence due to inherent low *Re* microchannel flows which makes mixing a very difficult task. Moreover, when it comes to mixing of liquids, it is even more complicated to design an efficient passive mixer due to their low diffusion coefficients (of the order of 10^{-9}). To overcome this limitation, the channel structure of passive mixer should be designed in such a way that the contact area between the samples is continuously enhanced in the residence time. This can be realized only when the geometry of passive mixer is capable of continuously inducing the stretching and folding of samples [39]. Studies of homogeneous kinetics in solution require that a system become well mixed on a time scale faster than the kinetics of the reaction. For most chemical reactions, it is preferable that mixing rate is faster than reaction rate to avoid creation of unwanted side products. Many biochemical assays, for example DNA microarrays, require that a reagent be brought into contact with the entirety of a functionalized surface, i.e., that the reagents in the system be well mixed [40]. Therefore, in order to effectively mix in a reasonable time, fluids must be manipulated such that the interfacial surface area between the fluids is increased massively and the diffusion path is decreased drastically, enhancing the molecular diffusion for complete mixing within the desired timeframe of selected application.

A wide variety of passive mixers based on various geometric structures and hydrodynamic principles have been proposed by many authors previously. Based on the literature, with respect to geometric structure, passive mixers can be broadly classified into i) planar, ii) three-dimensional and iii) complex microstructures as depicted in the classification below (Fig. 1.8).

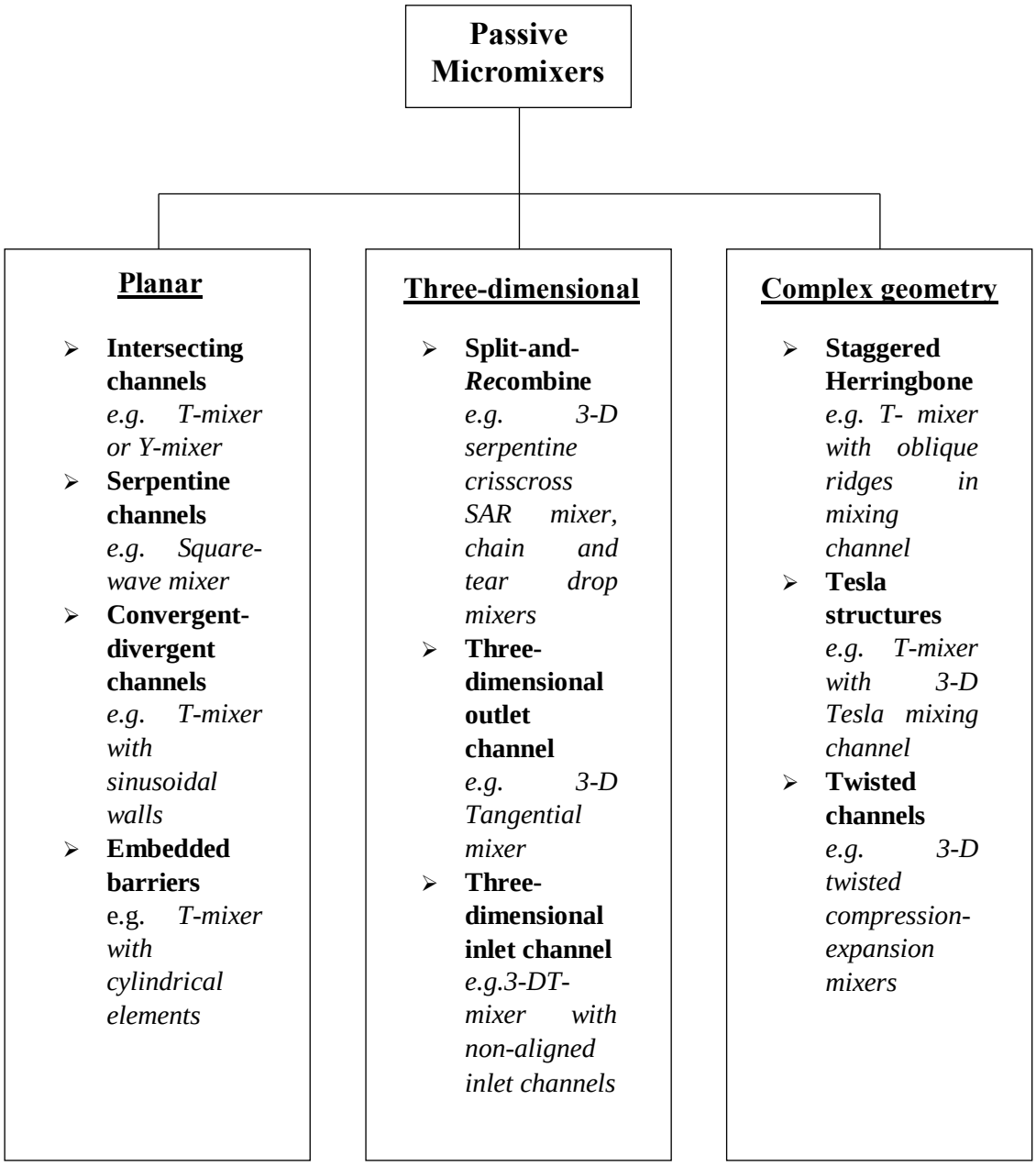

Fig. 1.8 Classification depicting types of passive micromixers based on geometric structure

1.5.1 Planar micromixers

Planar micromixers refer to the type of geometries that need only a two-dimensional control over the raw material to fabricate the required shape of channels on the substrate. This important feature of planar passive mixers facilitates a fairly simple and less time consuming fabrication procedure. They also incur lower pressure drops during their operation. However the two-dimensional flow in planar micromixer channels is more restrictive towards the stretching and folding of samples which is required for mixing enhancement. The various types

of planar designs reported in the literature including the lab-tested micromixers as well as successfully implemented real-time application micromixers can be generally grouped under following four categories, i) Contacting or Intersecting sub-streams (e.g. T-mixer, Y-mixer), ii) Serpentine channels (e.g. square-wave mixer, zig-zag wave mixer), iii) Convergent-divergent channels and iv) Embedded barriers (e.g. T-mixer with cylindrical elements).

1.5.1.1 Contacting or intersecting sub-streams

The samples are allowed to meet at the confluence of the branches (inlet channels) of T-mixer, Y-mixer or Arrow-head mixer. The samples collide and come in contact with each other at the junction and subsequently flow into the mixing channel for mixing process before exit from the outlet of micromixer. Following studies refer to the use of different contacting type passive micromixers in various applications. The analyte concentration of a continuous flow is measured using a basic T-mixer (Fig. 1.9) in the work of Kamholz et al. [41]. A simple Y-mixer was used in Wu et al. [42] to validate the nonlinear diffusive model of diffusion mixing in microchannels. Hadd et al., [5] used an electrokinetically driven T-mixer was used to perform enzyme assays. A micro swirl type of T-mixer was used in the work of Kawasaki et al. [29] to mix aqueous solutions of metal salts and supercritical water in the synthesis of NiO nanoparticles. A simple passive T-type micromixer is used to separate particles and molecules based on their diffusion coefficients in the work of Brody et al. [43].

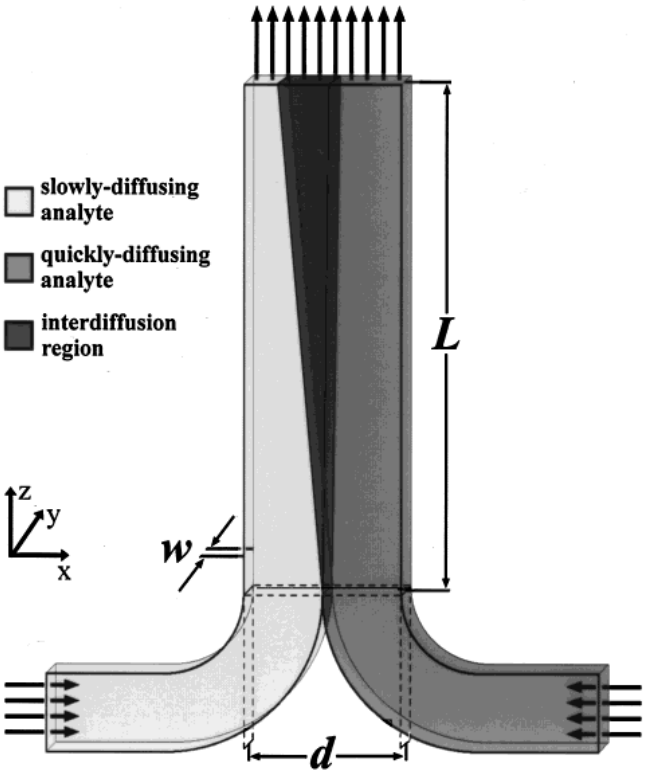

Fig. 1.9 Schematic of T-sensor for measuring analyte concentrations (Kamholz et al. [41])

1.5.1.2 *Serpentine channels*

Serpentine type micromixers (square wave, curved, zig-zag) (Fig. 1.10) performs reasonably good mixing with lower pressure drops and simple structure favoring easier integration as compared to complex and 3-D structured micromixers. In a study conducted by Hossain et al. [44], three different passive micromixers were investigated numerically. The micromixers had zig-zag, square-wave, and curved geometries, and the analysis focused on the mixing and flow fields across a wide range of Reynolds numbers. The researchers used Navier-Stokes equations to study the behavior of water and ethanol, which served as the working fluids. Notably, the findings revealed that the square-wave microchannel exhibited the most efficient mixing performance. However, the curved and zig-zag microchannels showcased comparable performance across the majority of Reynolds numbers. Regarding pressure drop, the curved microchannel experienced the least drop, while the square-wave and zig-zag channels displayed similar pressure drops. Similarly, Nonino et al. [45] conducted a comparative numerical analysis of serpentine microchannels with square cross-sections. Their objective was to assess the mixing performance of each geometry by calculating mixing indices at different axial locations. The study employed two streams of fluid with varying solute concentrations and considered Reynolds numbers ranging from 5 to 150. The comprehensive evaluation provided insights into the mixing performance of the microchannels and offered a comparison with straight microchannels of identical length. Another investigation by Kuo et al. [46] explored the flow characteristics and mixing performance of three microfluidic blood plasma mixing devices, each with a distinct microchannel geometry. The researchers discovered that the device equipped with a square-wave microchannel outperformed the others in terms of mixing efficiency. As a result, this particular design was selected for further optimization. The team fabricated four micromixers with square-wave microchannels of different widths and subjected them to both numerical simulations and experimental analysis. The results indicated that careful specification of the microchannel geometry could achieve a remarkable mixing efficiency of approximately 76% within a mere 4 seconds. To demonstrate the practical feasibility, the researchers conducted prothrombin time (PT) tests using a total liquid volume of 4.0 μL. The tests revealed that the mean time required to complete the entire PT test was less than 30 seconds.

Even though serpentine channels are planar in structure and easy to fabricate, they require larger area on the Lab-on-chip which may not be always feasible.

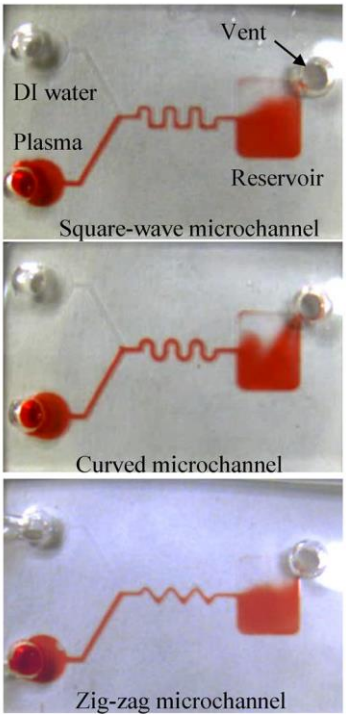

Fig. 1.10 Different types of serpentine micromixers in blood plasma mixing (Kuo et al. [46])

1.5.1.3 *Convergent-divergent channels*

Convergent-divergent walled microchannels have emerged as a promising approach to enhance mixing quality in comparison to conventional straight mixing channels. For instance, Parsa et al. [47] investigated mixing performance within a sinusoidal microchannel incorporating convergent-divergent sections. Their findings revealed the formation of Dean Vortices at higher Reynolds numbers, accompanied by separation vortices within the divergent crest and trough regions. These vortices played a pivotal role in facilitating convective diffusion and consequently improving the efficiency of mixing. In a similar vein, Wu and Tsai [48] developed a meandering microchannel design that integrated convergent-divergent portions. Their research showcased significant enhancements in mixing performance, particularly under high flow rates. The presence of Dean and separation vortices, manifested in multiple directions within the microchannel, contributed to the improved mixing efficiency. Another numerical study by Afzal et al. [49] delved into the mixing characteristics of a split and recombination type micromixer employing convergent-divergent walls (see Fig. 1.11). Notably, the researchers observed an increase in both the mixing index and pressure drop as the number of split and recombination units rose. Consequently, the optimization of design necessitated careful consideration of a trade-off between improved mixing performance and the associated pressure drop.

Collectively, these investigations emphasize the effectiveness of utilizing convergent-divergent walled microchannels to enhance mixing quality. The presence of Dean and separation vortices within these microchannels plays a critical role in augmenting convective diffusion and promoting efficient mixing. However, it is important to meticulously consider specific design parameters, such as the number of split and recombination units, in order to strike an appropriate balance between improved mixing performance and the accompanying pressure drop.

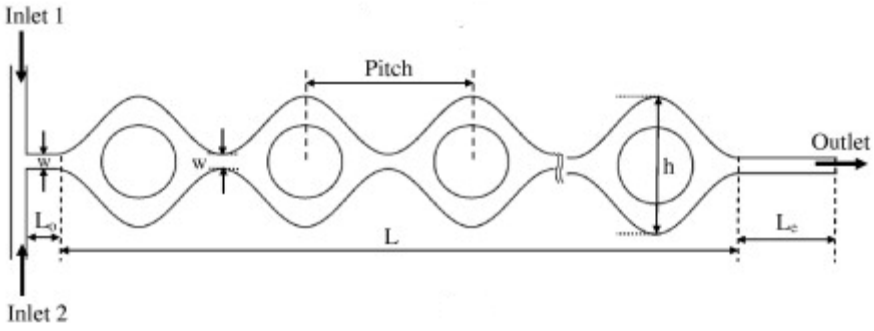

Fig. 1.11 Split and recombine mixer with convergent-divergent channel walls (Afzal et al. [49])

1.5.1.4 Embedded barriers

Several studies have investigated the utilization of embedded barriers, such as obstacles in microchannels, to improve mixing by promoting chaotic advection. In a study conducted by Chen et al. [50], the passive mixing behavior of a poly(dimethylsiloxane) microfluidic mixer with pillar obstructions was evaluated using fluorescence microscopy (Fig. 1.12). The researchers examined the impact of various parameters on the efficiency of mixing.

In a different approach, Tseng et al. [51] employed computational fluid dynamics (CFD) to optimize a micromixer that incorporated diamond-shaped obstacles and boundary protrusions. By manipulating the flow field and optimizing the geometric design, their aim was to enhance the mixing performance. Fang et al. [52] conducted research on mixing enhancement in microchannels by introducing simple periodic geometric features. They specifically explored how different shapes of these features influenced mixing efficiency. Afzal and Kim. [49] conducted a comparative analysis of three types of passive micromixers with convergent-divergent sinusoidal walls. Their evaluation involved assessing the mixing efficiency of each design and identifying the configuration that yielded the most favourable results. Similarly, Alam et al. [53]

investigated the mixing performance of a planar micromixer that incorporated circular obstructions within a curved microchannel. They studied the influence of various operational and geometric parameters on mixing efficiency. Santana et al. [54] focused on optimizing the mixing conditions for the transesterification of sunflower oil in microchannels with circular obstructions. Their objective was to improve the reaction rate and conversion efficiency through careful adjustment of the mixing parameters.

Embedded barriers in microchannels have the disadvantages of higher pressure drops and clogging effect which limits their re-use.

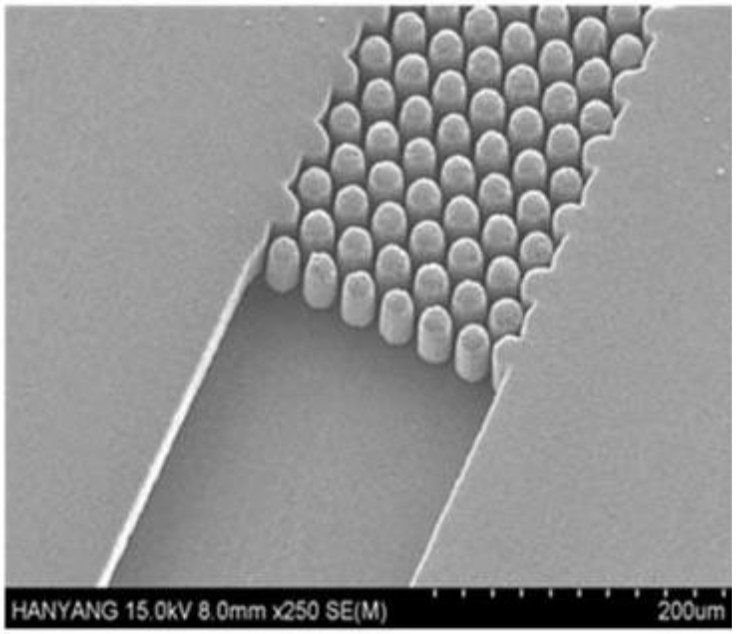

Fig. 1.12 Micromixer with pillar obstructions in mixing channel (Chen et al. [50])

1.5.2 Three-dimensional micromixers

The three-dimensional micromixers refer to the type of passive mixers that are designed to induce a third dimensional flow at some point or periodically throughout the micromixer by inserting three-dimensional shapes into micromixer to enhance mixing. The different types of three-dimensional structure are i) SAR mixers (split-and-recombine mixers), ii) Three-dimensional outlet channel (e.g. Tangential mixer) and iii) Three-dimensional inlet channel (e.g. Vortex T-mixer). Fabricating three-dimensional structured micromixers can be very time consuming as well as their integration is relatively challenging compared to planar type micromixers.

1.5.2.1 *SAR (Split-And-Recombine) mixers*

Split-and-Recombine micromixers refer to the type of channel geometries that are divided and joined repeatedly along the length of micromixer to reduce the thickness of

samples and increase the interfacial area. Hossain et al. [55] proposed a three-dimensional split and recombine type micromixer with O-H shaped periodic units and evaluated the mixing performance in the *Re* range of 0.1 to 70. For *Re* as low as 30 the split and recombine micromixer is able to achieve nearly 88 % of mixing quality. They also observed the mixing performance is strongly influenced by the geometrical parameters of the split and recombine mixer. Raza et al. [56] designed a novel micromixer by combining the three-dimensional serpentine mixer and crisscross split and recombine structure and evaluated the mixing performance in the *Re* range of 0.1 to 200. The micromixer achieved very short mixing lengths in the order of 1500 μm for the *Re* range of 0.1 to 120. A nearly complete mixing is achieved by this design for $Re > 40$. Hermann et al. [57] developed a validated CFD model to study and optimize the three-dimensional split and recombine mixer for better exploitation of secondary flows in order to enhance the mixing performance particularly at lower Re. The results suggested that the consideration of the effect of secondary flows is very important to improve the mixing performance of micromixers. Nimafar et al. [58] carried out experimental investigations to evaluate and compare mixing efficiency of three different micromixers viz., simple T-mixer, split and recombine planar O-type mixer and split and recombine three-dimensional H-type mixer (Fig. 1.13) in the laminar regime. It is found that H-type performed significantly better owing to the split and recombining process in combination with three-dimensional flow pertaining to its geometric structure.

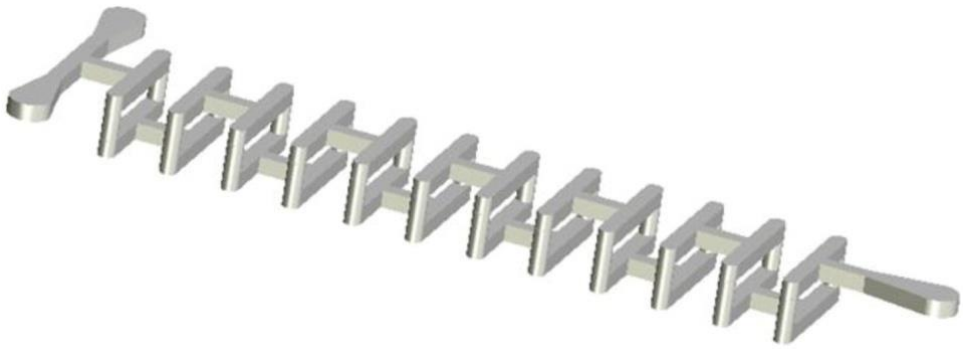

Fig. 1.13 Schematic of three-dimensional split and recombine H-type mixer (Nimafar et al. [58])

1.5.2.2 *Three-dimensional outlet channel (Tangential mixer)*

Kockmann et al. [59] conducted experiments to explore different three-dimensional passive mixers with the aim of identifying an optimal micromixer suitable for high-flow-rate

chemical processing applications. Among the mixers tested, the tangential micromixer (shown in Figure 1.14) demonstrated superior performance compared to the conventional T-mixer, caterpillar micromixer, and interdigital micromixer. In the tangential mixer, the two liquid samples are introduced tangentially into a cylindrical mixing chamber and exit through a central transition hole, inducing a swirling motion that promotes efficient mixing. These findings highlight the effectiveness of the tangential micromixer design in achieving enhanced mixing capabilities for high-flow-rate applications.

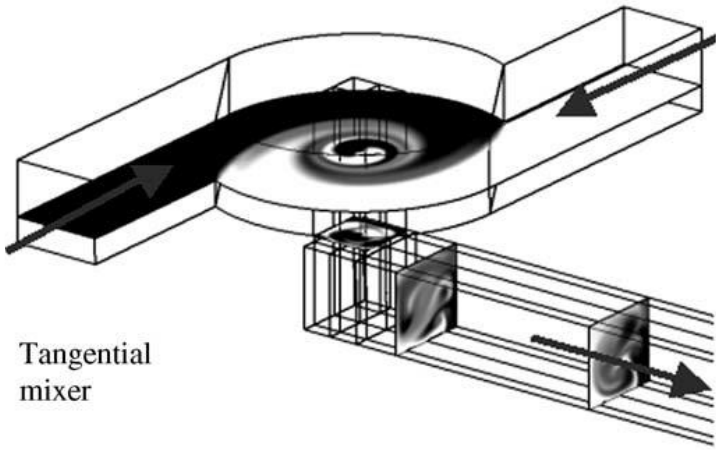

Fig. 1.14 Three-dimensional outlet Tangential mixer (Kockmann et al. [59])

1.5.2.3 *Three-dimensional inlet channel (Vortex T-mixer)*

Cortes-Quiroz et al. [60] conducted an evaluation of flow characteristics to determine which factors contribute to higher mixing performance in a three-dimensional (3-D) T-mixer compared to a typical T-mixer. They studied the flow patterns and vortex formation within the mixers and analyzed their influence on mixing efficiency. The research aimed to identify the design parameters that enhance vortex formation and subsequently improve mixing performance in T-mixers. Ansari et al. [61] proposed a vortex micro T-mixer with non-aligned inputs (Fig. 1.15). Their study focused on the formation of vortices within the mixer by introducing non-aligned input streams. By manipulating the angle and position of the inlet streams, they aimed to enhance the generation of vortices, which are known to promote efficient mixing. The research investigated the effect of these non-aligned inputs on the flow patterns and mixing efficiency of the T-mixer.

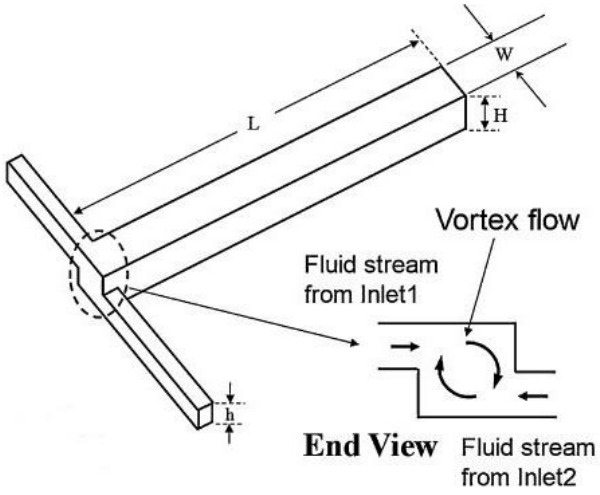

Fig. 1.15 Three-dimensional inlet Vortex T-mixer (Ansari et al. [61])

1.5.3 Complex structured micromixers

Complex structured micromixers refer to the passive mixer geometries designed with complicated and intricate geometric features in order to intensely create stretching and folding of samples and induce chaotic motion to significantly enhance mixing. the different types of complex micromixer structures are i) Staggered herringbone mixer ii) Tesla structures and iii) Twisted channels. The fabrication of complex structured micromixers may pose many challenges with respect to fabrication process, cost and time. Along with difficulty in integration, they can also cause severe pressure drops at relatively higher *Re*.

1.5.3.1 *Staggered herringbone mixers*

Staggered herringbone mixers refer to inclined grooves of herringbone like structures placed in a staggered manner in the bottom of mixing channel to induce chaotic advection. Stroock et al. [62] introduced the concept of a chaotic mixer for microchannels. They demonstrated that chaotic advection, achieved by introducing a staggered herringbone pattern in the mixer's design (Fig. 1.16), enhances mixing efficiency. The researchers investigated the flow characteristics and chaotic mixing behavior in microchannels with staggered herringbone structures. This pioneering work laid the foundation for utilizing staggered herringbone micromixers for improved mixing performance. Chen and Wang [63] focused on the optimized modular design and experimental evaluation of staggered herringbone chaotic micromixers. They aimed to further enhance the mixing performance by optimizing the geometric parameters of the staggered herringbone structures. The study involved both numerical simulations and experimental validation to investigate the effects of different module configurations on mixing efficiency in the micromixer. Du et al. [64] evaluated floor-grooved micromixers, which

incorporate a staggered herringbone pattern, by analyzing concentration-channel length profiles. They examined the mixing efficiency by quantitatively assessing the concentration distribution along the channel length. The researchers investigated the impact of geometric parameters, such as groove width and depth, on the mixing performance of staggered herringbone micromixers.

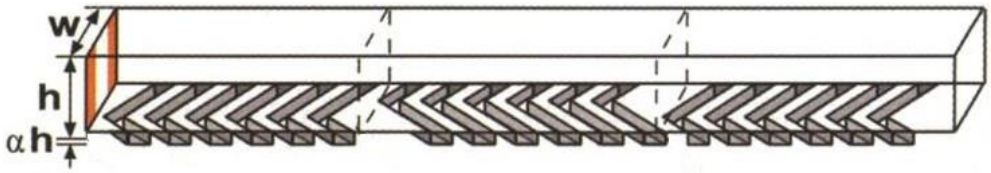

Fig. 1.16 Schematic of staggered herringbone micromixer (Stroock et al. [62])

1.5.3.2 Tesla structures

The utilization of Tesla structures in the design of mixing channels has been shown to significantly enhance mixing performance. This improvement can be attributed to the shape of the mixing channels, which incorporates curved trajectories. Near these curved paths, the Coanda effect comes into play, causing substantial sample movement in the transverse direction. As a result, the mixing performance is greatly enhanced, as the Coanda effect induces effective fluid mixing within the channels. Hong et al. [65] introduced a novel in-plane passive microfluidic mixer with modified Tesla structures. The modified Tesla structures induce chaotic advection, which enhances mixing performance. The flow physics involve the creation of vortices and fluid mixing through the interaction of the fluid with the geometric features of the Tesla structures. This chaotic advection mechanism promotes efficient mixing within the microfluidic device. Hossain et al. [66] conducted an analysis and optimization study on a micromixer with a modified Tesla structure. They investigated the flow physics associated with the modified Tesla structures and their impact on mixing performance. By analyzing the velocity profiles and flow patterns, they gained insights into the underlying flow physics governing mixing within the micromixer. This understanding allowed for the optimization of the geometric parameters of the Tesla structures to achieve improved mixing performance. Yang et al. [67] presented a high-performance micromixer that utilized three-dimensional Tesla structures for bio-applications (Fig. 1.17). The three-dimensional Tesla structures facilitated enhanced mixing by generating strong vortices and promoting fluid mixing through chaotic advection. The

underlying flow physics involve the creation and interaction of vortices within the three-dimensional structures, resulting in improved mixing efficiency for bio-applications.

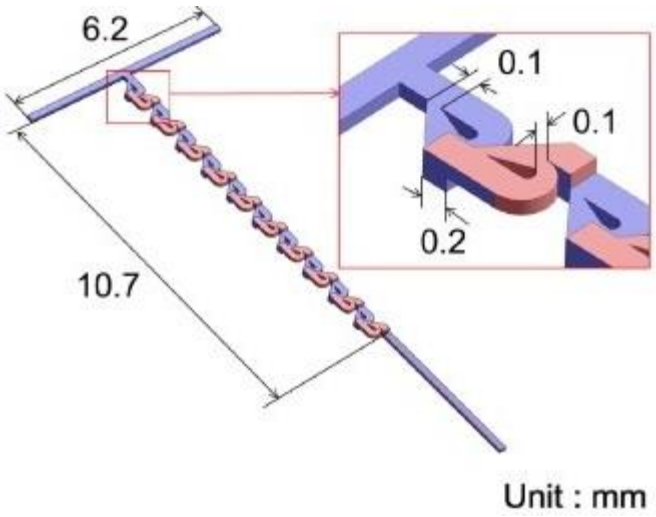

Fig. 1.17 Three-dimensional Tesla structured micromixer (Yang et al. [67])

1.5.3.3 *Twisted channels*

Zhang et al. [68] designed a novel micromixer with clamped capillaries that are twisted in orthogonal direction periodically at each section (Fig. 1.18). It is shown that the angle of clamping with 450 has better mixing performance with lower pressure drop. In the research conducted by Bahiraei and Mazaheri [69], they investigated the thermal and energy efficiency considerations of a hybrid nanofluid containing graphene-platinum nanoparticles. This nanofluid was applied in a chaotic twisted geometry for miniature devices. The study focused on manipulating fluid flow patterns and heat transfer properties by introducing chaotic twisted geometries. The goal was to enhance mixing performance and overall energy efficiency. Similarly, Bahiraei et al. [70] utilized computational fluid dynamics (CFD) simulations to examine irreversibilities and energy efficiency in the laminar flow of a power-law nanofluid within a minichannel. They introduced chaotic perturbations to the flow to generate chaotic advection, promoting better fluid mixing and reducing thermal gradients. The study aimed to improve the mixing performance and energy efficiency of the system. Furthermore, Bahiraei et al. [70] investigated the development of chaotic advection in the laminar flow of a non-Newtonian nanofluid. They explored the generation of chaotic flow patterns and vortices, which enhanced mixing performance by facilitating efficient fluid mixing. The objective was

to utilize these flow physics phenomena to achieve energy-efficient fluid transport and mixing. Lastly, Bahiraei et al. [71] conducted a second law analysis of a hybrid nanofluid in tubes equipped with double twisted tape inserts. By manipulating fluid flow patterns and leveraging the interaction between the fluid and the twisted tape inserts, the study aimed to enhance mixing performance by creating turbulence and promoting effective fluid mixing.

Many studies showed that twisted channels generating swirling flows have significantly improved the heat transfer efficiency. However, studies on the effect of swirling flows on mixing performance of micromixers are very few.

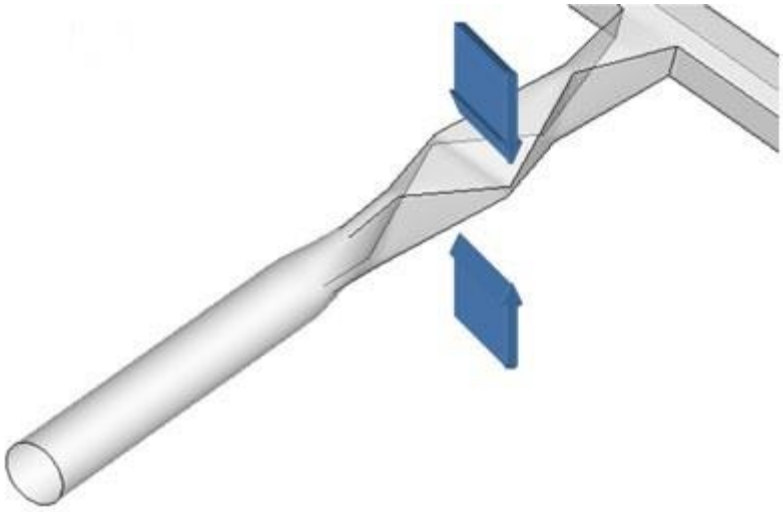

Fig. 1.18 Schematic model of rectangular twisted 90-mixer (Zhang et al. [68])

1.5.4 Passive T-type micromixer

1.5.4.1 *Flow and mixing phenomenon of T-mixer*

The T-micromixer is the most widely employed mixing device among all the simplest passive designs available in the literature. Many authors studied the effect of flow and geometric variables on mixing phenomenon of T-mixer at various *Reynolds* numbers. Particularly, the engulfment regime in T-mixer which occurs at a relatively higher *Re* than the typical operating range of μTAS is of great interest in many studies as it yielded a significant amount of mixing in T-mixer. Engler et al. [72] conducted numerical and experimental investigations on liquid mixing in static micromixers, exploring parameters such as flow rates, channel geometry, and mixing element design to understand their impact on the mixing performance of T-type micromixers. In a similar vein, Wong et al. [73] focused specifically on the micro T-mixer as a rapid mixing micromixer, optimizing parameters like channel dimensions, flow rates, and Reynolds numbers to achieve fast and efficient mixing in T-type

micromixers. Soleymani et al. [74] delved into numerical and experimental investigations of liquid mixing in T-type micromixers, analyzing parameters such as channel dimensions, fluid properties, and flow rates to evaluate their influence on the mixing performance and efficiency of these micromixers. Hoffmann et al. [75] adopted an experimental approach to study liquid-liquid mixing in T-shaped micro-mixers, utilizing techniques like μ-LIF and μ-PIV. Their focus was on parameters such as flow rates, viscosity ratios, and channel dimensions to understand their effects on the mixing performance of T-type micromixers. Shifting to numerical simulations, Bothe et al. [76] examined reactive mixing in a T-shaped micromixer, investigating parameters like reaction kinetics, species concentration, and mixing element geometry to gain insights into their influence on the mixing performance and reaction efficiency of T-type micromixers. Dreher et al. [77] investigated the characterization of laminar transient flow regimes and mixing in T-shaped micromixers. Parameters such as flow rates, fluid properties, and channel geometry were analyzed to explore their effects on flow patterns and mixing performance during transient flow conditions in T-type micromixers. Fani et al. [78] explored the steady engulfment regime in a three-dimensional T-mixer, examining parameters such as flow rates, channel dimensions, and fluid properties to comprehend their influence on the engulfment phenomenon and mixing performance within T-type micromixers. Cherlo and Pushpavanam [79] studied the effect of depth variations on the onset of engulfment in rectangular microchannels, including T-type geometries. They investigated parameters such as channel depth, flow rates, and fluid properties to understand their impact on the mixing performance and the initiation of engulfment in T-type micromixers. Calado et al. [80] characterized the mixing regimes of Newtonian fluid flows in asymmetrical T-shaped micromixers. Parameters like flow rates, channel geometry, and asymmetry ratios were examined to gain insights into their effects on the mixing performance and efficiency in asymmetrical T-type micromixers. Silva et al. [81] experimentally characterized pulsed Newtonian fluid flows inside T-shaped micromixers with variable inlet widths, analyzing parameters such as pulse frequency, pulse amplitude, and inlet width variations to understand their influence on the mixing performance and efficiency during pulsed flow conditions in T-type micromixers. Siconolfi et al. [82] employed numerical simulations and stability analysis to investigate the effect of geometry modifications on the engulfment phenomenon in micromixers. Parameters such as channel dimensions, modifications in geometry, and flow rates were scrutinized to comprehend their impact on the stability of the mixing process and mixing performance in T-type micromixers.

1.5.4.2 *Applications of T-mixer*

The passive T-mixer has been employed widely in a diverse range of micromixing applications owing to its simple design, robustness, ease of integration and low cost of fabrication. Bökenkamp et al. [83] conducted an experimental study on two "T" micromixers connected by a channel, etched on a 1 cm x 1 cm silicon chip. They carried out hydrolysis of PCA (phenyl chloroacetate) in the T mixers arrangement to utilize it in quench-flow analysis for protein folding studies that require sub-millisecond time scale of mixing. They successfully tested the mixer to be capable of performing sub-millisecond quench-flow analysis at higher *Re* numbers ($Re > 1000$). Stahl et al. [84] utilized a T-mixer for crystallization of benzoic acid at higher *Re* (6000 to 7000). They evaluated different mathematical models and validated the size distribution of microparticles obtained in the experiments. A T-shaped micromixer is employed in Iwasaki et al. [85] for cationic polymerization of vinyl ethers. Yamamoto et al. [86] carried out the synthesis of zeolitic imidazolate framework (ZIF-8) nanoparticles in a passive T-mixer. They observed the size of nanoparticles is dependent on flow rates for $Re < 2000$ whereas the size as well as shape of nanoparticles is independent of flow rates for $Re > 2000$. Santana et al. [87] carried out synthesis of biodiesel (transesterification of sunflower oil) in a passive T-mixer with and without static elements. They noticed that the use of static elements in T-mixer improved biodiesel synthesis. Yasukawa et al. [88] employed two T-micromixers for mixing of substrate and catalyst solution and slug flow generation respectively. Their designed system showed higher yields of ethyl pyruvate per unit time with lesser energy consumption compared to conventional batch reaction systems. Montillet et al. [89] utilized three different configurations of T-shaped micromixers and produced water in oil emulsions with a mean size smaller than 10 μm. They found that the size and cross-section shape of mixing channels has an important role to determine the feasibility of emulsion formation.

1.5.5 Geometry optimization in micromixing

In the field of micromixer optimization, researchers have proposed various methodologies to enhance mixing performance. Shakhawat Hossain et al. [66] conducted a study focusing on the analysis and optimization of a micromixer with a modified Tesla structure. They selected design variables and defined the design space. Objective functions were calculated through a three-dimensional Navier-Stokes analysis. To save computational time, surrogate models were constructed based on these objective function values. These surrogate models were then utilized to predict superior designs and determine the optimal points. Another approach was presented by Kwang-Yong Kim et al. [53] who concentrated on shape optimization of the micromixer. They employed a numerical optimization model along

with the response surface method. Four design variables related to micromixer performance were chosen. By utilizing a design of experiments (DOE) framework, a surrogate model was created based on discrete numerical analysis. The objective function values were obtained by performing a three-dimensional Navier-Stokes analysis. The RSA method was employed as an optimization tool to improve the mixing performance. M Jain et al. [90] proposed a different optimization methodology that involved utilizing Bezier curves to represent the groove shape. The control points of these curves were optimized to identify the best shape for achieving maximum mixing. The Optimization Toolbox in Matlab was used for the optimization process. The study explored various Peclet numbers and groove arrangements. Mixing performance was evaluated using the mixing index. The Bezier curve approach was found to effectively represent a wide range of groove shapes using the same number of parameters. Optimal groove shapes identified through the Bezier curve approach demonstrated superior mixing performance compared to previously studied groove shapes such as diagonal and herringbone grooves.

These studies demonstrate the diverse methodologies employed in micromixer optimization, including the analysis of mixing performance, shape optimization, and the use of surrogate models to save computational time. By considering these approaches, researchers can effectively enhance the performance of micromixers and contribute to the field of microfluidics.

1.5.6 Shortcoming in the Literature

The literature review presented in the preceding sections provides an overview of micromixers, including their function, types, implementation in different applications, and various fabrication techniques. While there have been numerous reports on highly efficient active micromixers and complex structured/three-dimensional passive micromixers, there are still some shortcomings that need to be addressed. In particular, there is a need for the design and development of simple structured passive micromixers that offer enhanced efficiency for a wide range of applications.

i. One major challenge with active mixers is their difficulty in scaling up for large-scale production, as well as their high cost. Additionally, the fabrication process for complex-structured mixers is often time-consuming and not suitable for applications involving biological and chemical processing due to the associated large pressure drops. On the other hand, the simpler planar structures described in the literature are easier to manufacture but lack high mixing performance. There is limited literature available on the design and development of simple structured passive micromixers

that can provide comparable mixing quality to the three-dimensional/complex-structured mixers.

ii. The mixing performance of a simple structured passive T-micromixer is efficient within a limited range of Reynolds numbers, specifically in the engulfment regime. Experimental investigations have shown that a similar planar design, the T-T mixer, exhibits better mixing characteristics at higher Reynolds numbers compared to the conventional T-mixer. However, there are limited studies on this efficient planar design, and there is a lack of research analyzing the flow and mixing phenomena of the T-T mixer at various Reynolds numbers.

iii. The inclusion of embedded barriers in the mixing channel of passive micromixers has significantly improved their mixing performance. However, most studies in the literature focus on obstacles placed in single contacting type passive mixers such as T-mixers and Y-mixers. It has been reported that a passive T-T mixer (double contacting type) holds promise as a superior mixing device compared to the conventional T-mixer. Nevertheless, there is a dearth of studies on the effects of obstacles in a double contacting type passive mixer like the T-T mixer. Furthermore, existing studies are mainly limited to lower Reynolds numbers ($Re < 100$), where the mixing mechanism relies more on diffusion and less on convection. It is equally important to investigate the impact of obstacles in micromixers in the convective mixing regime observed at higher Reynolds numbers ($Re > 200$).

iv. Most research on passive micromixers has predominantly concentrated on geometric modifications of the mixing channel to improve the mixing efficiency of conventional designs. However, among the various simple passive mixer designs, only a few studies have explored geometric modifications of the inlet channels, which can influence the flow field and potentially enhance the efficiency of conventional passive micromixers.

1.5.7 Objectives and scope of present research work

The primary focus of the present thesis is to optimize the geometry and characterize the flow and mixing phenomenon in various simple structured passive T-type micromixers, specifically targeting low Reynolds numbers ranging from 1 to 100. Detailed investigations have been conducted on diverse geometric modifications of the conventional T-mixer, which have consistently proven to be highly efficient designs. The dissertation addresses existing limitations in the available literature through the following numerical investigations:

i. This study aims to examine the flow behavior and mixing phenomenon in both Serpentine Square and convergent-divergent passive T-mixers across a range of Reynolds numbers (Re). The investigation analyzes the influence of Reynolds numbers on flow patterns and mixing performance in these specific types of mixers.

ii. The focus of this study is to enhance the mixing performance in planar micromixers by optimizing the geometry of a T-mixer using Bernstein polynomials. The objective is to leverage Bernstein polynomials to improve the mixing capabilities of the T-mixer in planar micromixers.

iii. This study aims to investigate the impact of cylindrical and prismatic obstacles on the mixing phenomenon in a T-T mixer. The objective is to optimize the geometrical parameters of these obstacles to improve the mixing performance at different Reynolds numbers (Re).

iv. The objective of this research is to optimize the geometric parameters of In-Step T-Type micromixers to enhance their mixing performance. Additionally, the study includes an analysis of the pressure drop associated with these optimized micromixers. The primary focus is to improve mixing efficiency while considering the pressure drop characteristics of the micromixers.

1.5.7.1 Organization of thesis

The present dissertation is organized into seven chapters:

1. The first chapter provides a concise introduction to the evolution and significance of miniaturized reaction systems, highlighting the role of micromixers in diverse biomedical, biochemical, and chemical engineering applications. It explores the advantages and disadvantages of different fabrication techniques in terms of cost, accessibility, and mass production. The literature review encompasses a comprehensive range of passive micromixers, discussing their operational principles, strengths, limitations, applications, and relevant studies. Special attention is given to the flow and mixing phenomena in passive T-micromixers, forming the foundation for the current research. Building upon insights from the literature survey, various deficiencies have been identified and highlighted.

2. The second chapter of the thesis introduces the equations that govern the fluid flow and mass transfer in passive micromixers. Additionally, it presents the equation used to evaluate the mixing quality, which is based on the relative variance of concentration. These equations provide a fundamental understanding of the flow and mixing phenomenon in passive micromixers, laying the groundwork for further analysis and investigation.

3. In chapter three, the research delves into the examination and comparison of the flow behavior and mixing phenomenon in two passive micromixer types: Serpentine Square and convergent-divergent T-mixers. The investigation encompasses a range of Reynolds numbers (Re) for the analysis. The main objective is to gain insights into how varying Reynolds numbers impact the flow patterns and mixing performance in these specific micromixers.

4. In chapter four, the focus of this study is to enhance the mixing performance in planar micromixers by employing Bernstein polynomials to optimize the geometry of a T-mixer. The main objective is to leverage the use of Bernstein polynomials to improve the mixing capabilities of the T-mixer in planar micromixers.

5. The fifth chapter of this study aims to investigate the influence of cylindrical and prismatic obstacles on the mixing phenomenon in a T-T mixer. The primary objective is to optimize the geometrical parameters of these obstacles to improve the mixing performance across a range of Reynolds numbers (Re).

6. Chapter six of this research focuses on optimizing the geometric parameters of In-Step T-Type micromixers to enhance their mixing performance. The study also includes an analysis of the pressure drop characteristics of these optimized micromixers. The primary objective is to improve mixing efficiency while considering the impact of pressure drop effects on the micromixers.

7. Chapter seven of the thesis provides a concise summary of the key findings and conclusions derived from the research conducted throughout the thesis. It highlights the significant outcomes of the study and their implications. Furthermore, the chapter discusses the potential future directions and areas of exploration for further advancement in the field based on the current research work. The aim is to identify avenues for future research and to stimulate further progress and innovation in the subject area.

CHAPTER 2

2 GOVERNING EQUATIONS AND NUMERICAL SCHEMES TO EVALUATE MIXING QUALITY

In the present chapter, the equations governing the momentum transfer (Navier-Stokes) and mass transfer (convection-diffusion) in the numerical study of various micromixers described in the upcoming chapters are presented first. Secondly, the mathematical formulation used for the evaluation of mixing performance of various micromixers at different *Re* is presented. Later, the numerical schemes employed in the commercial code ANSYS FLUENT 15.0 and COMSOL Multiphysics which aid to solve the governing equations and obtain the flow and concentration fields in the micromixer are also presented.

2.1 Mathematical Modeling

The fluid flow in the microchannel is considered to be incompressible and Newtonian. The flow field is solved by the governing equations of continuity and Navier-Stokes as shown in Eqs. (1) and (2) respectively,

$$\nabla \cdot V = 0 \tag{1}$$

$$V \cdot \nabla V = -\frac{1}{\rho}\nabla P + v\nabla^2 V \tag{2}$$

where 'V' denotes velocity vector, 'ρ'denotes density, 'P' denotes pressure, and 'v' denotes kinematic viscosity. The governing equation for mixing of samples in the microchannel is given by Eq. (3) as shown below.

$$(V \cdot \nabla)c = D\nabla^2 c \tag{3}$$

where 'c' denotes concentration and 'D' denotes diffusion coefficient.

2.2 Mixing quality evaluation

The relative variance of the concentration of species in a cross-section of the mixing channel can be utilized to determine the amount of mixing that is taking place in the mixing channel. Therefore, the mixing quality 'α' is evaluated by using the Eq. (4) at different cross sections along the length of the mixing channel.

$$\alpha = 1 - \sqrt{\frac{\sigma_M^2}{\sigma_{\max}^2}} \tag{4}$$

Here, $\sigma_{\max}^2$ is the maximum variance of the mixture (0.5) and σ_M^2 is the variance of the mixture in the cross sectional plane, it is calculated as

$$\sigma_M^2 = \frac{1}{n}\sum_{i=1}^{n}(c_i - \bar{c}_M)^2 \tag{5}$$

where, $\bar{c}_M$ is the mean value of concentration taken over *n* elements of the grid for a particular cross section of mixing channel. The value of mixing quality 'α' becomes 'zero' for no mixing and 'unity' for complete mixing.

2.3 Numerical Schemes

The numerical schemes as shown in Table 2.1 have been employed in ANSYS FLUENT 15.0 to solve governing equations pertaining to fluid flow and mixing phenomenon in the micromixer. Second order upwind schemes are selected to solve the momentum and species equations to obtain the solutions at higher order of accuracy. SIMPLEC scheme has been employed for pressure-velocity coupling in order to improve the convergence of solution.

Table 2.1: The solution methods used in the numerical simulation

Pressure-velocity coupling	SIMPLEC
Pressure	Standard
Momentum	Second order Upwind scheme
Species	Second order Upwind scheme

In COMSOL Multiphysics, the fluid flow equations were solved using the Laminar Flow physics interface model, while the mass fraction equations were solved using the Transport of Concentrated Species (tcs) model. To account for mass transport, the Reacting Flow

Multiphysics coupling feature was utilized, allowing the fluid flow to depend on the mixture composition.

For the fluid flow problem, a P2+P1 discretization scheme was employed, while a quadratic discretization scheme was used for the concentration field in the mass fraction equations. This approach allowed for accurate and efficient simulation of the fluid flow and mass transport interactions, considering the influence of mixture composition on the fluid dynamics.

CHAPTER 3

NUMERICAL EVALUATION OF LIQUID MIXING IN A SERPENTINE CONVERGENT-DIVERGENT PASSIVE MICROMIXER

3.1 Introduction

Micromixers play an important role in μTAS (micro-Total Analysis Systems) or lab-on-chips to carry out chemical, biomedical and biomedical analyses. Nowadays, microreactors are widely utilized in the field of chemical processing for organic synthesis, reaction kinetic studies and chemical production. The main advantages of micromixers over macro batch reactors are rapid analysis, portability, low cost, spending fewer amounts of costly reagents and high safety in case of explosive chemical reactions. Some of the important applications of micromixers are protein folding studies, DNA arrays, cell analysis, organic synthesis and chemical assays [91]–[95]. Micromixers can be categorized into two types 1) active and 2) passive micromixers. Active mixers need an external energy source such as electrokinetic, ultrasonic, piezoelectric or magnetohydrodynamic instabilities to induce mixing [96]–[98]. In passive mixers, samples are only pressure driven but they do not require any external energy source to induce mixing. The channels of passive mixer are designed in such a way that the interfacial area between samples is reduced by splitting, recombining, stretching and folding mechanisms to enhance mixing [58], [99], [100]. The passive type micromixers are mostly employed in various applications due to their ease in fabrication, ease of integration into complex micro systems and low cost of manufacturing.

In spite of the advantages of passive mixers over active mixers, the inherent laminar nature of microfluidic flows and the absence of turbulence make mixing very difficult in passive mixers. Many complex designs of passive mixers were proposed earlier to improve the mixing performance of the passive device. Stroock et al. [62] experimentally investigated mixing in a staggered herringbone mixer. The mixer consists of ridges placed on the bottom wall of mixer. These ridges created transverse flow in the channel and thereby significant improvement in mixing is obtained in *Re* range of 0 to 100. Hsiao et al. [101] experimentally and numerically studied mixing in a T-mixer rectangular winglet pairs (RWPs) placed on the bottom wall of the

mixer. They observed that strong vortices are created behind RWPs at high *Re* which lead to better mixing performance. Chen et al. [102] carried out numerical analysis to study the mixing behaviour of stacking type and folding type E-shaped micromixers. It is observed that chaotic advection started in both mixers above a *Re* of 5 and thus mixing has enhanced significantly. They found that the folding type E-shaped mixer performed better than stacking type mixer due to the advection mechanism of continuous rotation along with 3D stretching. Cortes et al. [60] carried out numerical investigations on mixing phenomenon in a 3-D T-Mixer. They found that an earlier onset of vortex formation took place in 3-D T-Mixer with increase in *Re* as compared to planar T-mixer. Studies on 3-D passive mixers [103], [104] have found similar results.

It is observed that the complex designs of passive micromixers [62], [102], [105] and 3-D type passive mixers improve the mixing efficiency at the cost of fabrication challenges and severe pressure drops in the flow during their operation. Studies [44], [106] showed that a simple planar design of serpentine square wave passive mixer performed better mixing with easier fabrication of the device and minimum pressure drops during flow. In the present work to further enhance the mixing of simple passive designs, a serpentine square wave with convergent-divergent type passages in the mixing channel has been studied in the *Re* range of 0 to 100

3.2 Methodology

3.2.1 Numerical Modelling

The geometries of serpentine Square and Convergent-Divergent wave micromixers are created in ANSYS Design Modeler. Figure 3.1 shows the 3D schematic of Square and Convergent-Divergent wave micromixers. The dimensions of the geometries are Pitch, Pi = 400 µm, Width, W = 100 µm and L_c = 3400 µm. The depth of the channel for both mixers is taken as 100 µm. The whole domain of Square and Convergent-Divergent wave micromixers is meshed with hexahedral elements as shown in Fig. 3.2. This type of elements aligns very well with the flow direction and results in improved accuracy. The hexahedral meshing also results in less number of elements as compared to tetrahedral meshing for the same domain. This reduces the computational effort.

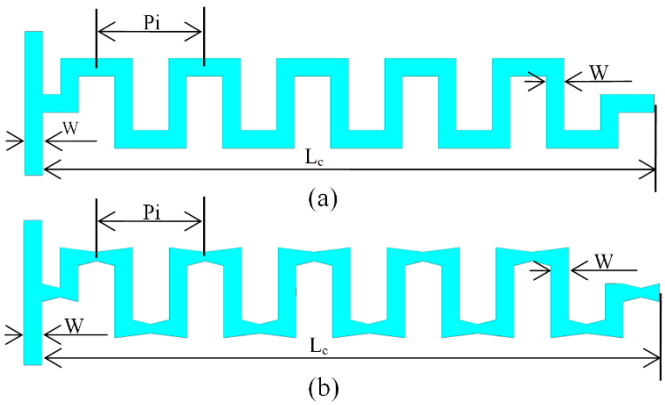

Fig 3.1: Schematics of (a) Square and (b) Convergent-Divergent wave micromixers

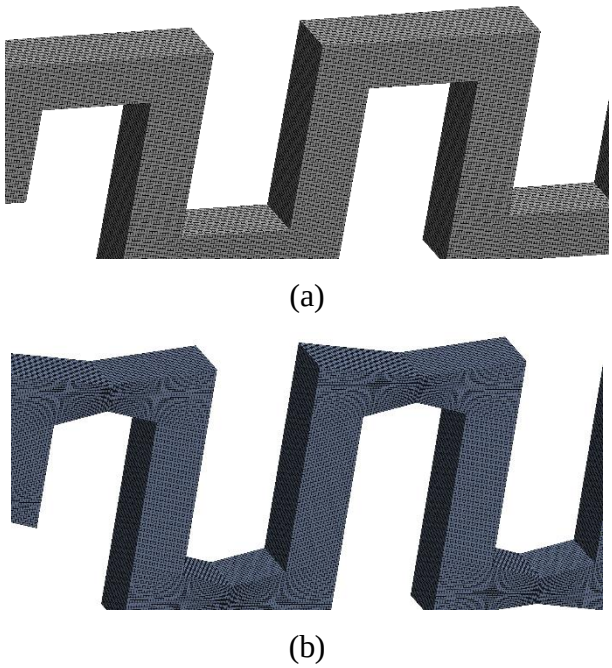

Fig 3.2: Hexahedral mesh of (a) Square and (b) Convergent-Divergent wave micromixers

The commercial numerical tool, ANSYS Fluent, is used to solve the flow and mixing phenomenon in the Square and Convergent-Divergent wave micromixers. Two liquid species '*a*' and '*b*', with same properties of liquid water at 20°C (density ρ = 998.2 kg/m^3, dynamic viscosity μ = 0.001 Pas and diffusion coefficient D = 2 x 10^{-9} m^2/s, were chosen to be mixed in the micromixer for all the simulations. The concentration in terms of the mass fraction for the boundary condition is set to one for species 'a' and set to zero for species 'b' at the left inlet and vice versa at the right inlet. The pressure at the outlet of the mixer is set to atmospheric pressure. The boundary conditions are provide in Table 3.1. Steady laminar flow model along with the species transport model is used to solve the flow mixing problem. The pressure-velocity coupling and the spatial discretization methods used for pressure, momentum, and species

transport equations are tabulated in Table 3.2. The convergence criterion for the residuals is set to 10^{-6} for continuity and 10^{-5} for momentum and species equations.

Table 3.1: Boundary conditions used in numerical simulations

Case	Velocity at left inlet (m/s)	Velocity at right inlet (m/s)	*Reynolds* number
I	0.02	0.02	2
II	0.05	0.05	5
III	0.1	0.1	10
IV	0.2	0.2	20
V	0.3	0.3	30
VI	0.4	0.4	40
VII	0.5	0.5	50
VIII	0.65	0.65	65
IX	0.75	0.75	75
X	1	1	100

Table 3.2: The solution methods of numerical simulation

Pressure-velocity coupling	SIMPLEC
Pressure	Standard
Momentum	Second order Upwind
Species	Second order Upwind

3.2.2 Grid Independence Test

Grid independence test has been carried out to find the required mesh size for the accurate analysis of fluid flow and mass transfer in the serpentine Convergent-Divergent wave micromixer. Figure 3.3 shows the variation of axial velocity at the outlet centreline of serpentine Convergent-Divergent wave mixer at a *Re* of 65. The minimum deviation in the axial velocity is found between 5 and 4 micron size elements. Therefore, the grid with 5 micron size element is selected for the current study.

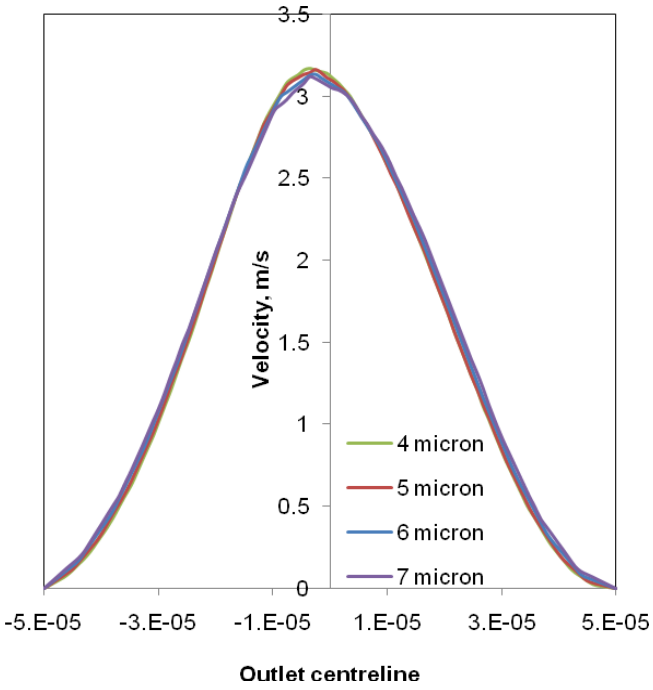

Fig 3.3: Velocity profiles at outlet centreline of Convergent-Divergent wave micromixer for different mesh sizes

3.2.3 Validation

The governing equations of fluid flow and species transport for the T-mixer in the current study have been solved numerically with similar conditions as that of Cortes-Quiroz et al. [60]. These results are compared with the results of Cortes-Quiroz et al. [60] to check the accuracy of the solution obtained from the present study. The mixing quality comparison between T-mixer of present study and Cortes-Quiroz et al. [60] is shown in Fig. 3.4. It is observed that the present results agree well with the existing literature.

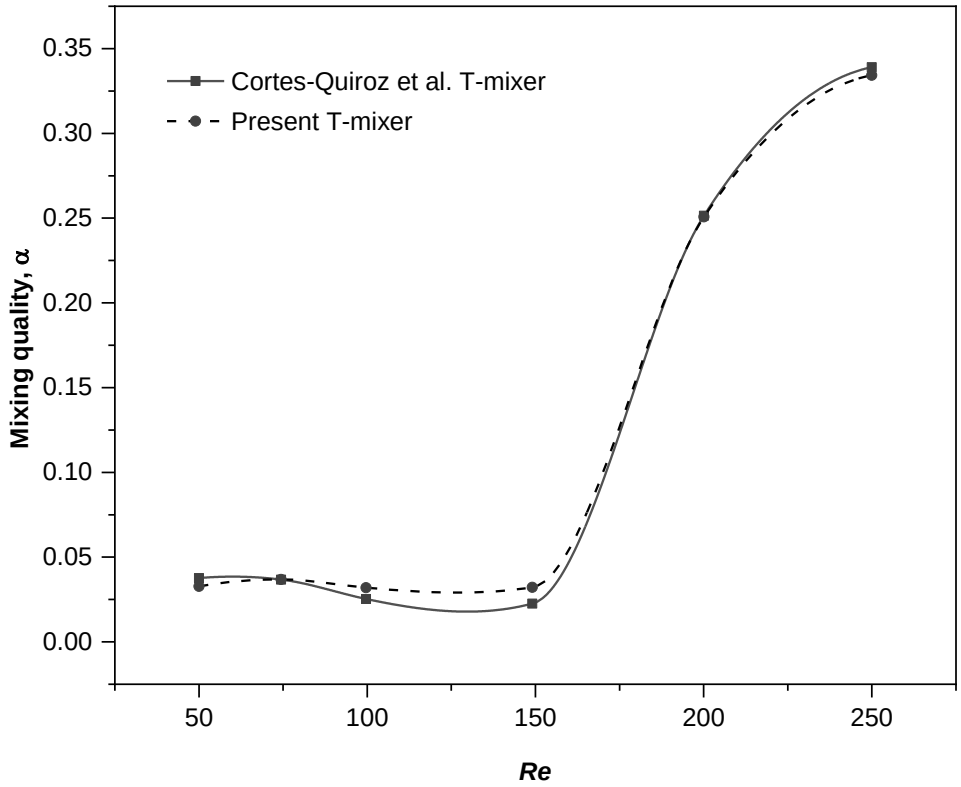

Fig. 3.4 Comparison of mixing index between T-mixer of present study and T-mixer of Cortes-Quiroz et al. [60] at different *Reynolds* numbers

3.3 Results and discussion

3.3.1 Low Re flows

At low *Re* (< 10), the nature of flow in two mixers (Square and Convergent-Divergent wave) is completely in laminar regime (Figs 3.5a and 3.5b) Mixing is governed only by diffusion and proportional to residence time of samples in the mixer. Therefore, mixing is reduced as the *Re* is increased from 0 to 10 (Fig 3.6). The geometries of both mixers could not enhance mixing due to the dominant viscous forces of low *Re* range of 1 to 10 (Figs 3.7a and 3.7b).

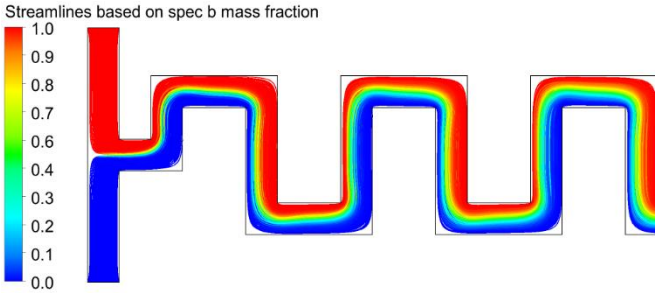

(a)

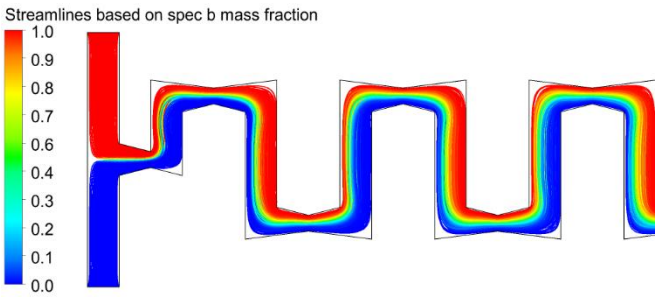

(b)

Fig 3.5: Streamlines at *Re* = 5 (a) Square wave (b) Convergent-Divergent wave micromixers

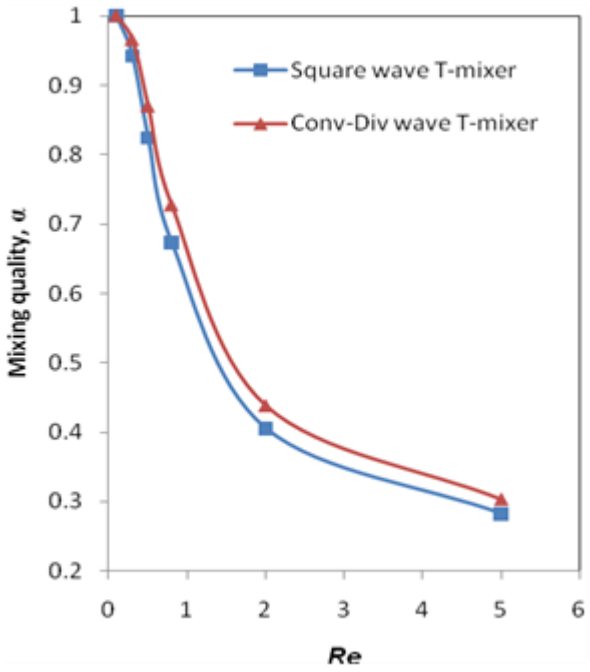

Fig 3.6: Variation of mixing quality with Re of Square and Convergent-Divergent wave micromixers.

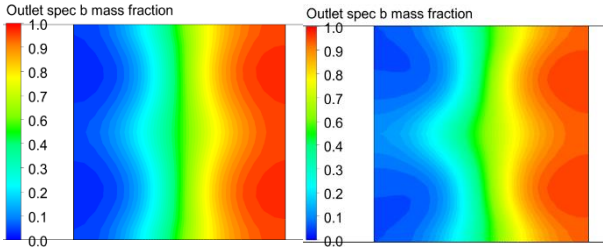

(a) (b)

Fig 3.7: Outlet mass fraction contours at *Re* = 5 (a) Square wave (b) Convergent-Divergent wave micromixers

3.3.2 High Re flows

As the *Re* is increased (> 10), it is observed that the process of stretching and folding have initiated in the mixing channel of both mixers (Figs 3.8a and 3.8b). However it can be observed that the degree of stretching and folding is higher for Convergent-Divergent wave mixer along with recirculating secondary at bends (Fig 3.8b) as compared to Square wave mixer (Fig 3.8a). The intermediate convergent-divergent passages in the horizontal sections of mixing channel have created a greater scope for the stretching and folding of samples along with recirculation at bends. Therefore the mixing is enhanced at high *Re* flows of 10 to 100 (Fig 3.9) with Convergent-Divergent wave mixer (Fig 3.10b) as compared to Square wave mixer (Fig 3.10a).

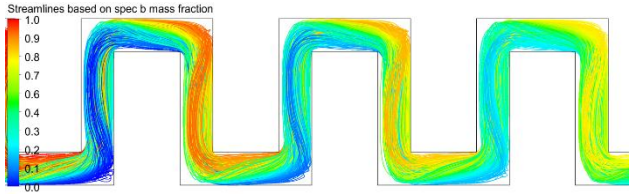

(a)

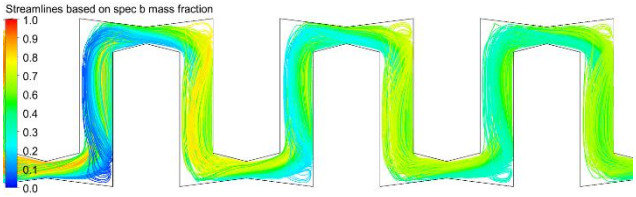

(b)

Fig 3.8: Streamlines at *Re* = 30 (a) Square wave (b) Convergent-Divergent wave micromixers

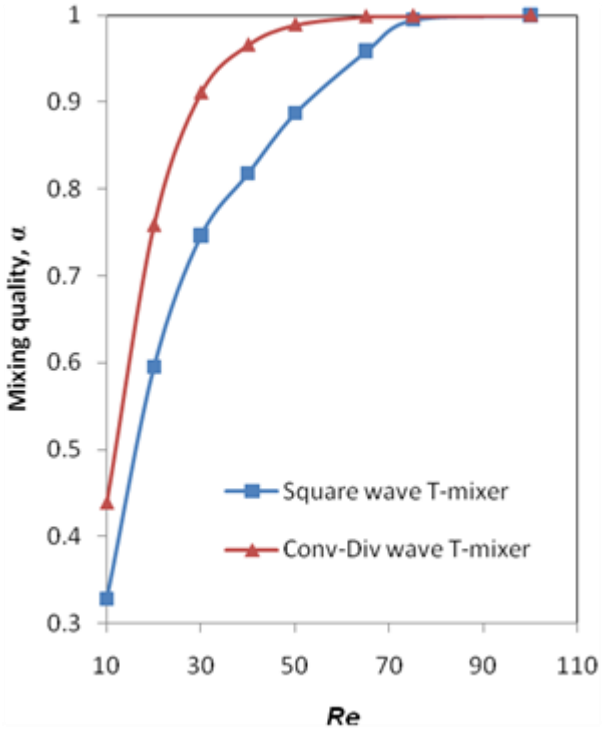

Fig: 3.9 Variation of mixing quality with Re of Square and Convergent-Divergent wave micromixers.

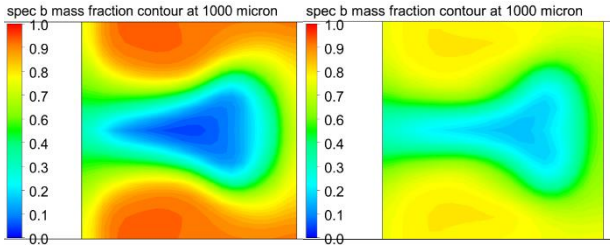

(a) (b)

Fig 3.10: Outlet mass fraction contours (*Re* = 30) at 1000 micron (a) Square wave (b) Convergent-Divergent wave micromixers

3.4 Conclusions

To improve the mixing efficiency of planar type passive micromixer, the mixing phenomenon in a serpentine mixer with Convergent-Divergent passages in the horizontal sections of mixing channel has been investigated in the *Re* range of 0 to 100. It is observed that at low *Re* (0 to 10), the flow is completely laminar and the mixing relied purely on diffusion in both Square

wave and Convergent-Divergent mixers. Therefore, as *Re* is increased from 0 to 10, mixing continuously decreased in both mixers due to reduction in the residence time. The action of stretching and folding is initiated in both types of mixers when the *Re* is increased (> 10), and therefore mixing continuously increased. However, it is found that the degree of stretching and folding is intense in the Convergent-Divergent wave mixer as compared to Square wave mixer. Also, the flow in the Convergent-Divergent wave mixer is associated with recirculation zones in the bends which enhanced the mixing efficiency considerably. Therefore, it is concluded that it is more beneficial to employ convergent-divergent passages in serpentine type mixers which can further enhance its mixing capability.

CHAPTER 4

4 MIXING ENHANCEMENT OF PASSIVE TYPE T–MIXER THROUGH SHAPE OPTIMIZATION

4.1 Introduction

Micromixers are an important component in microfluidic devices and microfluidic systems. They have significant applications in biomedical and chemical analysis [91], [92], [94], [95], [107]. Mixing has prime importance in microfluidics. At the same time, mixing is very challenging in micro channels. At macroscale we exploit the velocity of the fluid so that the flow can easily turn into turbulent mode by increasing the flow velocity so that turbulence in the flow helps in mixing of the fluids at macroscale. At microscale however the turbulence effects are not present, and flows are inherently laminar because of the small length scale of the system. Micromixers can be primarily classified into two types. 1) Passive micromixers and 2) Active micromixers. Active micromixers require external force to induce mixing such as electrodynamic, magneto hydrodynamic, acoustic, and ultrasonic [96]–[98]. The pressure driven passive micromixers require no external force to induce mixing. In passive micromixers, diffusion and chaotic advection are dominant physical phenomenon. Passive micromixers can increase mixing by stretching, folding, splitting and recombining mechanisms [58], [99], [100]. Different passive micromixers are designed by considering the mechanisms mentioned above to enhance mixing efficiency.

Due to ease of design and fabrication, many passive micromixers have been developed to improve mixing efficiency. Chen et al. [102] carried out a numerical study to investigate the mixing behavior of stacking and folding type E-shaped micromixers. It was found that mixing enhanced significantly due to chaotic advection. Above *Re* of 5, chaotic advection played a major role in improving the mixing in stacking and folding type E-shaped micromixers. Strook et al. [62] carried out an experimental study to investigate mixing performance in a staggered

herringbone mixer. Ridges were placed on the bottom wall of the mixer. A transverse flow was created in the channel due to the ridges. Moreover, transverse flow helped in improving the mixing of the channel. Hsiao et al. [101] carried out both experimental and numerical study in a T-mixer with rectangular winglet pairs (RWPs) placed on the bottom wall of the mixer. At higher *Re*, strong vortices were created behind RWPs and thus, mixing efficiency improved significantly. J. M. Ottino et al. [108] studied chaotic mixing in microchannels. It was observed an increase in interfacial contact area by creating repeated stretching and folding of fluids in a microchannel. Ekta et al. [109] carried out a numerical study to investigate the mixing characteristics and pressure drop of a spiral micromixer by varying width and depth of the micromixers. They found that for $Re>50$, the mixing efficiency doesn't improve significantly. Dundi et al. [110] developed passive type T-T mixer with cylindrical elements. And they numerically proved that the developed mixer showed significant improvement in micro mixing compared to basic T-mixer. Muhammad et al. [111] developed non-aligned input M-type micromixers with different shaped obstacles. They found that the proposed four novel micromixers showed improved mixing performance. Masoud et al. [112] studied the confluence angle, flow rate and flow rate ratio effect on passive mixing. The effectiveness increased with increase in flow rate ratio and decrease in angle. Mranal et al. [113] studied the effect of heterogeneous charge patterns at the microchannel bottom on electro kinetic mixing performance. They identified optimal heterogeneous charge pattern by formulating a binary numerical optimization problem. Furthermore, other studies were able to create chaotic mixing by different geometry modifications in microchannel shapes such as serpentine channels, zig-zag channels, and curved microchannels [114]–[116]. Jain et al. [117] used a shape optimization technique to optimize groove shape in a microchannel. In this study, the groove shape has been represented parametrically using Bezier curves. The control points of the Bezier curve were chosen as optimization parameters to identify the optimal groove shape which maximizes mixing for a given set of operating conditions.

It was observed that different passive micromixers provide improved mixing efficiency [62], [101], [102]. Other studies [46], [118] showed that simple planar designs like square, wave, and serpentine micromixers which showed better mixing were easy to manufacture and had minimum pressure drops during the flow. All micromixers mentioned previously were developed by trial-and-error method. And there was a need to develop a systematic approach to address this problem. This was achieved by employing the features of Bernstein

polynomials. Sergei Natanovich Bernstein (1880–1968) proposed the Bernstein basis in order to offer a useful demonstration of Weierstras' theorem. Due to Bernstein polynomials' sluggish convergence as function approximants, they were not commonly used until the development of digital computers. The Bernstein polynomials were eventually used widely once it was discovered that the coefficients of these polynomials could be easily changed to alter the shape of the curves they described. In the 1960s, two French car engineers, Paul de Casteljau and Pierre Etienne Bezier, were interested in putting this idea into action. Clay model sculpting turned out to be a time-consuming and expensive procedure for creating intricate designs for car bodies. De Casteljau and Bezier set out to create mathematical tools that would enable designers to make and modify complex objects naturally. Bernstein polynomials, also called Bezier curves, brought Bezier's name to people's attention. This is because de Casteljau published most of his research when at work. Bernstein polynomials are based on current research and modern technologies, and they have a number of useful properties that can be used in many fields. Inspired by the successful application of the Bernstein polynomial based optimization approach for numerous aerodynamic applications, this approach has been employed for the outer wall profile of the T- mixer also [119]. In this approach, the shape variation is governed by equation (8) such that the need for grid generation at every iteration is eliminated. On the flipside, a minor drawback of restriction of the available shape owing to the choice of deformation vectors exists. However, this could be solved by varying the order of parameterization as well as control points' displacement. The present article attempts to perform optimization by choosing the former method.

In the present work, the basic T-mixer and the effect of channel shape on the mixing efficiency of the T-mixer were studied. Shape optimization technique to enhance mixing efficiency by altering the shape of T–mixer channel was used. The optimized T-mixer showed significant improvement in mixing compared with basic T-mixer. Numerical analysis was conducted in 2D to reduce computational time and the complexity of setting up the shape optimization problem. At low *Re* (*Re*<30), the extent of mixing evaluated using 3D and 2D models was nearly same. This was due to the absence of secondary flows and flow vortices at low *Re* [120].

4.2 Methodology

The 2D planar type T-micromixer geometry was created using COMSOL Multiphysics 5.5 software, shown in figure 4.1a. The length of the microchannel (L_c) is 3000 µm, width (W_c) is 200 µm, height (h_c) is 800 µm and inlet channel width (W_i) is 100 µm.

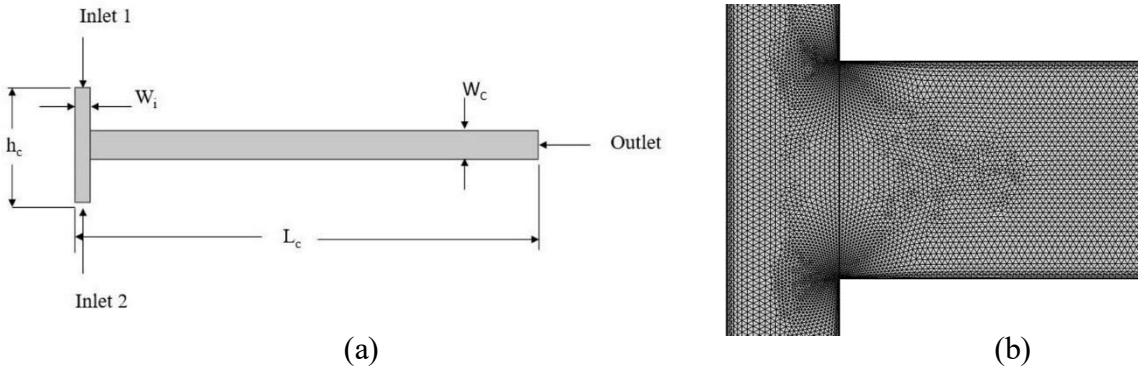

Fig. 4.1 Schematic diagram of the T-micromixer and its mesh (a) Schematic diagram of the computational domain and (b) free triangular mesh of T-micromixer.

In this problem, two liquid species A and B were chosen for mixing in planar type T-micromixer channel. Both species had the same properties as liquid water at 20^0C, mentioned in Table 4.1. Concentration gradient was created by providing the boundary conditions at the inlet, so that mass fraction was set to unity for species ‘A’ and zero for species 'B' at inlet one and vice versa at inlet two. Normal inflow velocity boundary condition (Re = 2 to 30) was given at inlet one and inlet two along with mass fraction boundary conditions. At the outlet, the pressure boundary condition was provided. It was set to atmospheric pressure. Except for inlet and outlet, all other boundaries were applied with no-slip boundary conditions.

Table 4.1: Properties of the species materials

Properties	**Species A & Species B**
Type of material	Liquid Water
Density, ρ [Kg/m^3]	998.2
Dynamic Viscosity, μ [Pa. s]	0.001
Diffusion coefficient, D [m^2/s]	2×10^{-9}

Fluid flow equations were solved using Laminar flow physics interface model, while mass fraction equations were solved using the Transport of concentrated species (tcs) model. Reacting flow Multiphysics coupling feature was used to simulate mass transport where the fluid flow depends on mixture composition. For solving the fluid flow problem, P2+P1 discretization scheme was used, and for concentration field, a quadratic discretization scheme was used.

A free triangular mesh was used for the whole computational domain, as shown in figure 1b. Because this mesh is like a 'workhorse' for 2D Computational fluid dynamics problems, it was easy to create this kind of mesh with high element quality[121]. However, this ease comes with a cost. This free-unstructured triangular mesh gives greater numerical diffusion. The triangular meshes must be extra fine to overcome the difficulty. In this study, extremely fine mesh was used with a maximum element size of 5.36 μm, and the number of elements was 63864. The details of mesh independence are mentioned in the following section. The different meshes that were considered for the mesh independence test are given in Table 2.

4.2.1 Grid independence study

To determine the optimum mesh size for planar type T-mixer analysis, a grid independence study was performed. This study considers axial velocity and mixing quality distribution at the outlet of planar type T-mixer for *Re*=5. Figure 4.2a depicts the axial velocity distribution at the outlet while figure 4.2b depicts the mixing quality distribution at the outlet. Between meshes 6 and 7, the axial velocity has the smallest variation. In addition to axial velocity, the mixing quality difference between mesh 6 and mesh 7 is also minimal. Hence, mesh 6 was considered for the current study.

Table 4.2: Grid independence test parameters

Meshes	**Maximum element size**	**Minimum element size**	**Maximum element growth rate**	**Number of elements**	**Mixing quality, α**
Mesh 1	176	5.6	1.4	18704	0.2497
Mesh 2	69.6	3.2	1.25	23966	0.1826
Mesh 3	36	1.6	1.15	30208	0.1726
Mesh 4	22.4	0.32	1.1	37052	0.1684
Mesh 5	10.4	0.12	1.08	41974	0.1674
Mesh 6	5.36	0.016	1.05	63864	0.1669
Mesh 7	5.00	0.016	1.05	73280	0.1668

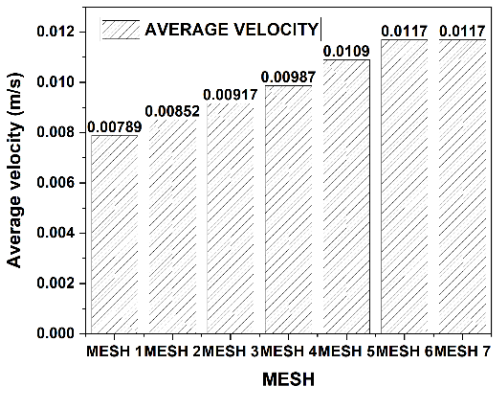

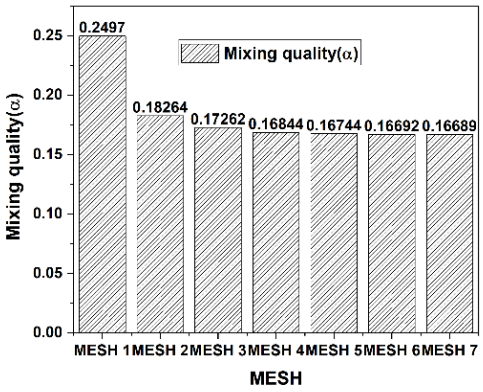

(a) (b)

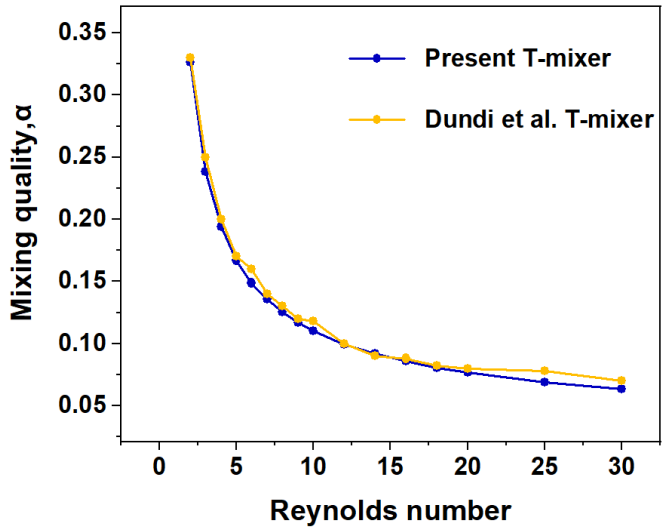

(c)

Fig. 4.2 Grid independence study and validation (a) Average axial velocity profiles at outlet of T – micromixer for different meshes, (b) Mixing quality at outlet of T–micromixer for different meshes and (c) Comparison of Mixing quality with various Reynolds number for T-mixer of the present study and Dundi et al. [110].

4.2.2 Validation

The governing equations of the flow field and species transport of the T-mixer have been solved in this study using conditions comparable to those used by Dundi et al. [110]. To validate the accuracy of the current numerical scheme, the results obtained were compared to the results of Dundi et al. [110]. Equations (4, 5) were used to assess mixing quality at the T-mixer outlet. Figure 4.2c shows that the current study's findings are in close accord with those of Dundi et al. [110].

4.2.3 Optimization approach

The effect of the outer wall's shape of the T-micromixer on the mixing performance was examined. Bernstein polynomial was used to deform the geometry. After deformation, mixing

quality was evaluated for different Reynolds numbers from 2 to 30. The following equations represent the Bernstein polynomial of n^{th} degree with n+1 control point.

$$P(t) = \sum_{i=0}^{n} B_i J_{n,i}(t) \qquad 0 \le t \le 1 \qquad (6)$$

In the above equation, B_i represents the control points of the Bezier curve, and $J_{n,i}(t)$ is the Bernstein basis polynomial mathematically defined as follows:

$$J_{n,i}(t) = \frac{n!}{i!(n-i)!} t^i (1-t)^{n-i} \qquad (7)$$

In this study, the COMSOL Multiphysics 5.5 optimization module's features were used to deform the geometry. The two external walls of T-micromixer were represented by n^{th} order Bernstein polynomial, which is available through the polynomial boundary feature. Inspired by the successful application of the Bernstein polynomial based optimization approach for numerous aerodynamic applications, the approach was employed for the outer wall profile of the T- mixer also [119]. In this approach, the shape variation is governed by equation (8) such that the need for grid generation at every iteration is eliminated. This representation helps in deforming the geometry. It controls the deformation of interior nodes by a smoothing equation, while the deformation of walls is given by:

$$d = \sum_{i}^{n} B_i^n(s) c, \qquad -d_{max} \le c_i \le d_{max,} \qquad (8)$$

B_i represents the control points of Bezier curve. The initial value of B_i could be anything depending on the COMSOL parameter(s), which ranges from $0 \le s \le 1$. For example, in a linear curve, when S = 0.25, $B_i(S)$ is one quarter of the way from starting point to ending point. "d_{max}" Represents the maximum displacement of Bernstein polynomial of n^{th} order.

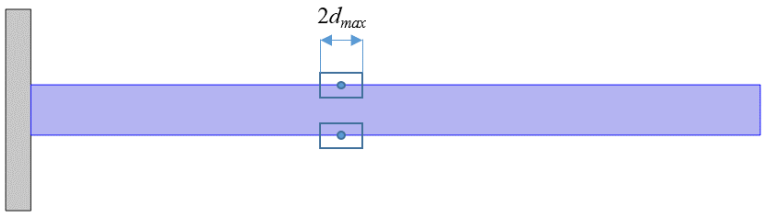

Fig. 4.3 Geometry bounding box realization on the microchannel.

On the flipside, a minor drawback of restriction of the available shape owing to the choice of deformation vectors exists while using Bernstein polynomials. However, this could be overcome by varying the order of parameterization (n) and/or control points' displacement (d_{max}). The present study attempts to perform optimization by choosing the former method.

Maximum displacement was limited to 5% of the total length of the curve which was to be altered. In this problem, upper and lower walls of micro channel were considered to alter the channel shape. Both walls were of equal length of 2900µm and the maximum displacement of each wall was 145µm, which was 5% of total length of inlet/outlet boundary. The geometry bounding box is a square box with a side length of $2d_{max}$. It is to be noted that the mass of the species held in T-mixer at any point of time is not constrained and it varies with wall profile. Initially, the polynomial order was fixed to second-order. Bernstein polynomials satisfy the bounds of coefficients across the whole line. It means that each point on the line is confined to move in a square box. The higher-order and higher maximum displacement lead to clashing of boundaries and reduce the tendency for inverted elements. So, it is necessary to find a balance between them for convergence of the solution. The optimization technique uses adjoint sensitivity method [122], [123] to perform sensitivity analysis. Initially, shape optimization was performed at Reynolds number (Re = 5). Here the flow rate was fixed, and the maximization of mixing quality (α) was considered an objective function to perform shape optimization.

The COMSOL numerical solver initially solves the fluid flow and species conservation equations for the rectangular domain and transfers the data to the optimization module. In the optimization module, the objective function i.e., mixing quality for different data points in control space is searched. If the stopping criteria is reached i.e., optimum value is obtained, the corresponding outer wall profile is given as the output and the search procedure is terminated. However, if the optimum profile is not found in the initial run I_0, further iterations are performed in the optimization module to search for the optimum geometric configuration which exhibits maximum mixing quality. The flowchart depicted in figure 4.4 shows the implementation of the optimization algorithm in the COMSOL based module.

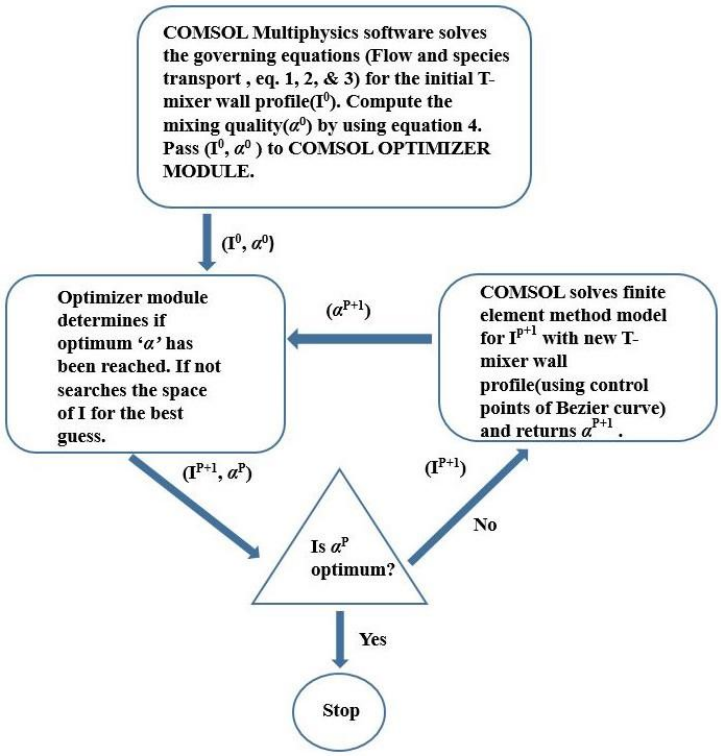

Fig. 4.4 Flowchart showing steps for optimization problem implementation in COMSOL Multiphysics.

4.3 Results and Discussion

The profile of the walls of the T- micromixer was modified using the adjoint based shape optimization technique. Figure 4.5a shows the geometric model of T-mixer with the walls being highlighted. Initially, the length of both walls was 2900 µm each. Numerical simulations were carried out by varying the inlet velocity such that the Reynolds number varied from 2 to 30. As the Reynolds numbers pertain to laminar flow regime throughout the channel as shown in

figure 5b, the mixing was observed to be diffusion dominant. Therefore, the residence times played a pivotal role in effective mixing of the constituent species. The effect of Reynolds number on the mixing quality depicted in figure 4.2c reinforces the dependence of mixing quality on residence time. The increase in Reynolds number represents an increase in inlet velocity. As the inlet velocity increases, the residence time available for the constituent species inside the mixer decreases. This adversely affects diffusion and thus results in ineffective mixing.

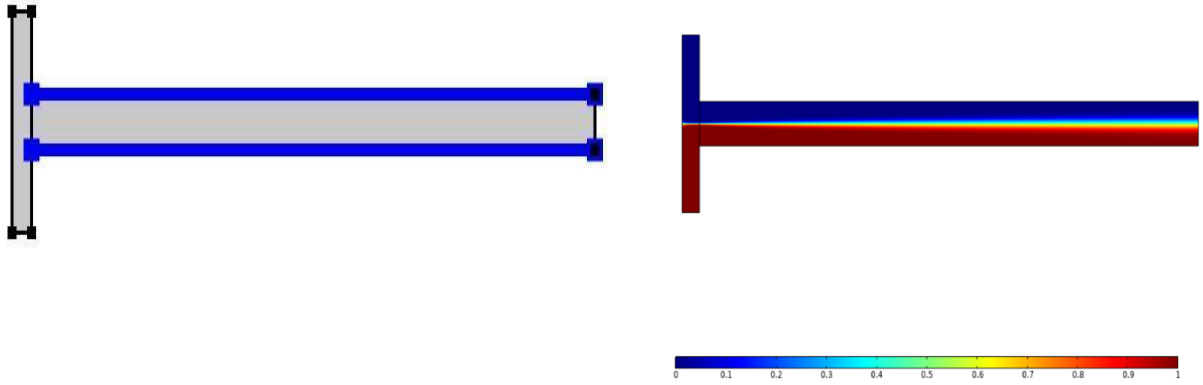

(a) (b)

Fig. 4.5 Streamlines and polynomial boundary representation (a) Polynomial boundary representation of boundary walls of T-micromixer, and (b) Streamlines based on Spec B Mass fraction at $Re = 5$.

4.3.1 Optimized T-micromixer

The optimized order of the Bernstein polynomial for improved mixing significantly depends on the geometric bounding box size and its geometry. The side of the square bounding box selected in the present study was 5 % of the total length of the straight channel T-micromixer (2900 microns) i.e. 145 microns. Considering the intersection of the walls at higher orders, the order of the polynomial was limited to “12” in this study. Figure 4.6 shows different T-micromixer configurations obtained by varying the order of the polynomial. Each wall profile results in different mixing quality as well as pressure drop.

Table 4.3 shows the effect of the order of the polynomial on the mixing quality as well as pressure drop at $Re = 5$. It is observed that with increasing order of the polynomial, the mixing quality monotonously increases accompanied by an increase in pressure drop. The channel profile following the 12^{th} order Bernstein polynomial was observed to exhibit the highest mixing quality. It is observed from the table that a significant increase in the mixing quality i.e. 139.9 % was also accompanied by an increase in pressure drop. However, the relative increase in the mixing quality as well as the pressure drop with increasing polynomial order decreased at higher orders of the polynomial i.e. (n = 4 to 12). It is to be noted that the aforementioned maximum mixing quality in case of 12^{th} order polynomial was obtained by only a 1 % increase in the length of curved boundary i.e. 2932.4 µm. A similar kind of optimization procedure was also performed at higher Reynolds numbers. However, the optimized wall profile obtained by performing the aforementioned optimization procedure does not depend on the Reynolds number of the flow.

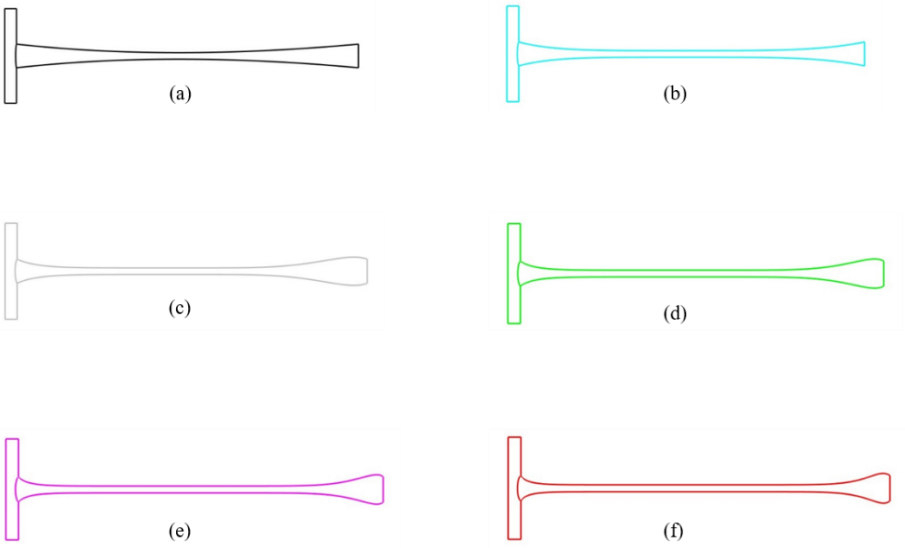

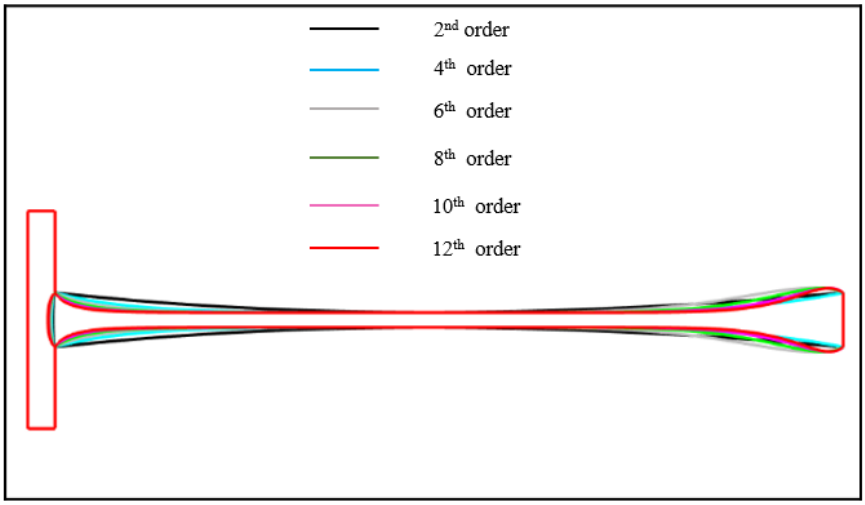

(g)

Fig. 4.6 Optimized shapes for different polynomial order (a) 2nd, (b) 4th, (c) 6th, (d) 8th, (e) 10th, (f) 12th orders, (g) Overlapping images of all orders.

Table 4.3 Mixing quality and Pressure drop variation for different polynomial order at *Re = 5*

Polynomial order	**Mixing quality, α**	**Pressure drop, (Pa)**
Linear	0.16692	18.113
2nd	0.29598	195.63
4th	0.34675	324.92
6th	0.35914	320.4
8th	0.38013	366.32
10th	0.39265	397.65
12th	0.4005	419.82

Figure 4.7 shows the effect of Reynolds number on the mixing quality and pressure drop at various Reynolds number for the optimized 12th order T – micromixer. From figure 4.7a it is

observed that the mixing quality decreases with an increase in *Re*. It is understood that with an increase in *Re*, the sample's residence time is reduced which resulted in reduced mixing quality as discussed earlier. On the contrary, it is observed that with an increase in *Re*, the inlet pressure requirement increases monotonously as expected. It is also observed that the major portion of the pressure loss across the channel occurs in the throat region owing to the gradually reduced cross section. This indicates that the minimum throat area and the channel profile significantly impact pressure losses across the channel.

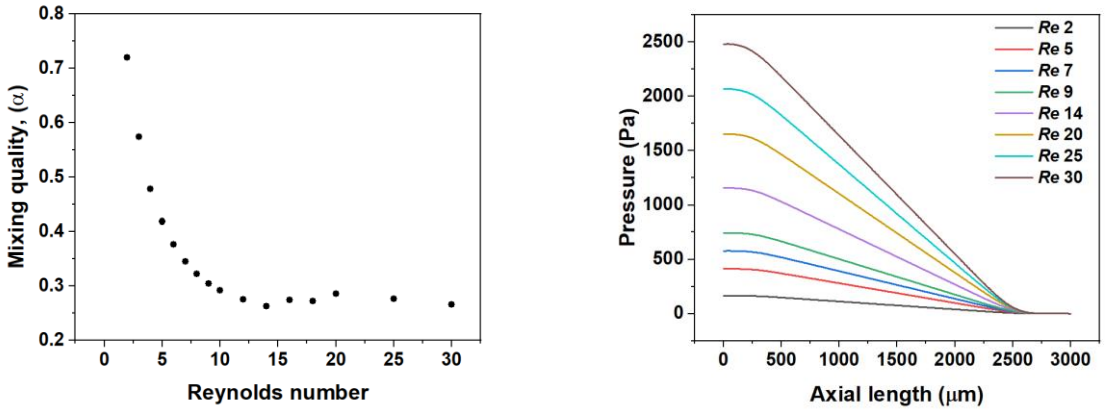

(a) (b)

Fig. 4.7 Variation of Mixing quality and pressure with *Re* of Optimized T-mixer (a) Variation of Mixing quality with *Re* of Optimized T-mixer and (b) Pressure variation of optimized T-micromixer along the axial length of the channel for different *Re*.

4.3.2 Comparison between Basic T-micromixer, Optimized T-micromixer, and Basic T-mixer with width equals to the throat width of the optimized channel

In this section, the mixing performance of the optimized T-mixer was compared with the basic T-mixer and thin T-mixer. The thin T-mixer refers to the configuration where the thickness of the straight channel is equal to throat thickness of the optimized channel. The geometric model of the aforementioned thin T-mixer is shown in figure.4. 8a. It is observed that the mixing quality monotonously decreases with *Re* for all geometries. However, the rate at which the mixing quality decreases significantly depends on the profile of the mixer walls. Though all the mixer configurations exhibit similar mixing performance at very low *Re*, the effects are amplified with increasing *Re*. The optimized T-mixer exhibits maximum mixing quality followed by thin T-mixer and the basic T-mixer.

From figure 4.8b and Table 4.4, an improvement of 100% to 300% in the mixing quality of optimized T-mixer is observed compared to basic T-mixer. There is an increase in mixing quality with decreasing channel thickness. At same values of *Re* at the inlet i.e. same flow rates of the species, the decrease in the channel gap results in a decrease in the transverse distance between the fluid streams, thereby reducing diffusion length. This reduction in diffusion length at smaller channel gaps significantly improves rate of diffusion. However, the improvement of the optimized T-mixer over the thin T-mixer is due to increased residence times owing to the diverging section at the outlet. The residence time is calculated for both mixers at $Re = 10$. A streamline along the center-line of the channel is considered and the time taken for a particle to traverse this length is numerically calculated by considering the velocities on the discrete nodes of the aforementioned streamline. The residence time calculated for optimized T-mixer is 0.136 sec and for thin T-mixer, it is 0.039 sec. The residence time of the Optimized T-mixer is nearly 2.5 times that of the thin T-mixer.

Table 4.4 Mixing quality of Basic T-mixer and Optimized T-mixer

Reynolds number, (*Re*)	**Mixing quality of Basic T-mixer**	**Mixing quality of Optimized T-mixer**	**Increase percentage (%) of mixing quality**
2	0.326	0.72	120
4	0.193	0.477	147.15
6	0.148	0.375	153.37
8	0.125	0.321	156.8
12	0.099	0.275	177.77
16	0.085	0.273	221.17
20	0.076	0.285	275
25	0.068	0.276	305.88
30	0.063	0.265	320.63

Figure 4.8c shows the pressure drop variation for different configurations of the T-mixer vis-à-vis Reynolds number. The pressure drop across a T-mixer is calculated by evaluating the average pressures at the inlet and outlet and their corresponding difference. It is observed that though the pressure drop across the channel monotonously increases with *Re*, the rate of increase depends on the mixer configuration. The thin and optimized T-mixers exhibit significantly higher-pressure drop compared to the basic T-mixer. It is due to deformed boundaries of the T-mixer. Figure 4.8d shows a comparison of the longitudinal pressure distribution of the basic T-mixer, Optimized T-mixer, and thin T-mixer at $Re = 5$. Basic T-mixer has very low pressure drop when compared to Optimized T-mixer and thin T-mixer. The pressure drop of an Optimized T-mixer is roughly identical to that of T-mixer with a width equal to Optimized channel throat width. The difference in inlet pressure requirement between thin T-mixer and Optimized T-mixer is relatively insignificant. The longitudinal distribution of pressure along the centerline, however, depends on the channel profile. It is observed that in locations upstream, pressure in the Optimized T-mixer is slightly higher than its value in thin T-mixer. On the contrary, in location downstream, the thin T-mixer has higher pressure compared to Optimized T-mixer. This is due to the converging and diverging profiles at the inlet and outlet. Due to the converging and diverging sections, the pressure gradient is relatively low at the inlet and outlet, as shown in the figure. These effects result in nearly the same values of pressure drops.

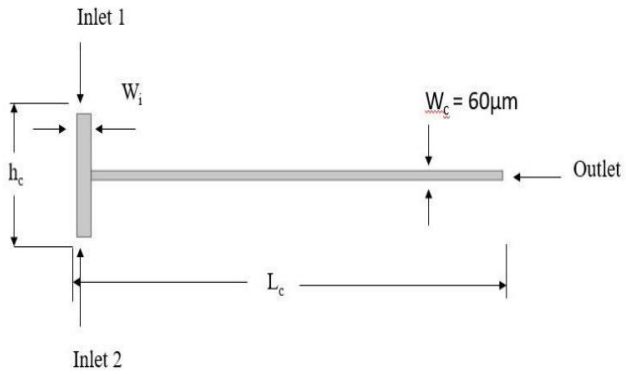

(a) The schematic of T-mixer with width equals to the throat width of the Optimized channel

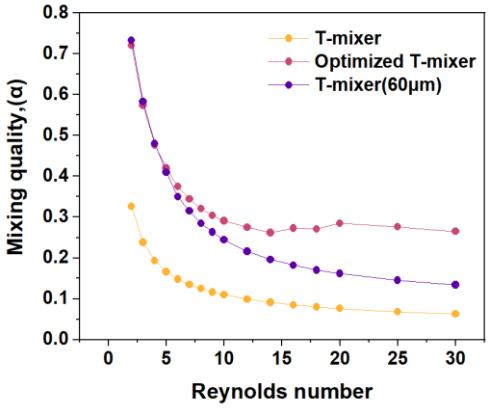

(b) The mixing quality variation with *Re* of T-mixer, Optimized T-mixer, and T-mixer with width equals to the throat width (60µm) of the optimized channel at different *Re*

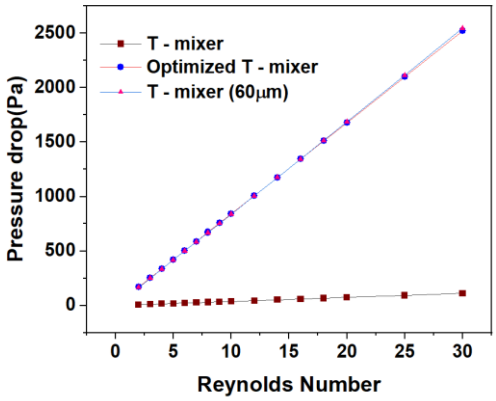

(c) Pressure drop variation with *Re* of T – mixer, Optimized T – mixer, and T – mixer with width equals to the throat width (60μm) of the Optimized channel

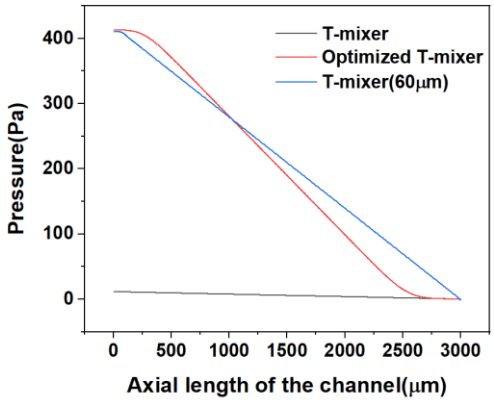

(d) Pressure variation of T-mixer, Optimized T-mixer, and T-mixer with width equals to the throat width (60μm) of the Optimized channel along the axial length of the channel at *Re = 5*

Fig. 4.8 Schematic of T-mixer(60μm), the mixing quality and Pressure drop variation with *Re* of T – mixer, Optimized T – mixer, and T – mixer with width equals to the throat width (60μm) of the Optimized channel.

4.4 Summary and conclusions

An adjoint based shape optimization scheme was employed and the channel walls were modified to form Bernstein polynomial profiles. The shape optimization scheme was run by varying the order of Bernstein polynomial and Reynolds number. An upper limit on the maximum order of the polynomial was imposed as "12" in order to prevent the intersection of the channel walls. The optimized shape of T-mixer wall is independent of Reynolds number at which the algorithm is run. The mixing quality monotonously decreases with *Re* owing to reduced residence times. Also, the mixing quality monotonously increases with increasing order of the Bernstein polynomial. This is attributed to reduced throat thickness. The pressure drop across the T-mixer increases with an increasing order of Bernstein polynomial owing to reduced throat thickness. A thin T-mixer with the channel width equal to the throat width of the optimized T –mixer was also designed and the performance was evaluated. The mixing quality

in case of the thin T-mixer was lower than the optimized T-mixer. This is attributed to the converging-diverging profile in case of the latter. However, the effect of the wall profile on the pressure drop is relatively insignificant.

Therefore, it may be concluded that the developed shape optimization procedure is beneficial in providing a geometric configuration of the T-mixer with enhanced mixing performance without losing the advantage of ease of fabrication. Various studies could be performed by dividing the upper and lower walls into discrete line segments. It is to be noted that as the shape of the mixer changes, there will be a change in the amount of mass that the mixer can hold. There might be a possibility of change in the optimization result also. Therefore, future studies could be performed by using the mass held in the mixer also as one of geometrical constraint while designing the shape of T mixer. However, the application of this adjoint-based shape optimization procedure is limited. If the solution space contains multiple minima or maxima, it may fail to find a global minima or maxima. Hence, it is difficult to apply for non-differential loss functions and non-convex problems.

CHAPTER 5

5 OPTIMIZATION STUDY OF OBSTACLES IN T-T MIXING CHANNEL AT LOW *REYNOLDS* NUMBERS

5.1 Introduction

Microfluidic systems, specifically micro-mixers, have become essential tools in various biochemical and chemical studies, particularly in micro-Total Analysis Systems (TAS) or lab-on-chips [124]. Micro-mixers offer several advantages over traditional macro batch reactors, including higher mass transfer efficiency due to their large surface-to-volume ratio, compact

design, portability, reduced reagent usage, and faster analysis times. They are also less expensive and directly compatible with lab-on-chip platforms.

There are two types of micro-mixers: passive and active. Passive micro-mixers do not require external energy sources and can achieve mixing in the channels through pressure-driven flow. These devices are designed with channels that increase the surface area between fluid samples while decreasing the diffusion path, allowing for efficient mixing [125]. Passive micro-mixers are widely used due to their durability, operational stability, and ease of integration into more complex systems.

On the other hand, active micro-mixers rely on external energy sources, such as electrokinetic, ultrasonic vibrations, or magneto-hydrodynamic forces, to induce mixing through perturbations in the fluid flow [126]. Active micro-mixers offer more precise control over mixing parameters but may require additional equipment and energy sources for operation.

Micro-mixers are crucial in various applications, including the separation and detection of cells, chemical tests for analyte quantification, and studies of protein folding for understanding disease pathogenesis [127]. The high mass transfer efficiency and small-scale design of micro-mixers make them ideal for these applications, enabling rapid and efficient mixing of small volumes of fluids for precise chemical and biological analyses.

Extensive research has been conducted on micromixers, specifically T-micro-mixers, by various researchers, focusing on laminar flow regimes [128]–[130]. Studies have applied various techniques, such as imaging techniques using contrasting agents, and focusing techniques to reduce lamellae width and speed up mixing [130]. Other researchers have investigated the use of vorticity to improve mixing quality, even at low Reynolds numbers [72]. Feasibility studies have been conducted on micro T-mixers as rapid mixing micromixers, and the fast mixing is explained by the asymmetrical flow conditions at the inlets and the generation of vortices and secondary flow at the junction [73]. The impacts of various parameters on mixing performance, such as throttle size, mixing channel angle, flow rates, and aspect ratio, have also been investigated [131]. Experimental techniques, such as micro-scale Laser-induced fluorescence and Particle Image Velocimetry, have been used to study liquid-liquid mixing in T-micromixers and develop concentration and velocity fields models to understand local mass transport and hydrodynamics [75]. Numerical studies have also been conducted on pure water and glycerol mixing in T-micromixers, revealing the impact of glycerol concentration on mixing [62]. Furthermore, 3D T-mixer designs have been evaluated for convective micromixers, showing significant enhancements in mixing performance, lower pressure loss,

and similar levels of shear stress compared to typical T-mixers [60]. Micromixers with staggered herringbone structures with obliquely inclined ridges at the channel walls have also been created to study mixing phenomena experimentally, revealing chaotic motion and effective mixing in a certain Reynolds number range [117].

Passive micromixers have also been explored to enhance mixing performance at different Reynolds numbers. Designs such as three-dimensional mixer structures or complicated mixer designs have been used to improve mixing at low Reynolds number flows [67], [132], [133]. Barriers in microchannels, such as pillar obstructions, have been investigated for their ability to create secondary flows and enhance mixing [134], [135]. Other studies have utilized periodic mixing units, such as staggered bars, in T-shaped geometries to improve mixing performance [52]. Numerical simulations have also been conducted on micromixers with convergent-divergent channel walls of sinusoidal variation, evaluating mixing performance and pressure drop in different split-and-recombination arrangements [49]. The results show that the number of split-and-recombination units and channel amplitude have significant impacts on mixing performance and pressure drop. The throat-width was found to be a critical parameter affecting mixing performance, while the diameter of the circular wall had minimal impact over the chosen Reynolds number range. Additionally, studies have investigated the influence of micromixer design, such as circular obstructions, on fluid mixing and reaction conversion in microchannels [54]. Alternative placement of cylindrical obstacles was found to result in better performance. However, it should be noted that obstacles in microchannels may have limitations such as larger pressure drops and clogging effects, which may hinder their practical use.

The main objective of the present study is to optimize the geometry of obstacles in a T-T mixer in order to achieve an efficient mixing configuration. The aim is to minimize the rise in pressure drop caused by the presence of the obstacles while ensuring that clogging in the mixing channel is not a significant issue. Previous research has examined circular and triangular obstacles, so the current study focuses on optimizing the geometric parameters of these obstacles to improve mixing performance and minimize pressure drops.

5.2 Numerical Modeling

For this study, a 3-dimensional T-T micro mixer with dimensions of 3000 μm in length, 200 μm in width, and 800 μm in height was chosen. The inlet channels have a width of 50 μm, and a no-slip boundary condition is applied near the wall, while a velocity inlet boundary condition is imposed at the inlet. At the outlet of the channel, the pressure is set to atmospheric. The two species being mixed, species a and species b, have thermo-physical properties that are

the same as liquid water. Species a is given a mass fraction of 1 at two inlets, while species b is given a mass fraction of 1 at the other two inlets, as shown in Figure 5.1. The Reynolds number range studied indicates a laminar flow regime, so a laminar flow model was selected to solve the continuity and momentum equations. The Transport of Concentrated Species (TCS) model was used to solve the species conservation equations.

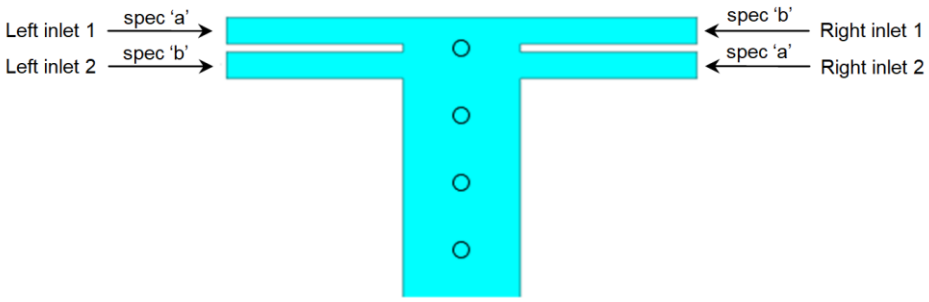

Fig. 5.1 T-T mixer with cylindrical obstacles and inlet conditions

5.2.1 Optimization methodology

Aimed at the optimizing the size and position of cylinder and prismatic obstacles in T-T Micromixer, the Nelder-mead algorithm available on COMSOL Multiphysics platform is chosen. In an N-dimensional solution space, N+1 vertices which form the simplest geometry called a simplex are solved for the objective function value. From the solution set obatined, the best, second best, and worst vertex values are selected and their center is also evaluated. The worst veterx is is replaced by exploring different geometric configurations by performing trivial geometric modifications such as reflection, expansion, contraction, and shrinkage. A new simplex is thus selected iteratively unitl the optimal veterx is obtained and the stopping criteria is met. Figure 5.2 gives a brief pictorial representation of the algorithm.

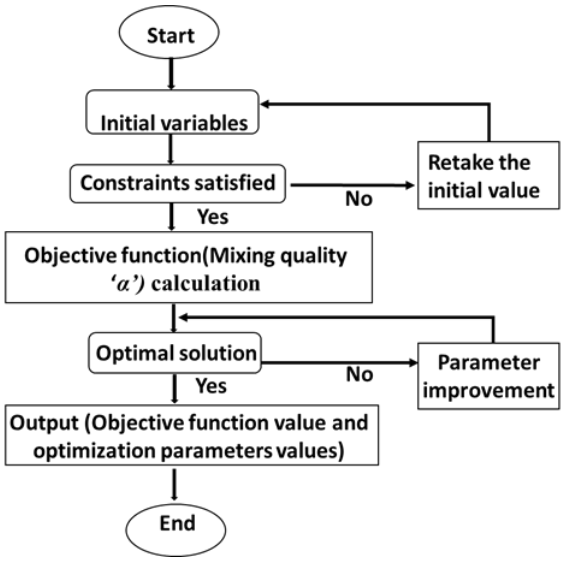

Fig. 5.2 Flowchart showing steps for optimization problem implementation in COMSOL Multiphysics.

The schematics of different geometries of T-T mixer with obstacles with geometric details considered in the present study is shown in figure 5.3. The size and pitch of the obstacles are selected as the optimization variables and mixing quality is selected as the objective function.

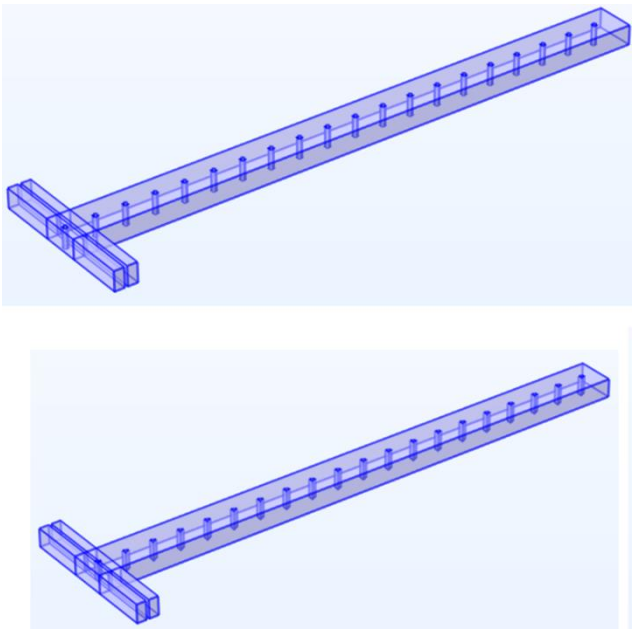

Fig. 5.3 Schematic showing dimensions of 3-D solid model used for numerical simulation of mixing.

5.2.2 Grid independence and Validation

To optimize the computational time, effort, and accuracy of a simulation, a grid independence study was conducted to determine the mesh configuration that would not require further refinement. Meshes with element counts of 16397, 30119, 87304, 159794, and 424535 were evaluated for mixing quality at a Reynolds number of 8, and the results were plotted in Figure 5.4. It was found that increasing the number of elements beyond 159794 had no significant impact on the mixing quality, so this mesh configuration was chosen for the study. The numerical scheme employed in this study was compared to data from previous research by Dundi et al. [110], and the results are presented in Figure 5.5. The mixing quality metric used in the grid independence study was also used to validate the numerical scheme, and it was found that the model developed using COMSOL multi-physics provided reasonably accurate predictions of mixing qualities for Reynolds numbers between 1 and 30.

Table 5.1 Mesh configuration parameters.

Meshes	**Maximum element size**	**Minimum element size**	**Maximum element growth rate**	**Number of elements**	**Mixing quality, α**
Mesh 1	109	23.1	1.4	16397	0.1488
Mesh 2	66	16.5	1.3	30119	0.1374
Mesh 3	42.9	13.2	1.25	87304	0.1313
Mesh 4	33	9.91	1.2	159794	0.1272
Mesh 5	22.1	6.6	1.15	424535	0.1270

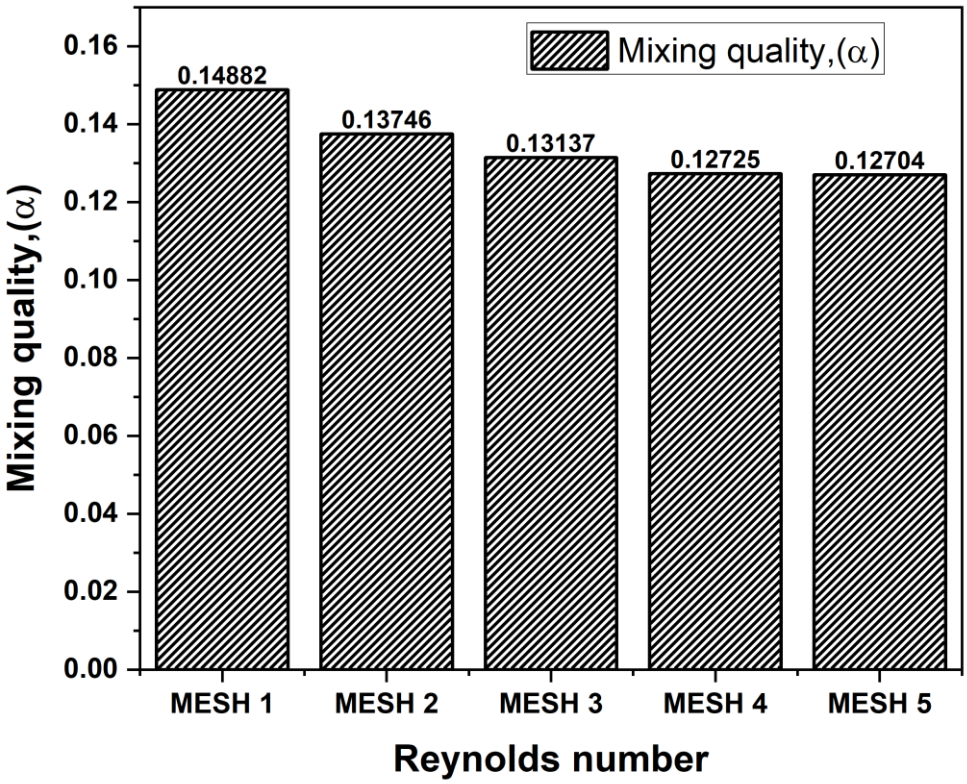

Fig. 5.4 Grid independence study

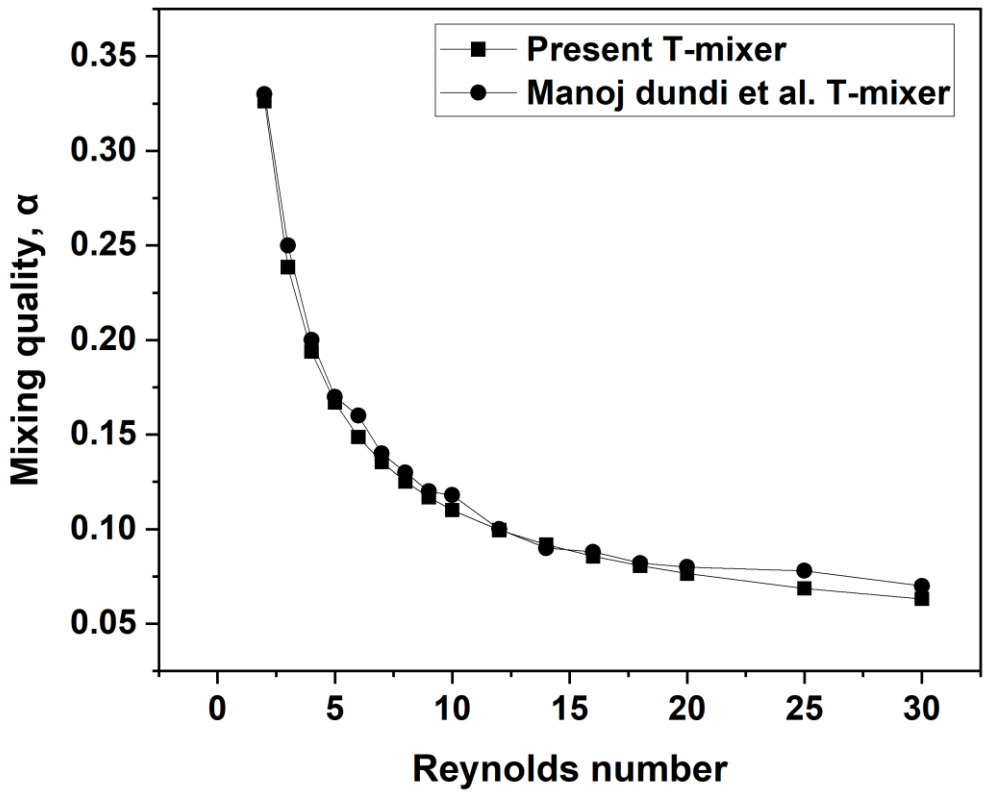

Fig. 5.5 Comparison of mixing quality vs Reynolds number for the present and study from the literature.

5.3 Results and Discussion

5.3.1 Mixing characteristics of T-T mixer with optimized and un-optimized cylindrical obstacles

5.3.1.1 Mixing characteristics of T-T mixer with un-optimized cylindrical obstacles

The extent of mixing in a study is measured by a parameter called mixing quality, which is defined using the variances of the concentrations of species[136]. The influence of the Reynolds number on mixing quality is shown in Figure 5.6 for $0 < Re < 100$. It is observed that mixing quality exhibits a non-monotonic trend with an increase in Reynolds number, as reported in previous studies[54]. The mixing quality initially decreases with an increase in Re from 0 to 15 due to the dominance of diffusion at low Reynolds numbers. However, with further increase in Re, the mixing quality increases, but beyond a certain Reynolds number (i.e., 90), it starts to decrease. The residence time, diffusion, and convection effects are the factors

affecting the mixing quality trend. The cylindrical obstacles used in the study only serve the purpose of increasing the residence time as the phenomenon of splitting and recombination is insignificant in this range of Re. It is worth noting that a mass fraction of 0 or 1 indicates no mixing, while a mass fraction of 0.5 indicates complete mixing, as illustrated in Figure 5.7a, where the streamlines of both species in the wake regions of the obstacles have mass fractions close to 1.

For Reynolds numbers ranging from 15 to 50, an increase in the Reynolds number leads to a significant improvement in mixing quality. This improvement is due to the splitting and recombination effect of fluid streams from both sides of the obstacle, as reported in [54]. This effect is evident in Figure 5.7b, where the fluid streams split at the front of the obstacle and recombine in its wake region repeatedly, leading to increased mixing. The higher mixing quality is reflected in the decreased mass fractions of both species between the obstacles. However, at higher Reynolds numbers ($90 < Re < 100$), the mixing quality decreases with an increase in Reynolds number. This is because the fluid streams do not have sufficient residence time and length to recombine with other streams before reaching the outlet boundary, as shown in Figure 5.7c. The final obstacle being too close to the outlet boundary hinders the recombination of fluid streams, resulting in a minor decrease in the mixing quality.

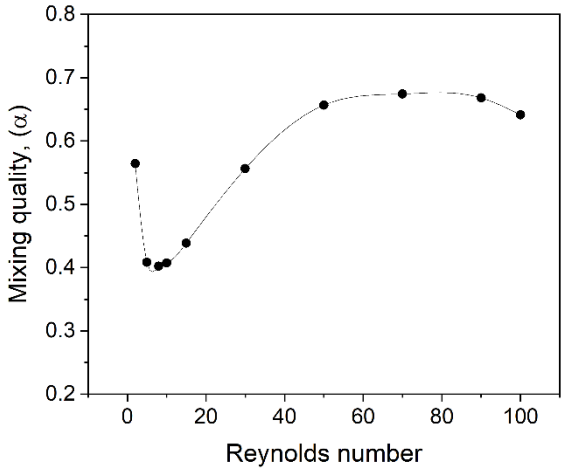

Fig. 5.6 Mixing quality vs Reynolds number for initial geometric configuration with cylindrical obstacles.

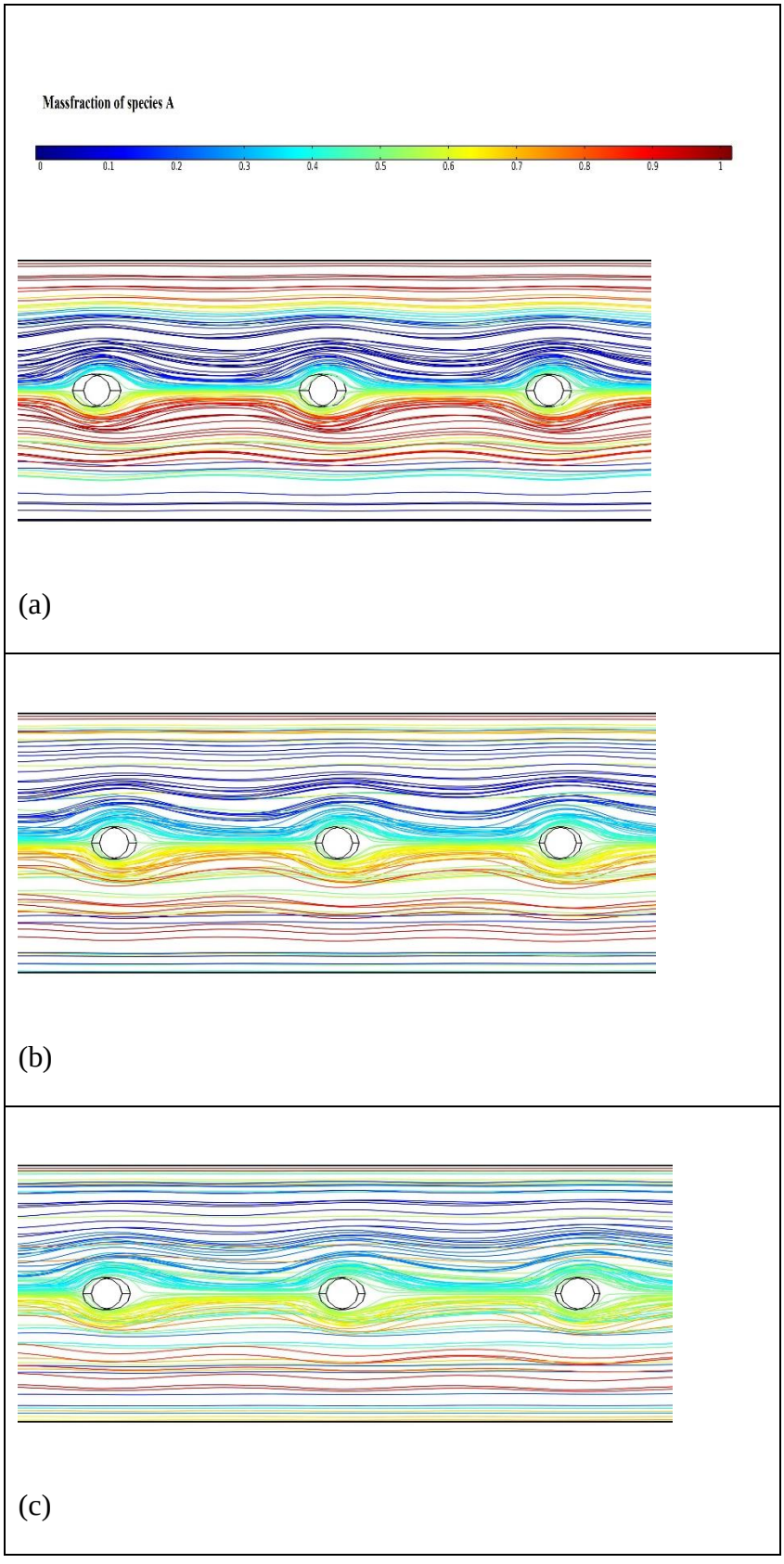

Fig. 5.7 Streamline distribution for initial geometric configuration color graded with the mass fraction of species A for Reynolds number of a) 10, b) 30 and c) 100.

5.3.1.2 Mixing characteristics of T-T mixer with optimized cylindrical obstacles

The optimization algorithm has been run on cylindrical obstacle geometry in the T-T mixer at *Re* = 15, and the mixing performance of the optimized geometry has been evaluated in the Reynolds number range of 2 to 100. The ranges of the diameter and pitch for which the optimization algorithm is run are 20 to 200 microns and 45 to 600 microns. It is observed that, compared to the initial mixer configuration with cylindrical obstacles, the number of the obstacles in the optimized configuration significantly decreased from 20 to 8.5. Also, the diameter of the obstacle has increased from 10 microns to 100 microns while the pitch has increased from 150 microns to 300 microns. Thereby, the mixing quality at the Reynolds number of 15 increased from 0.43867 to 0.60988. The reason for the increase in the mixing quality with the increased pitch and the size of the obstacle is studied by considering the streamline distribution of the fluid streams as shown in figure 5.8.

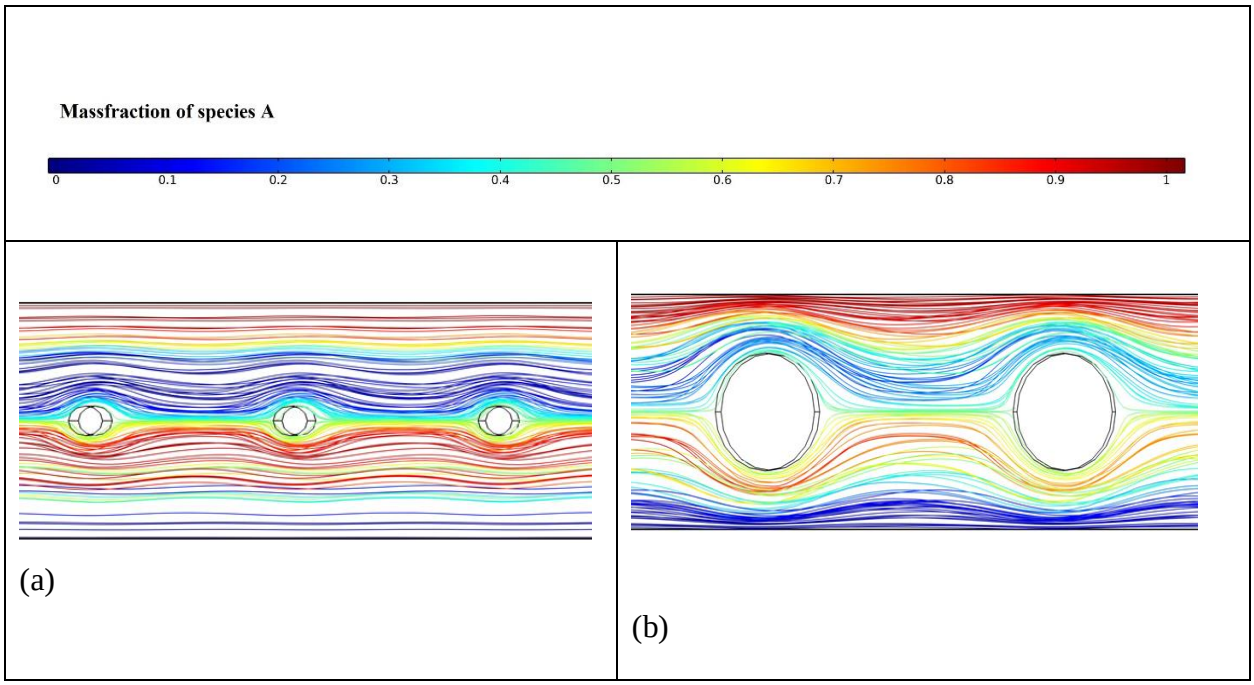

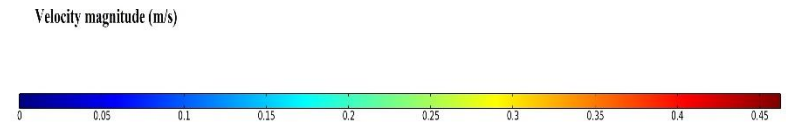

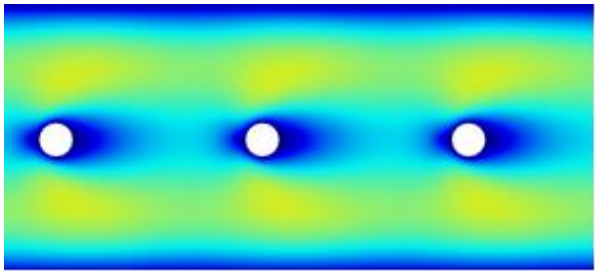

(c)

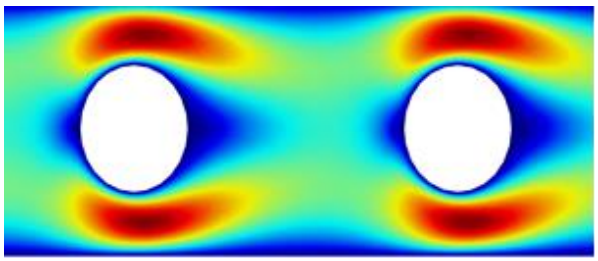

(d)

Fig. 5.8 Streamlines distribution color graded with massfraction of species A for a) Initial geometric configuration b) Optimized geometric configuration. Velocity contours of c) Initial geometric configuration d) Optimized geometric configuration at Reynolds number of 15.

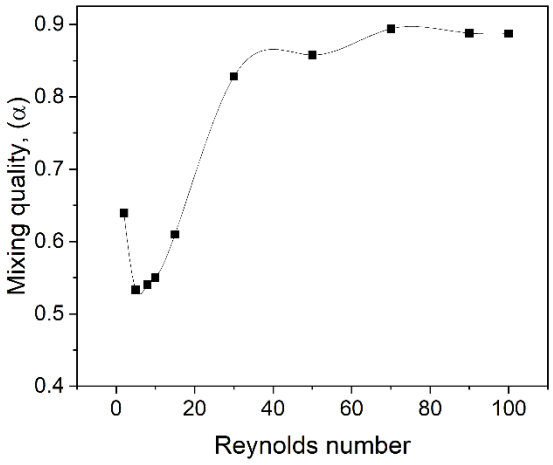

Fig. 5.9 Mixing quality vs Reynolds number for optimized geometric configuration with cylindrical obstacles.

Figure 5.8a and 5.8b shows the streamline distribution for the initial and the optimized geometric configurations at *Re* = 15. It can be seen that compared to the initial geometric configuration, the mass fractions of both the species in the wake regions of the obstacles are small, indicating effective mixing i.e., a higher mixing quality. This could be attributed to the dominance of the splitting and recombination pattern occurring at smaller Reynolds numbers itself for the optimized geometry i.e. the geometry with higher cylindrical diameter. The occurrence of this pattern at smaller Reynolds numbers itself is attributed to the large velocities of the fluid streams in the region between the obstacle and the wall of the channel as shown in figure 5.8c and 5.8d (velocity contours). These large velocities in these zones are attributed to the decreased gap between the transverse extremity of the obstacle and the channel wall.

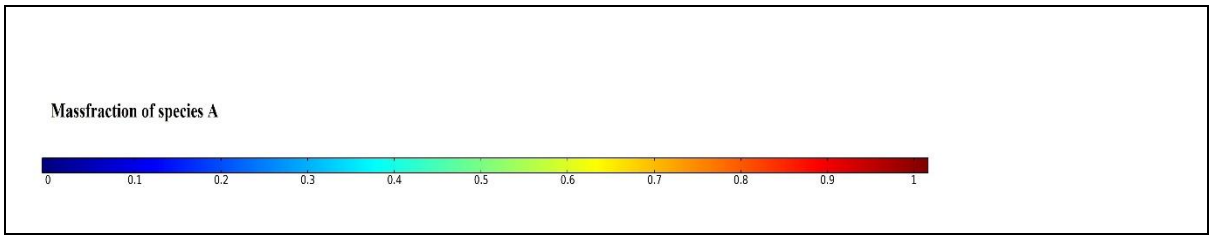

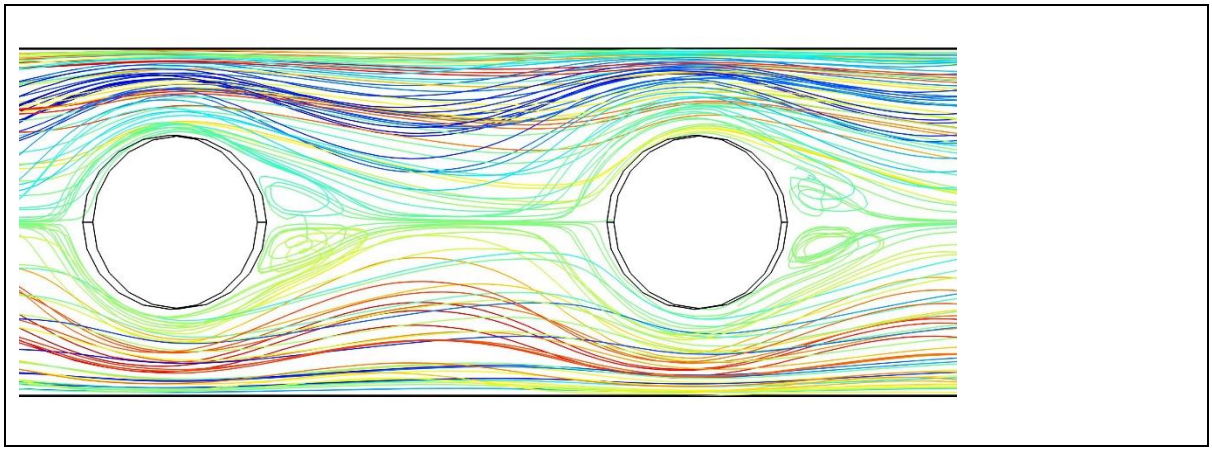

Fig. 5.10 Streamlines distribution color graded with massfraction of species A for optimized geometric configuration for Reynolds number of 30.

Further, the mixing characteristics of the optimized T-T mixer configuration with cylindrical obstacles are studied and are presented in Figure 5.9. At a low Reynolds number of 2, the mixing quality of the optimized configuration increases, indicating improved diffusion effects in this range. As the Reynolds number increases, a similar trend to the initial cylindrical T-T mixer configuration (Figure 5.6) is observed, but with two notable differences. Firstly, the slope of the rapid increase in mixing quality is steeper in the optimized configuration, indicating a shift in the dominance of convective effects at lower Reynolds numbers. Secondly, the minimum of the mixing quality vs Reynolds number curve shifts left, indicating that significant improvements in mixing quality can be achieved at lower Reynolds numbers in the optimized configuration. A benchmark mixing quality of 0.8, which could not be achieved in the initial mixer configuration over the studied Reynolds number range, can be achieved at a Reynolds number of 30 in the optimized configuration. This is attributed to the formation of symmetrical recirculation zones in the wake region of the obstacle, where fluid streams recombine, increasing mixing quality. The formation of these recirculation zones at a Reynolds number of 30 is attributed to flow separation occurring on the obstacle wall, which is caused by the increased diameter of the obstacle cylinder, increasing velocity in the gap between the cylinder and channel walls. It should be noted that a nearly complete mixing of around 0.85 mixing quality can be achieved at Reynolds numbers greater than 50. However, this significant increase in mixing quality comes with a pressure drop penalty, as shown in Figure 5.11, where the

pressure drop in the optimized configuration increases. The observed phenomena are summarized in Table 2.

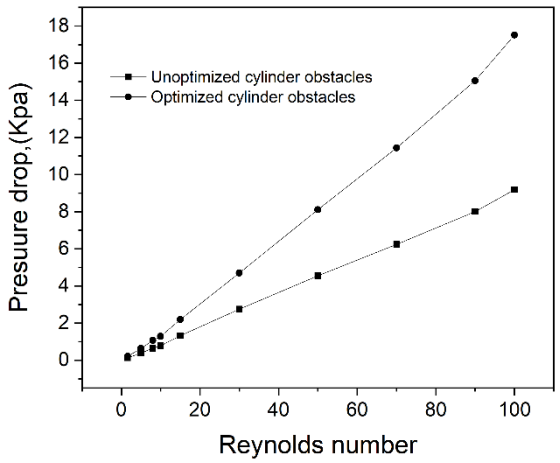

Fig. 5.11 Pressure drop vs Reynolds number comparison for optimized and initial geometric configurations.

Table 5.2: Comparison of few the Reynolds numbers for the occurrence of key flow and mixing characteristics.

Mixer type	Number of Cylindrical Obstacles	Symmetrical Two Vortex Formation	More than 80% mixing quality	Near complete mixing
T-T Mixer with initial cylindrical obstacle configuration	20	Not witnessed	Not witnessed	Not witnessed
T-T Mixer with optimized cylindrical obstacle configuration	8 ½	$Re \geq 30$	$Re \geq 30$	$Re \geq 50$

5.3.1.3 Mixing characteristics of T-T mixer with un-optimized prismatic obstacles

Initially, the mixing characteristics in a T-T mixer with prismatic obstacles has been studied to understand the geometric parameters which affect the mixing quality and are needed to be optimized. The initial geometric configuration consists of 20 prisms of equilateral triangular cross section of side 25 microns which are placed 150 microns from each other. Numerical simulations have been performed for the Reynolds numbers ranging from 2 to 100. Figure 5.12a shows the effect of *Re* on the mixing quality of the T-T mixer with initial geometric configuration. A trend similar to that of the configuration with cylindrical obstacles is observed. Also, similar splitting and recombination patterns in the fluid streams could be seen in figure 5.12b. At higher Reynolds numbers, similar to the case of cylindrical obstacles, incomplete recombination of the fluid streams occurs near the obstacle near the outlet, which results in a minor decrease in the mixing quality. These trends indicate that the size and shape of the triangular obstacle along with its transverse position and pitch significantly affect the flow filed and thereby mixing quality. Therefore, the aforementioned parameters are considered as the parameters to be optimized with a maximization being performed on the mixing quality. From the earlier discussed trends and phenomenon, it could also be inferred that under un-optimized conditions, shape of the obstacle has a minimal effect on the mixing characteristics in the studied operational range.

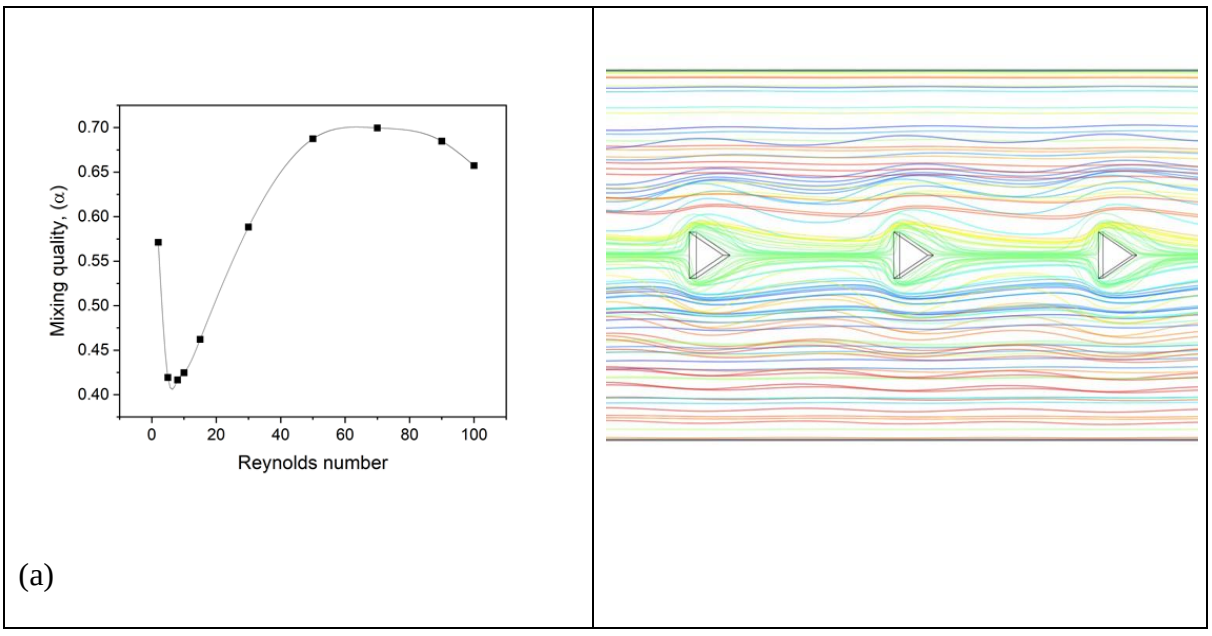

(a)

	(b)

Fig. 5.12 **(**a) Mixing quality vs Reynolds number for initial geometric configuration with prismatic obstacles. (b) Streamlines distribution color graded with mass fraction of species A for initial geometric configuration with prismatic obstacles for Reynolds number of 15.

5.3.1.4 Mixing characteristics of T-T mixer with optimized triangular obstacles

The shape, size, pitch and the position of the prismatic obstacles are optimized by employing the Nelder-mead algorithm. The thus obtained optimized configuration of the T-T mixer with prismatic obstacles is shown in figure 5.13. It could be seen that, the cross section of the prism has changed from an equilateral triangle to a scalene triangle which is significantly inclined towards one wall of the channel. Figure 5.13a shows the effect of the Reynolds number on the mixing quality in the optimized configuration of the T-T mixer with prismatic obstacles and the initial configuration. It is observed that, though the overall trend is similar to that of the initial geometry, the Reynolds numbers at which the different effects dominate are different. An increase in the Reynolds number monotonously increases the mixing quality for $Re > 5$.

Figure 5.13b shows the streamline distribution in the optimized T-T mixer at $Re = 50$. It is observed that, owing to the prism being asymmetric w.r.t., the centerline of the channel, only one recirculation zone attached to the wall of the channel is formed. These recirculation zones formed in the wake region of the obstacles induce significantly effective mixing of the fluid streams. It is indicated by the mass fraction of the species approaching 0.5 in that region. From figure 5.13a it is also observed that the mixing quality of the optimized configuration does not decrease from $Re = 90$ to 100. This is due to the increased gap between the rear end of the

obstacle and the channel outlet which gives the fluid streams enough length to recombine after the splitting near the obstacle's front end as shown in figure 5.13b. From figure 5.13a it is observed that the mixing quality for the optimized configuration is greater than the initial configuration throughout the operational range considered. The increase in the mixing quality in the optimized configuration could be attributed to the asymmetrical recirculation zone. From figure 5.13b it could be seen that in the optimized configuration, the gap between one transverse extremity of the obstacle and the channel wall is significantly small. This results in an increase in the velocity of the fluid stream passing through this gap. This high-velocity fluid stream comes into contact with the fluid stream from the other side of the obstacle enhancing the convective mixing. This is indicated by the smaller mass fractions (i.e., ≈ 0.5) of the species in the wake regions of the obstacle. On the contrary, in the case of the initial geometric configuration, the recirculation zone is not formed in the wake region of the obstacle. This decreases the residence time for the recombination of the fluid streams thereby resulting in ineffective mixing. The ineffective mixing is evident from the greater mass fractions (i.e., ≈ 1.0 or 0) of the species in the wake region of the obstacle.

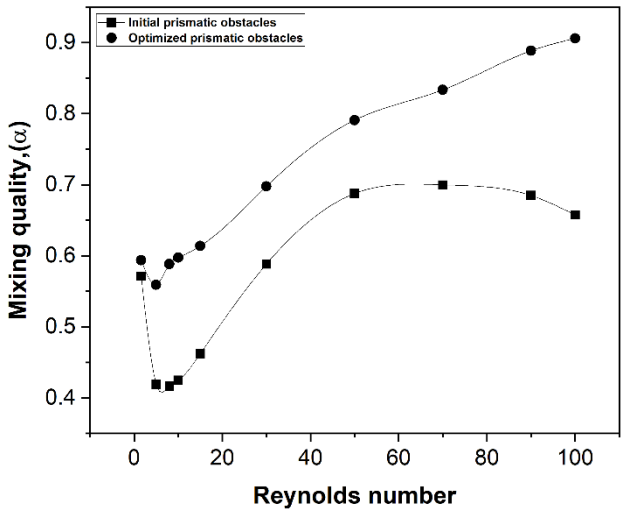

(a)

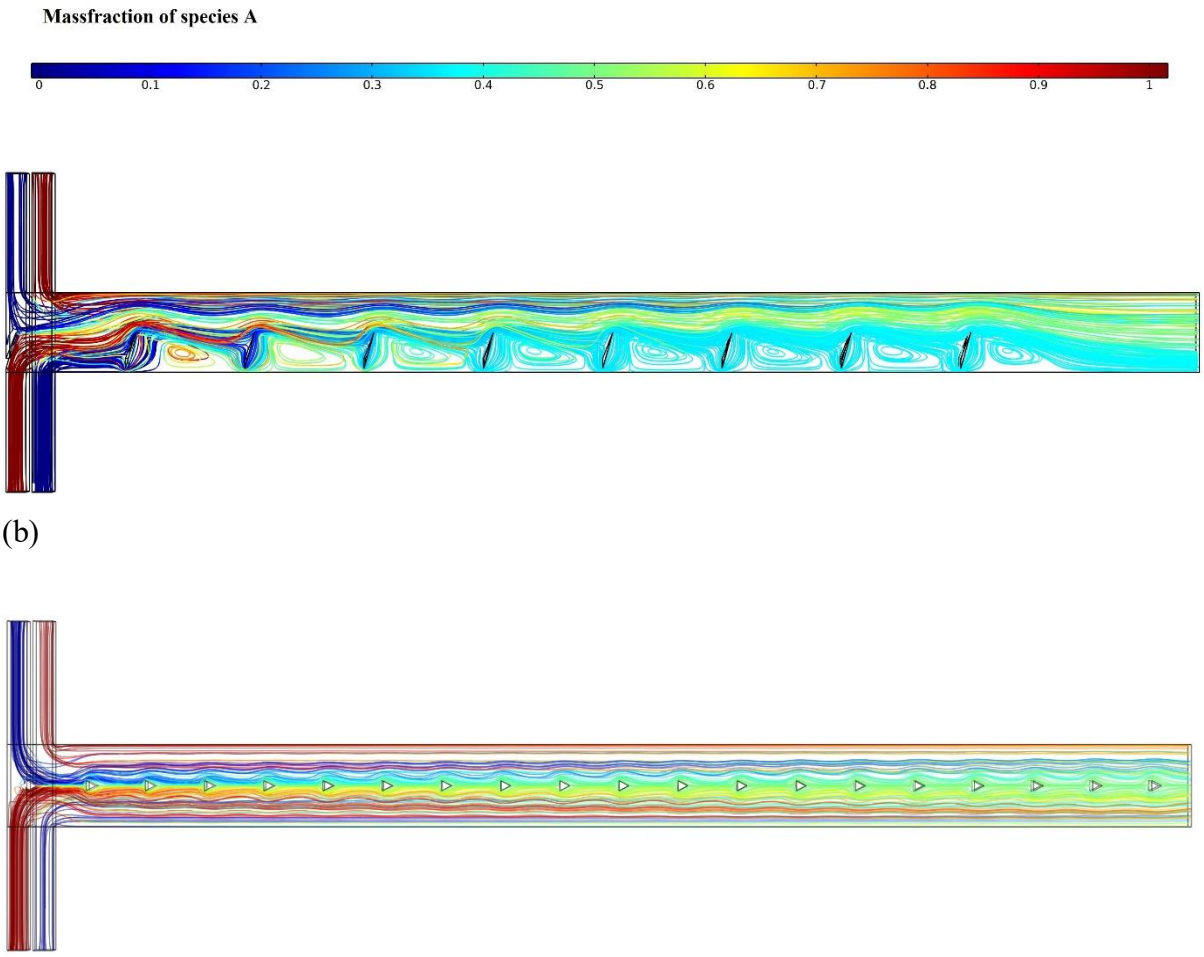

(b)

(c)

Fig. 5.13 (a) Comparison of the mixing quality vs Reynolds number distribution for initial geometric and optimized geometric configurations. (b) Streamlines distribution color graded with massfraction of species A for initial geometric configuration with prismatic obstacles for Reynolds number of 90. (c) Streamlines distribution color graded with massfraction of species A for optimized geometric configuration with prismatic obstacles for Reynolds number of 90.

Table 5.3: Comparison of few the Reynolds numbers for the occurrence of key flow and mixing characteristics

Mixer type	Number of triangular Obstacles	Vortex Formation	More than 80% mixing quality	Near complete mixing
T-T Mixer with unoptimized triangular obstacles	20	Not witnessed	Not witnessed	Not witnessed
T-T Mixer with optimized triangular obstacles	8 ½	$Re \geq 15$	$Re \geq 70$	$Re \geq 90$

5.3.2 Comparison of the optimized configurations with Cylindrical and prismatic obstacles

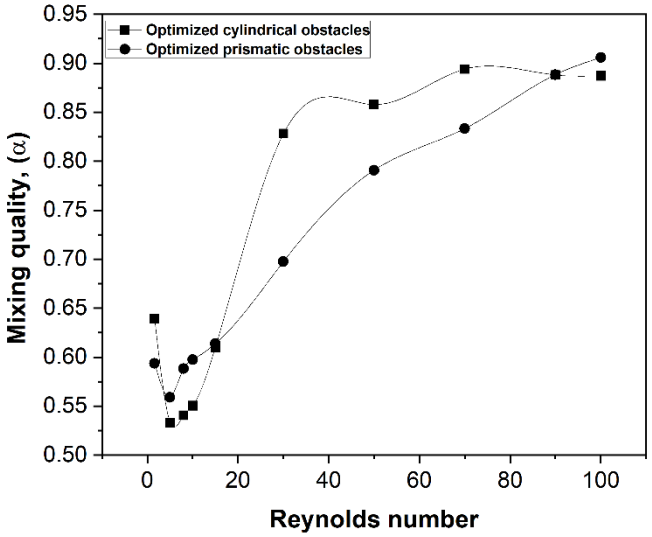

Fig. 5.14 Comparison of the mixing quality vs Reynolds number distribution for optimized geometric configurations for cylindrical and prismatic obstacles.

Figure 5.14 shows the comparison of the mixing qualities for the optimized configurations with cylindrical and prismatic obstacles. It is observed that at low Reynolds numbers (≤ 15), the prismatic configuration results in higher mixing quality. However, the smaller gradient in the increase of the mixing quality with the increase in the Reynolds number in case of the prismatic obstacles results for $Re > 15$ results in smaller mixing quality compared to the cylindrical obstacle mixer. However, at higher Reynolds i.e., ≈ 100, the increase in the Reynolds number results in a minor decrease in the mixing quality in case of cylindrical obstacle unlike the prismatic obstacle. These trends are explained by considering the species' massfraction contours at the channel outlet.

Figure 5.15a and b show the species mass fraction contours at $Re = 15$. From figure 5.15a it is observed that, as the cylindrical obstacle present symmetrically about the Centre line of the channel, a symmetric mass fraction distribution profile is obtained. Also, larger amounts of species leave the channel outlet un-mixed near both the channel walls. On the contrary, in case of the prismatic obstacles, the asymmetry in terms of prism geometry and location results in higher mass fractions of one species near the farther wall from the obstacle as shown in figure 5.15b. Whereas, near the wall close to the obstacle, species mass fractions nearer to 0.5 could be seen. This indicates effective mixing near the wall close to the obstacle resulting in higher overall mixing quality in the case of prismatic obstacles compared to the one with cylindrical obstacles.

The higher mixing quality for cylindrical obstacle compared to the prismatic one for $Re > 18$ is studied by considering the species mass fraction contours at $Re = 30$ as shown in figures 5.15c and 5.15d. The species mass fraction distribution for the cylindrical obstacle configuration is observed to be symmetrical about the centerline of the outlet. Also, the distribution of the species is observed to be more uniform in case of cylindrical obstacle compared. This is attributed to the symmetrical recirculation zones formed near the wake region of the obstacle which result in effective recombination of the fluid streams. On the contrary, in case of prismatic obstacle though the species mass fraction near the wall close to the obstacle is ≈ 0.5 indicating better mixing, the mass fraction ≈ 1.0 or 0 near the wall farther from the obstacle indicates ineffective mixing. This is attributed to the fluid stream near the farther wall leaving the channel un-disturbed as shown in figure 5.13b. Therefore, the cylindrical obstacle performs better than the prismatic configuration in this region. The decrease in the mixing quality in the case of cylindrical obstacles for $Re > 90$ is attributed to

lack of residence time for the high velocity of the fluid stream on either side of obstacle to recombine before the outlet. On the contrary, in the case of prismatic obstacles, owing to the large recirculation zone being formed near to one side of the channel wall, the flow stream diverts as shown in figure 5.15e and 5.15f thereby effectively recombining with the fluid stream from the other extremity of the obstacle.

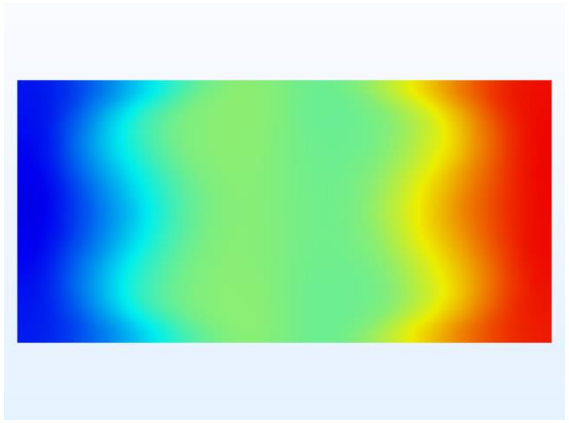

(a)

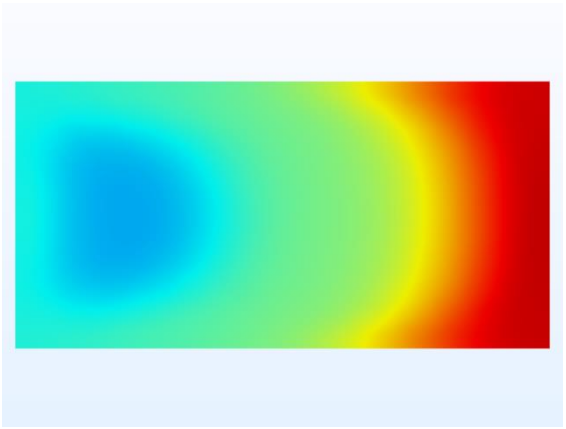

(b)

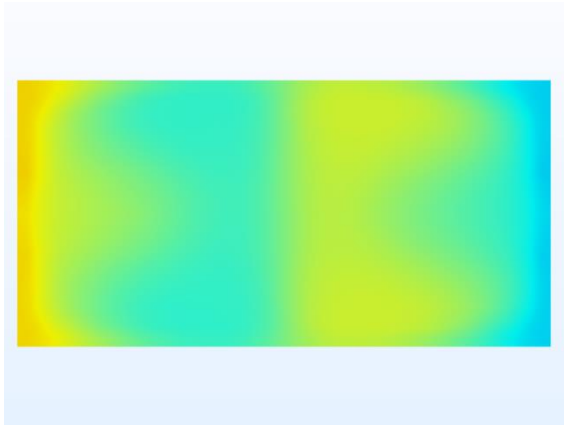

(c)

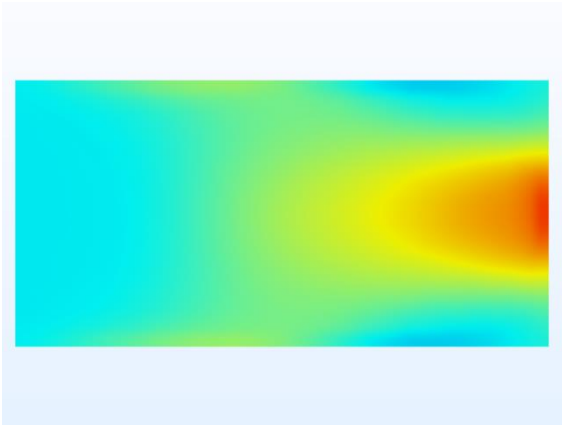

(d)

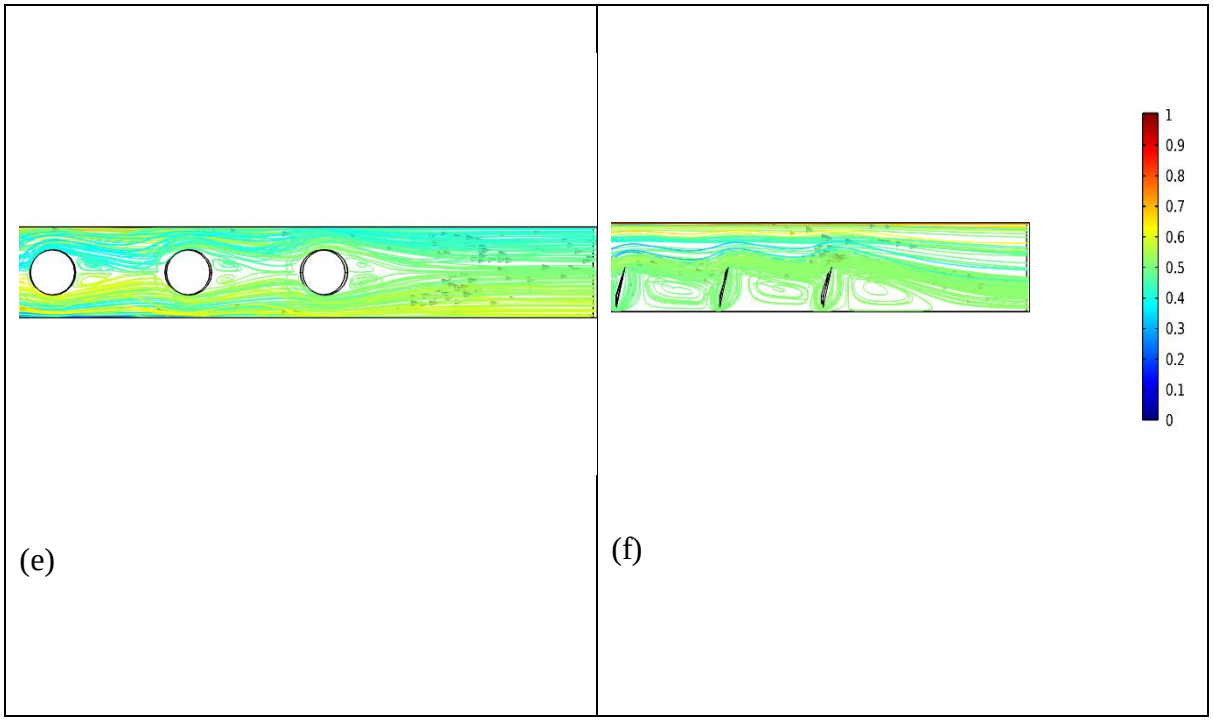

Fig. 5.15 Outlet massfraction contours for species A at *Re* = 15 for optimized geometric configurations with (a) Cylindrical (b) Prismatic obstacles. Outlet massfraction contours for species A at *Re* = 30 for optimized geometric configurations with c) Cylindrical d) Prismatic obstacles. Streamlines distribution color graded with massfraction of species A for initial geometric configuration with prismatic obstacles for Reynolds number of 15. Streamlines distribution color graded with massfraction of species A for optimized geometric configuration with e) cylindrical obstacles f) prismatic obstacles for Reynolds number of 90.

5.4 Summary and conclusions

In the current study, the optimization of obstacle geometry in T-T mixers using the Nelder-Mead algorithm in COMSOL has been investigated for Reynolds numbers ranging from 2 to 100. The study has yielded several conclusions.

- Firstly, before optimization, any obstacle geometry or shape of a similar size has a similar effect on mixing in T-T mixers within the Reynolds number range of 2 to 100.

- Secondly, after optimization, both cylindrical and prismatic obstacles improved mixing performance. However, optimized cylindrical obstacles produced better mixing quality than optimized triangular obstacles in the Reynolds number range of 2 to 100.

- Thirdly, both optimized geometries resulted in vortex formation, which improved mixing performance. However, the symmetrical vortex pair formed in the case of the optimized cylindrical obstacle produced better mixing quality than the single large intense vortex formed in the case of the optimized prismatic obstacle.

- Fourthly, the pressure drop in the optimized configurations was higher than that of the un-optimized configurations. However, the rise in pressure drop was smaller in the case of the optimized prismatic obstacles than in the case of the cylindrical obstacles.

Finally, the study found that the optimized prismatic obstacles provided a smooth transition of the mixing phenomenon from the diffusive regime to the convective regime as the Reynolds number increased. Moreover, the optimized prismatic obstacles reduced the choking effect as the Reynolds number approached a value of 100, whereas the choking effect was considerable in the other three configurations.

CHAPTER 6

6 SIMPLE STRUCTURED AND HIGHLY EFFECTIVE PASSIVE T-TYPE MICROMIXERS WITH A CIRCUMFERENTIAL IN-STEP IN MAIN CHANNEL

6.1 Introduction

Passive micromixers offer several advantages over active mixers for biomedical, chemical, and biochemical applications on μTAS or lab-on-chips. They are easily integrated into complex microsystems, have low manufacturing costs, and allow for straightforward scaling-up in large-scale production. Passive mixers are particularly suitable for maintaining isothermal conditions in chemical reaction kinetic studies, which can be challenging with active mixers due to their complex architecture.

However, one limitation of passive mixers is their slower mixing compared to active mixers, as they rely more on diffusion and less on chaotic advection or transverse directional flows. To address this issue, researchers have proposed various designs with complex structures to induce chaotic advection effects and transverse directional flows. Some examples include the staggered herringbone mixer[62]–[64], three-dimensional split and recombine (SAR) mixers[55]–[57], and mixing channels designed in the form of Tesla structures[65]–[67]. Although these designs improve mixing performance, they also come with challenges like complex fabrication, integration issues, and large pressure drops during operation, making them less suitable for some biological applications.

As a result, simple planar type passive mixers are preferred for many applications due to their low cost, ease of fabrication and integration, and lower pressure drops. However, most planar passive mixers have poor mixing efficiency. Some proposed designs in the literature operate efficiently only within a limited range of Reynolds number [137], [138] or require longer lengths for complete mixing, compromising the advantages of miniaturization.

To improve the mixing performance of simple planar T-micromixers, researchers have explored geometric modifications. For instance, a three-dimensional T-mixer, known as the T-T mixer, has been proposed by splitting each inlet channel into two halves[60]. Other modifications include the use of anti-symmetric barriers before the junction of inlet channels to induce swirl in the sample flow[74].

In the present work, the focus is on modifying the geometries of simple structured T-mixer by introducing a circumferential in-step in the channel. The main objective of the present study is to optimize the circumferential in-step in a T mixer in order to achieve an efficient mixing configuration.

In summary, passive micromixers have distinct advantages over active mixers, and efforts are being made to enhance their mixing efficiency through various design modifications. The use of circumferential in-steps in channels shows promise in improving the mixing performance of simple planar passive mixers.

6.2 Methodology

6.2.1 Numerical Modeling

The 2D planar type T-micromixer geometry with circumferential in-step was created using COMSOL Multiphysics 5.5 software, shown in figure 6.1a. The length of the microchannel (L_c) is 3000 µm, width (W_c) is 200 µm, height (H_c) is 800 µm and inlet channel width (W_i) i

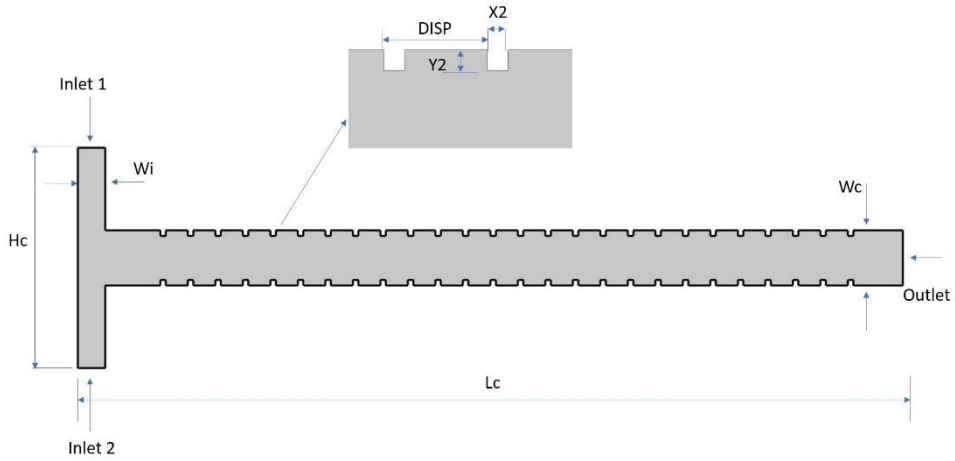

(a)

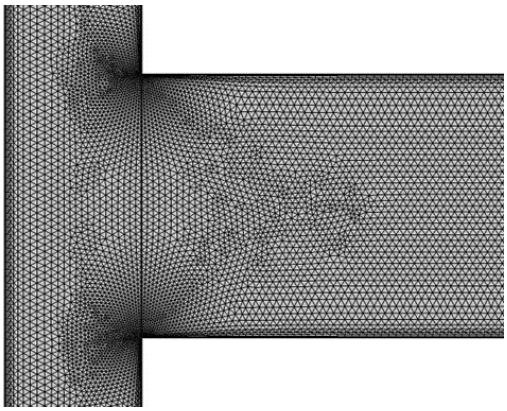

(b)

Fig. 6.1 Schematic diagram of the T-micromixer and its mesh (a) Schematic diagram of the computational domain and (b) free triangular mesh of T-micromixer.

In this problem, two liquid species A and B were chosen for mixing in planar type T-micromixer channel. Both species had the same properties as liquid water at 20^0C, mentioned in Table 6.1. Concentration gradient was created by providing the boundary conditions at the inlet, so that mass fraction was set to unity for species 'A' and zero for species 'B' at inlet one and vice versa at inlet two. Normal inflow velocity boundary condition (Re = 2 to 30) was given at inlet one and inlet two along with mass fraction boundary conditions. At the outlet, the pressure boundary condition was provided. It was set to atmospheric pressure. Except for inlet and outlet, all other boundaries were applied with no-slip boundary conditions.

Table 6.1: Properties of the species materials

Properties	**Species A & Species B**
Type of material	Liquid Water
Density, ρ [Kg/m^3]	998.2

Dynamic Viscosity, μ [Pa. s]	0.001
Diffusion coefficient, D [m^2/s]	2×10^{-9}

Fluid flow equations were solved using Laminar flow physics interface model, while mass fraction equations were solved using the Transport of concentrated species (tcs) model. Reacting flow Multiphysics coupling feature was used to simulate mass transport where the fluid flow depends on mixture composition. For solving the fluid flow problem, P2+P1 discretization scheme was used, and for concentration field, a quadratic discretization scheme was used.

A free triangular mesh was used for the whole computational domain, as shown in figure 6.1b. Because this mesh is like a 'workhorse' for 2D Computational fluid dynamics problems, it was easy to create this kind of mesh with high element quality[121]. However, this ease comes with a cost. This free-unstructured triangular mesh gives greater numerical diffusion. The triangular meshes must be extra fine to overcome the difficulty. In this study, extremely fine mesh was used with a maximum element size of 5.36 μm, and the number of elements was 62878. The details of mesh independence are mentioned in the following section. The different meshes that were considered for the mesh independence test are given in Table 6.2.

6.2.2 Grid independence study

To determine the optimum mesh size for planar type T-mixer analysis, a grid independence study was performed. This study considers axial velocity and mixing quality distribution at the outlet of planar type T-mixer for *Re*=5. Figure 6.2a depicts the axial velocity distribution at the outlet while figure 6.2b depicts the mixing quality distribution at the outlet. Between meshes 6 and 7, the axial velocity has the smallest variation. In addition to axial velocity, the mixing quality difference between mesh 6 and mesh 7 is also minimal. Hence, mesh 6 was considered for the current study.

Table 6.2: Grid independence test parameters

Meshes	**Maximum element size**	**Minimum element size**	**Maximum element growth rate**	**Number of elements**	**Mixing quality, α**
Mesh 1	176	5.6	1.4	18704	0.2497
Mesh 2	69.6	3.2	1.25	23966	0.1826
Mesh 3	36	1.6	1.15	30208	0.1726
Mesh 4	22.4	0.32	1.1	37052	0.1684
Mesh 5	10.4	0.12	1.08	41974	0.1674
Mesh 6	5.36	0.016	1.05	63864	0.1669
Mesh 7	5.00	0.016	1.05	73280	0.1668

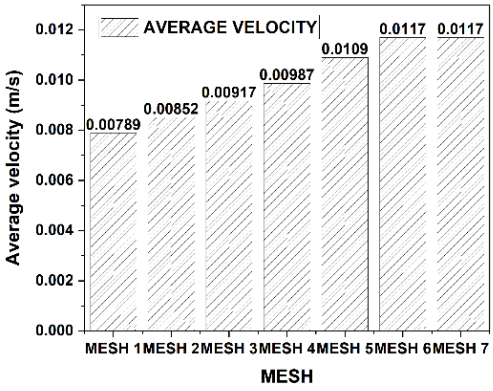

(a)

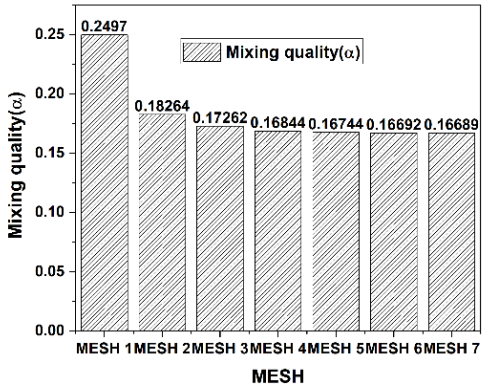

(b)

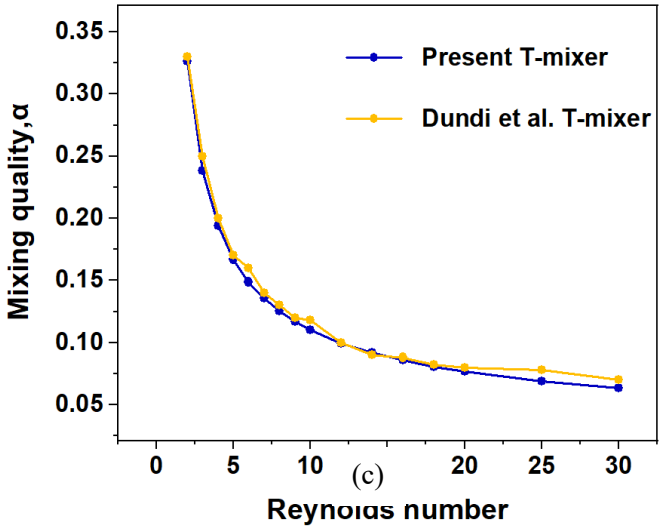

(c)

Fig. 6.2 Grid independence study and validation (a) Average axial velocity profiles at outlet of T – micromixer for different meshes, (b) Mixing quality at outlet of T–micromixer for different meshes and (c) Comparison of Mixing quality with various Reynolds number for T-mixer of the present study and Dundi et al. [110].

6.2.3 Validation

The governing equations of the flow field and species transport of the T-mixer have been solved in this study using conditions comparable to those used by Dundi et al. [110]. To validate the accuracy of the current numerical scheme, the results obtained were compared to the results of Dundi et al. [110]. Equations (4, 5) were used to assess mixing quality at the T-

mixer outlet. Figure 6.2c shows that the current study's findings are in close accord with those of Dundi et al. [110].

6.2.4 Optimization methodology

Aimed at the optimizing the geometrical parameters in T Micromixer with circumferential in-step, the Nelder-mead algorithm available on COMSOL Multiphysics platform is chosen. In an N-dimensional solution space, N+1 vertices which form the simplest geometry called a simplex are solved for the objective function value. From the solution set obatined, the best, second best, and worst vertex values are selected and their center is also evaluated. The worst veterx is is replaced by exploring different geometric configurations by performing trivial geometric modifications such as reflection, expansion, contraction, and shrinkage. A new simplex is thus selected iteratively unitl the optimal veterx is obtained and the stopping criteria is met. Figure 6.3 gives a brief pictorial representation of the algorithm.

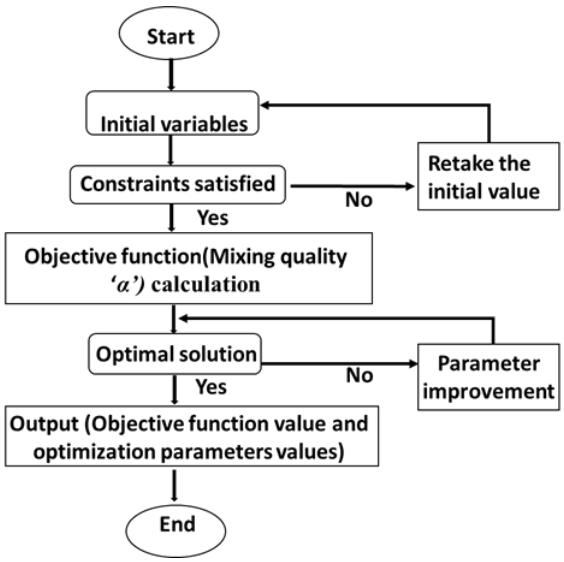

Fig. 6.3 Flowchart showing steps for optimization problem implementation in COMSOL Multiphysics.

The schematics of different geometries of T mixer with circumferential in-step with geometric details considered in the present study is shown in figure 6.1a. The size (X_2, Y_2) and pitch (DISP) of the instep are selected as the optimization variables and mixing quality is selected as the objective function.

6.3 Results and discussion

6.3.1 Optimizing the in-step configuration explicitly in the main channel:

Initially, the effect of the presence of an in-step in the main channel of the T-mixer is studied by considering the T-mixer with in-steps. The depth (Y_2) and width (X_2) of the in-step considered are 10 and 20 microns respectively, with the steps being 100 microns apart from each other. From figure 6.4a, 6.4b, it was observed that the mixing quality upon the in-steps' insertion into the main channel has increased nominally at smaller Re, while a maximum increase of 111% being achieved at Re = 100. However, the presence of these in-steps have also caused an increase in pressure drop across the T-mixer. Nevertheless, the % pressure drop penalty is noticed to be nearly constant, and invariable of Re.

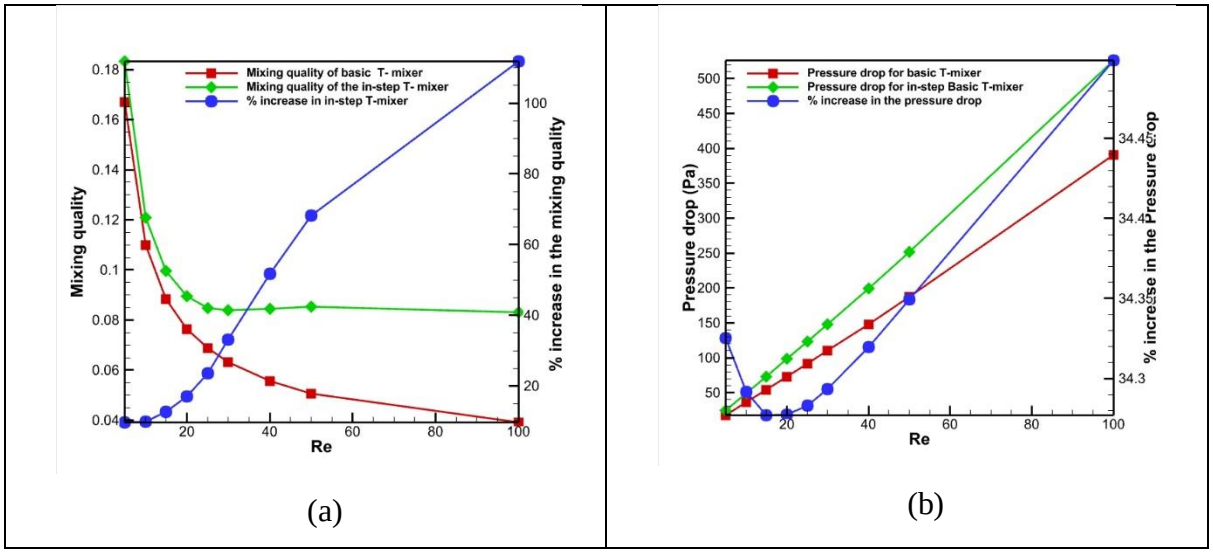

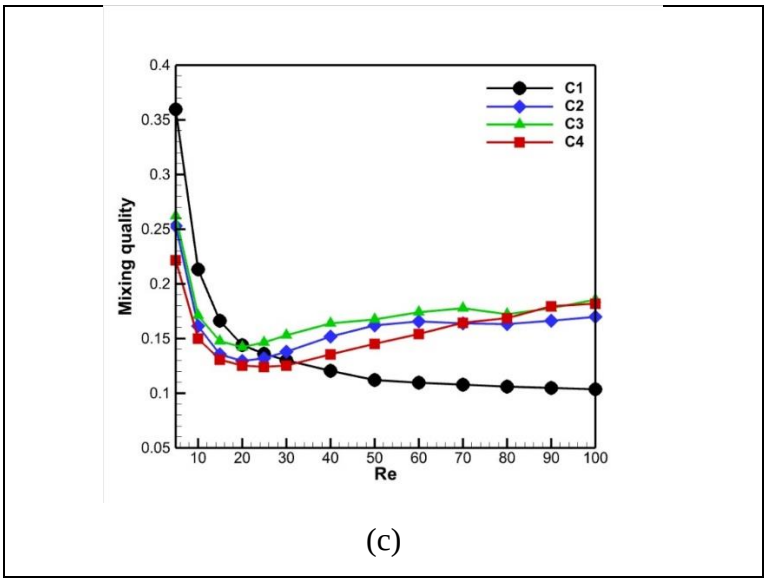

Fig. 6.4 (a) Mixing quality vs Reynolds number for basic T-mixer, in-step T-mixer and %increase in in-step T-mixer. (b) Pressure drop vs Reynolds number for basic T-mixer, in-

step T-mixer and %increase in in-step T-mixer. (c) Mixing quality vs Reynolds number for optimized configurations C1, C2, C3, C4.

In order to optimize the in-step depth, width and the pitch, an optimization algorithm is run for maximizing the mixing quality. The limits of X_2, Y_2 and DISP are considered to be 10 to 100, 50 to 200 and 50 to 1000 respectively. The optimized in-step configuration is found to be a function of the Reynolds number. It is observed that irrespective of Re, the optimum depth of the in-step is 75 microns. While the optimized in-step depth is an invariable of Re, the optimized width and pitch of the in-step depend significantly on Re. Figure 6.4c shows the mixing quality variation with Reynolds number for the in-step induced T-mixer configurations, optimized at different Reynolds numbers. It is observed that the T-mixer configuration (X_2, Y_2, DISP) = ($2e^{-5}$ m, $7.5e^{-5}$ m, $10e^{-5}$ m) (C1), the optimized configuration obtained when the algorithm is run at Re = 20, yields the highest mixing quality in the range $5 \leq Re \leq 20$. At the Reynolds numbers of 40, the optimization algorithm finds the configuration (X_2, Y_2, DISP) = ($2e^{-5}$ m, $7.5e^{-5}$ m, $26e^{-5}$ m) (C2) to provide with the maximum mixing quality. The optimization performed at the Reynolds number of 70 find the configuration (X_2, Y_2, DISP) = ($8.5e^{-5}$ m, $7.5e^{-5}$ m, $45e^{-5}$ m) (C3) to result in the highest mixing quality. It can be seen from the figure 6.4c that this configuration exhibits the highest mixing quality throughout the range $25 \leq Re \leq 80$. At Re = 80, 100, the algorithm finds the configuration (X_2, Y_2, DISP) = ($10e^{-5}$ m, $7.5e^{-5}$ m, $90e^{-5}$ m) (C4) to yield in the maximum mixing quality. However, this configuration is observed to result in maximum mixing quality only in the range $90 \leq Re \leq 100$. Also, it could be understood that the gradient based optimization algorithm though successfully evaluates the local maxima, the configurations thus obtained may or may not be the ones yielding global maximums. Further studies need to be performed for a range of Reynolds number to identify the optimized configuration throughout the operating ranges. Thus, a methodology of this kind, where optimization is performed at various discrete Reynolds numbers should be considered. The factors leading to the respective configurations in yielding maximum mixing quality in the corresponding ranges of Reynolds numbers are discussed further.

The phenomenon of micro-scale mixing is noticed to occur in two modes, namely, diffusion and convection. At smaller Reynolds numbers, where residence time is more, diffusion is the dominating mode of mixing. Owing to this, an initial increase in the Reynolds number results in a decrease in the mixing quality to a local minimum, as the residence time decreases. At moderate to high Reynolds numbers, i.e., Reynolds number above the local minimum of the mixing quality, convection is the dominating mode of mixing. This is due to the velocity

gradients across the flow. These modes of mixing are significantly impacted by the flow patterns in the micro-mixers. In case of the T-micro-mixers with in-steps, the flow pattern is found to be influenced by the in-step width as well as the longitudinal distance between two consecutive in-steps. The splitting and recombination of the streamlines is observed to be the factor defining the mixing in case of the micro-mixers with in-steps. As mentioned earlier, the height of the in-step for maximum mixing quality is observed to be the same irrespective of the Reynolds number at which optimization is being performed.

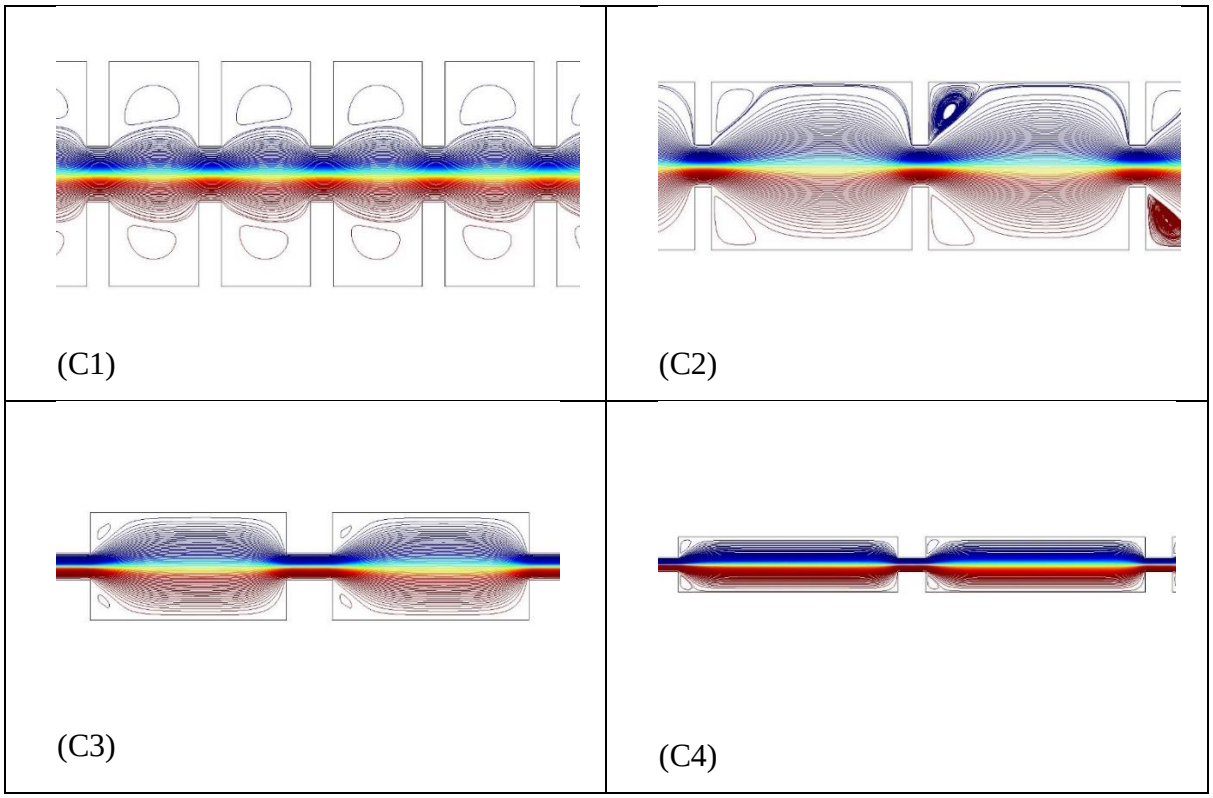

Fig. 6.5 Streamlines distribution color graded with mass fraction of species A for optimized configurations C1, C2, C3, C4 at Reynolds number of 10.

Figure 6.5 shows the flow pattern in the optimized configurations C1, C2, C3 and C4 at Re = 10 in terms of streamlines colour graded with the species mass fraction. At the lower Re = 10, in case of C1 the recirculation zone formed between two in-steps completely covers the region between the in-steps. As a result, the splitting and recombination of the streamlines is not observed in this configuration. Consequently, the interfacial length between the streamlines of the two species is more, resulting in effective diffusion dominated mixing. On the contrary, in case of the C2-4 configurations, it can be seen from the figures that splitting and recombination of the streamlines occurs, reducing the interfacial length between the

streamlines corresponding to the two species. Therefore, the diffusion dominated mixing weakens, resulting a reduced mixing quality.

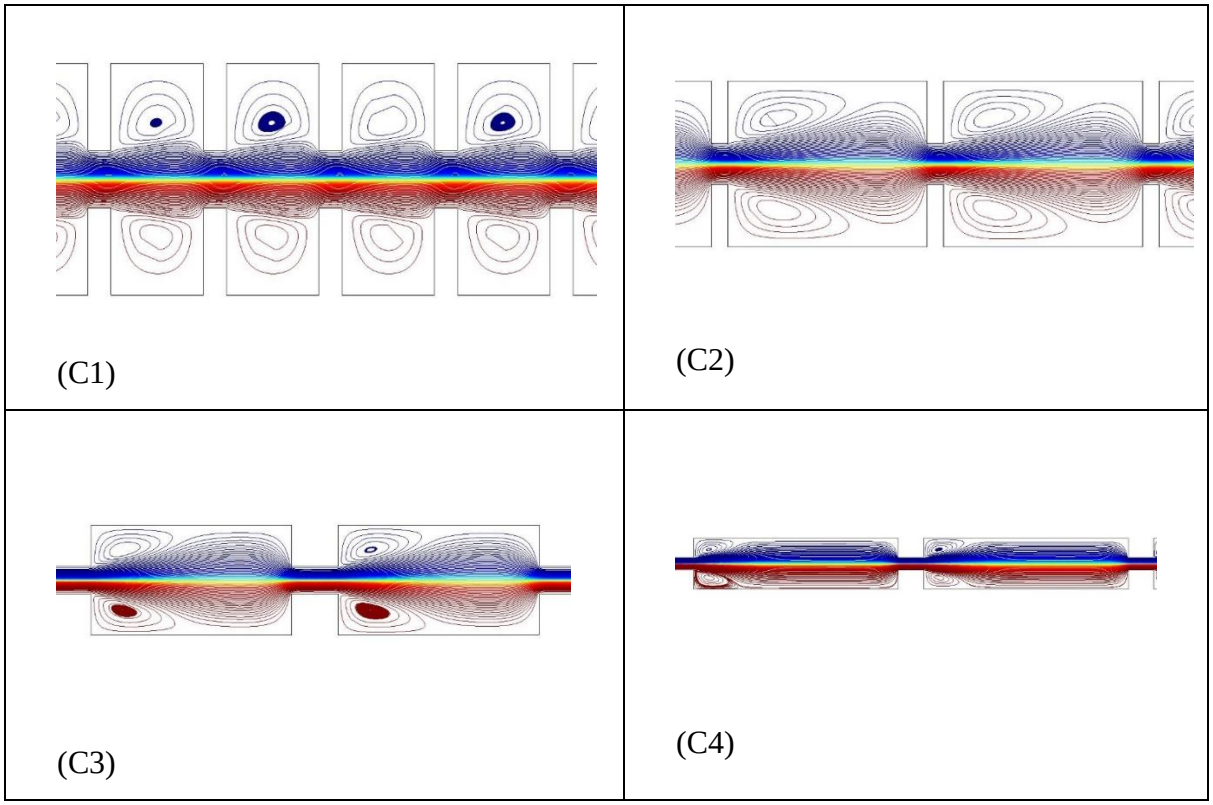

Fig. 6.6 Streamlines distribution color graded with mass fraction of species A for optimized configurations C1, C2, C3, C4 at Reynolds number of 40.

From figure 6.6, it is found that the configuration C3 yields maximum mixing quality in the range $25 \leq Re \leq 80$. Therefore, Re = 40 is considered for further analysis. Figure shows the flow pattern in the optimized configurations C1, C2, C3 and C4 at Re = 40 in terms of streamlines colour graded with the species mass fraction. At Re = 40, as seen from figure, the mixing occurs with both the modes i.e., diffusion and convection, equally contributing and complimenting each other. It should be noted that, along the width of the step, recombination occurs, as the velocity and thereby the gradients are high, convection mixing dominates. On the other hand, in the region between two consecutive steps, as the velocity is less and residence time is more, diffusion dominates. Therefore, an increase in the width of the in-step at a higher Reynolds number positively impacts the mixing quality, as the length of the recombination zone, i.e., convection dominated region increases. On the other hand, an increase in DISP, i.e., the distance between two consecutive steps increases, the number of recombination zones decreases. This adversely affects the mixing quality as the number of regions for convection dominated mixing decreases. Therefore, C2 and C3, with moderate number of recombination

zones as well as the moderate length of each recombination zone, result in the highest mixing quality. The C4 configuration, which has the lowest number of recombination zones, owing to the maximum DISP results in the further smaller mixing quality. However, the C1 configuration, which has the maximum number of the recombination zones exhibits lowest mixing quality as the recirculation zones formed fully occupies the area between two in-steps. Thus, splitting and recombination does not effectively occur.

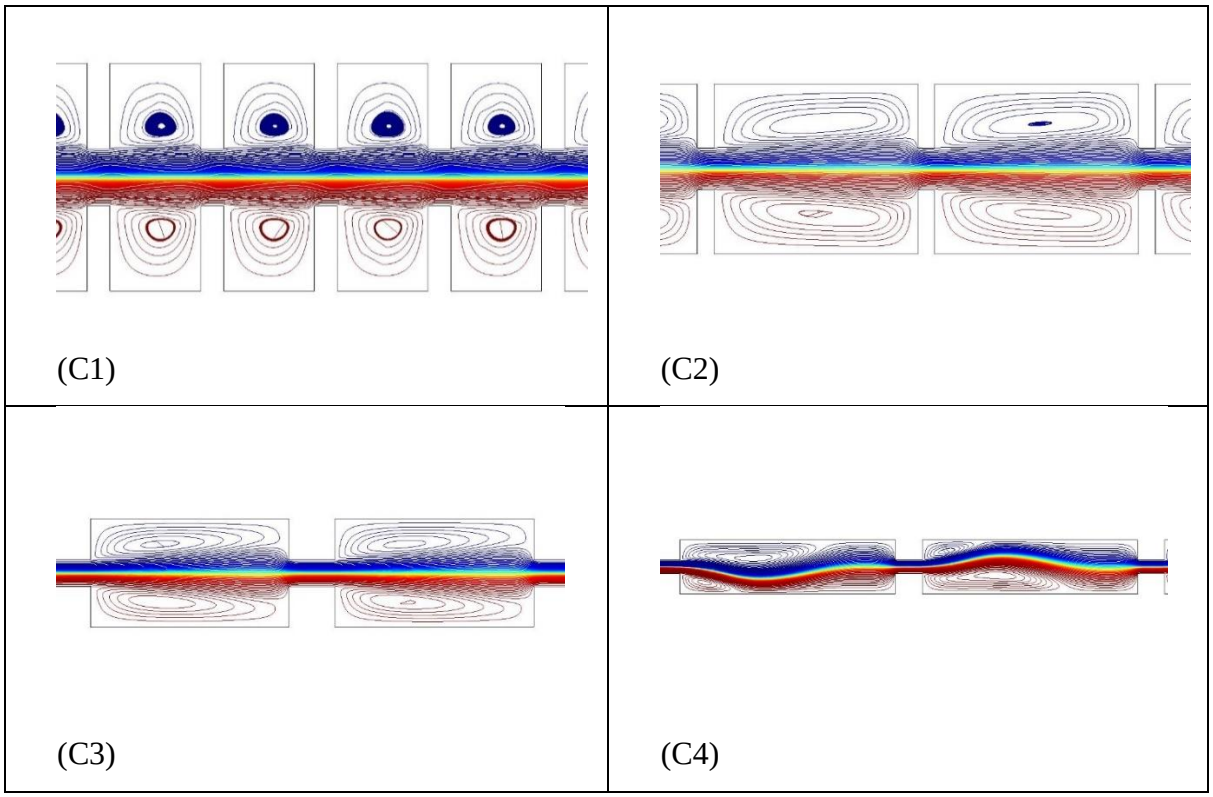

Fig. 6.7 Streamlines distribution color graded with mass fraction of species A for optimized configurations C1, C2, C3, C4 at Reynolds number of 100.

From figure 6.7, it is found that the configuration C4 yields maximum mixing quality in the range $90 \leq Re \leq 100$. Therefore, Re = 100 is considered for further analysis. Figure shows the flow pattern in the optimized configurations C1, C2, C3 and C4 at Re = 100 in terms of streamlines colour graded with the species mass fraction. It can be observed from the figure that at Re = 100, the region between the two-consecutive in-steps is completely covered with the recirculation zone for C1-3. Therefore, splitting and recombination does not occur along the width of the step. On the other hand, for C4, the region between two consecutive in-steps is occupied a smaller recirculation zone on one side and larger one on the other side. The side of these recirculation zones is also observed to be alternating. Therefore, at a higher Re, owing to the increasing size of the recirculation zones being formed, in order to facilitate the

phenomenon of splitting and recombination, a higher DISP accompanied by a higher X_2 is required for maximum mixing quality.

6.3.2 Pressure drop

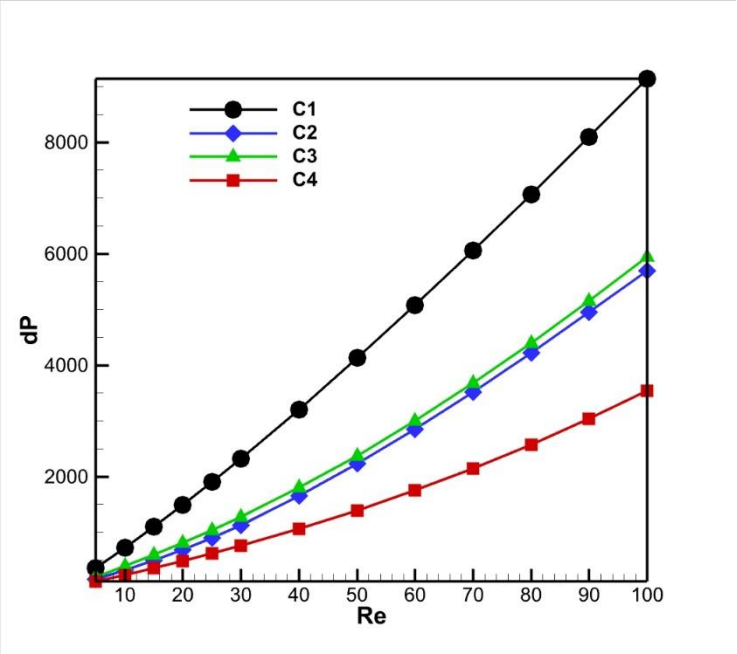

Fig. 6.8 Pressure drop vs Reynolds number for optimized configurations (C1, C2, C3, C4).

Figure 6.8 shows the pressure drop variation with Reynolds number for different configurations. It is found that the C1 configuration, which has the highest number of in-steps imposes the maximum pressure drop across the range of the Reynolds numbers considered. It is followed by C3, C2 and C4. It is observed that, the pressure drop across the micro-mixer decreases with the increase in DISP, i.e., decrease in the number of in-steps. It should also be noted that from C1 to C4, apart from the DISP increasing, the width of the step also increases. At smaller values of the step-width i.e., in case of C1 and C2, the pressure drop across each step is significantly small (≈ 100 Pa). With an increase in the step width, the pressure drop across each step also increases, i.e., ≈ 300 Pa in case of C3 and C4. However, despite of the configuration C3 having a smaller number of in-steps compared to C2, it has a slightly higher pressure drop. This higher pressure drops in C3 compared to the C2 is attributed to the increased width of the step by nearly 4 times ($2e^{-5}$ m to $8.5e^{-5}$ m) while the displacement increases by less than 100% ($26e^{-5}$ m and $45e^{-5}$ m). However, for the C4 configuration, where the DISP increases by 100% while the width of the step increased from $8.5e^{-5}$ m to $10e^{-5}$ m, a significant decrease in the pressure drop is observed.

6.3.3 Performance evaluation criteria

In case of micro-channel heat sinks, the hydraulic and heat transfer performance i.e., Nu and the hydraulic load i.e., the pressure drop across the micro-channel are evaluated. It is observed from the literature that the improvement in the heat transfer performance is many a times achieved at the cost of an increase in the pressure drop across the channel. Therefore, a parameter combining both the heat transfer improvement as well as the pressure drop penalty was devised. A parameter called performance evaluation criteria, which is the ratio of the increase in the Nusselt number to the increased in the friction factor is proposed []. Its value near to 1 or greater than 1 are preferred. In this study, similar to the heat transfer related performance evaluation criteria (PEC), a mixing related performance evaluation criteria is proposed. It is the ratio of the enhancement in the mixing quality to the increase in the friction factor. It is mathematically defined as,

$$PEC = \frac{\frac{MQ_O}{MQ_i}}{\left(\frac{\bar{\bar{f}}_O}{\bar{\bar{f}}_i}\right)^{\frac{1}{3}}} \qquad (1)$$

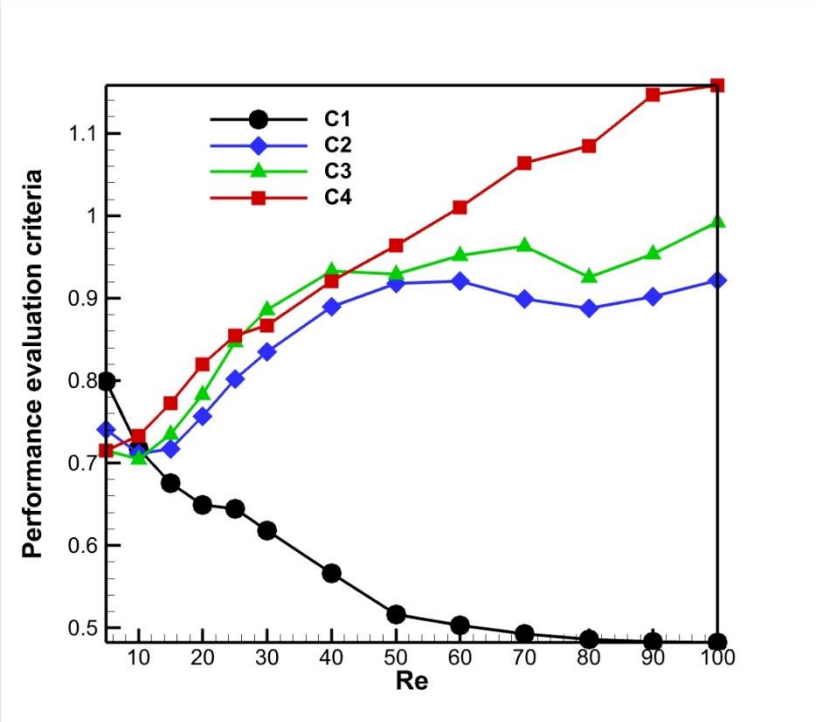

Fig. 6.9 PEC vs Reynolds number comparison for optimized configurations (C1, C2, C3, C4).

Figure 6.9 shows the PEC variation with Reynolds number for different configurations. It can be seen that at lower Reynolds number, C1 exhibits highest PEC. This could be attributed

to its significantly greater mixing quality, accompanied by only a slightly higher pressure drop. At higher Reynolds numbers on the other hand, C4 configuration owing to its significantly smaller pressure drop results in the highest PEC followed C3, C2 and C1. It can also be noticed that the PEC for the C4 configuration at higher Reynolds numbers exceeds 1.1. However, the C3 configuration despite of its higher pressure drops, results in a PEC ≥ 0.95 at higher Reynolds numbers. This indicates the improvement in the mixing quality C3 exhibits. It could be concluded that the configurations C3 and C4, could be preferred over the range of Reynolds numbers considered owing to the higher average mixing quality throughout the range of the Reynolds numbers and PEC respectively.

6.4 Summary and conclusions

The effect of the in-step on the mixing characteristics and the pressure drop are studied. The mixing quality was observed to significantly increase upon the insertion of in-step in the main channel of the T-micro mixer. The geometric parameters of the in-step such as the width, height and the pitch are optimized for maximum mixing quality using the gradient based Nelder-Mead algorithm. The findings are summarized as follows: -

- The optimized width and the pitch are dependent on the Reynolds number at which the algorithm is run, while its effect on the height of the in-step is insignificant.
- With an increase in the Reynolds number, the pitch and width of the in-step configuration for maximum mixing quality increases.
- The highest mixing quality in case of the lowest width and pitch at smaller Reynolds numbers (20) is attributed to the enhanced diffusion as a result of the recirculation zone occupying the entire region between the two consecutive steps.
- At moderate Reynolds numbers (40-70), moderate values of pitch and width of the in-step resulted in the highest mixing quality. This is due to the convection as well as diffusion contributing considerably in terms of the larger length of the recombination zones as well as the longer residence times in between two consecutive steps, respectively.
- At higher Reynolds numbers (80-100), larger values of pitch as well as width are preferred, as a larger pitch enables better splitting and a larger width facilitates longer distance for recombination.

- The increase in pitch as well as width increases the pressure drop also, significantly. Therefore, a mixing PEC is proposed to study the combined effect on the mixing as well as the pressure drop penalty.
- The configuration with largest pitch and width of the in-step was observed to result in the highest PEC. However, considering the range over which the configuration with moderate pitch and width exhibits highest mixing quality, and its moderately high PEC, it could be preferred.

CHAPTER 7 7 CONCLUSION AND FUTURE SCOPE

7.1 Conclusion

In this thesis, the mixing efficiency of planar type passive micromixers, particularly serpentine mixers with square and Convergent-Divergent passages in the horizontal sections, was thoroughly investigated in a wide range of Reynolds numbers (Re) from 0 to 100.

At low Re values (0 to 10), the flow was completely laminar, relying solely on diffusion for mixing in both square wave and Convergent-Divergent mixers. Consequently, mixing decreased with increasing Re due to reduced residence time. However, as Re increased beyond 10, the action of stretching and folding was initiated in both mixers, leading to an improvement in mixing efficiency. Remarkably, the Convergent-Divergent wave mixer exhibited more intense stretching and folding, and the presence of recirculation zones in the bends considerably enhanced its mixing efficiency. Thus, it was concluded that incorporating convergent-divergent passages in serpentine mixers can significantly enhance their mixing capabilities.

To optimize the mixing performance further, an adjoint-based shape optimization scheme was employed using Bernstein polynomial profiles to modify the channel walls of a T-mixer. The optimization showed that the shape of the T-mixer's wall was independent of the Reynolds number at which the algorithm was run. However, the mixing quality decreased with increasing Re due to reduced residence times. On the other hand, the mixing quality increased with the order of the Bernstein polynomial, attributed to reduced throat thickness. While pressure drop increased with the polynomial's order, the optimized T-mixer with converging-diverging profiles still outperformed a thin T-mixer with uniform channel width.

The study also investigated the optimization of obstacle geometry in T-T mixers using the Nelder-Mead algorithm in COMSOL for Reynolds numbers from 2 to 100. Before

optimization, different obstacle geometries had a similar effect on mixing, but after optimization, both cylindrical and prismatic obstacles improved mixing performance. Optimized cylindrical obstacles proved to be more effective than triangular ones in the given Reynolds number range, primarily due to the formation of a symmetrical vortex pair that enhanced mixing.

Furthermore, the effect of an in-step on mixing characteristics and pressure drop was studied. The insertion of an in-step in the main channel significantly increased mixing quality. The optimized width and pitch of the in-step were dependent on the Reynolds number, with higher Reynolds numbers requiring larger pitch and width to achieve maximum mixing quality. Smaller width and pitch led to enhanced diffusion through recirculation zones at lower Reynolds numbers. Moderate values of pitch and width resulted in the best mixing quality at moderate Reynolds numbers due to a balanced contribution from convection and diffusion. Larger pitch and width were preferred at higher Reynolds numbers, but this led to an increase in pressure drop. A mixing performance enhancement criterion (PEC) was introduced to consider both mixing efficiency and pressure drop. Overall, configurations with moderate pitch and width exhibited the highest mixing quality and moderate PEC, making them favorable choices.

In conclusion, this thesis provides valuable insights into improving mixing efficiency in micromixers using various optimization techniques, demonstrating the potential of employing convergent-divergent passages, optimizing obstacle geometries, and utilizing in-steps to enhance mixing performance across different Reynolds number ranges.

7.2 Future Scope

The current study has provided valuable insights into improving mixing efficiency in planar type passive micromixers, particularly focusing on serpentine mixers with Square and Convergent-Divergent passages and the optimization of obstacle geometries in T-T mixers using different algorithms. Based on the findings, there are several potential future directions for further research:

Optimization Algorithms Comparison: Conduct a comparative study of different optimization algorithms to identify the most efficient and robust approach for shape optimization in micromixers. Compare the results obtained from the adjoint-based scheme and the Nelder-

Mead algorithm with other optimization methods, such as genetic algorithms, particle swarm optimization, or simulated annealing.

Effect of Multiple Geometrical Constraints: As suggested in the study, consider additional geometrical constraints, such as the mass held in the mixer, while optimizing the shape of the T-mixer. Investigate how incorporating these constraints affects the mixing performance and pressure drop characteristics. This could lead to more realistic and practical designs.

Dynamic Flow Conditions: Extend the study to investigate the performance of the optimized micromixers under dynamic flow conditions. Explore how mixing efficiency and pressure drop are affected when the flow rates change or during pulsatile flow scenarios, which are more representative of real-world applications.

Multi-Objective Optimization: Consider multi-objective optimization approaches to balance conflicting design objectives, such as mixing quality, pressure drop, and fabrication complexity. This will help in finding optimal compromises between these competing factors.

Alternative Geometries: Explore other innovative geometries for micromixers and obstacle configurations to improve mixing efficiency. Investigate the potential of combining different mixing enhancement techniques to achieve superior performance.

REFERENCES

[1] G. S. Jeong, S. Chung, C. B. Kim, and S. H. Lee, "Applications of micromixing technology," *Analyst*, vol. 135, no. 3, pp. 460–473, 2010, doi: 10.1039/B921430E.

[2] C. Y. Lee and L. M. Fu, "Recent advances and applications of micromixers," *Sensors Actuators B Chem.*, vol. 259, pp. 677–702, Apr. 2018, doi: 10.1016/J.SNB.2017.12.034.

[3] C. Y. Lee, W. T. Wang, C. C. Liu, and L. M. Fu, "Passive mixers in microfluidic systems: A review," *Chem. Eng. J.*, vol. 288, pp. 146–160, Mar. 2016, doi: 10.1016/J.CEJ.2015.10.122.

[4] R. H. Liu, J. Yang, R. Lenigk, J. Bonanno, and P. Grodzinski, "Self-Contained, Fully Integrated Biochip for Sample Preparation, Polymerase Chain Reaction Amplification, and DNA Microarray Detection," *Anal. Chem.*, vol. 76, no. 7, pp. 1824–1831, Apr. 2004, doi: 10.1021/AC0353029/ASSET/IMAGES/LARGE/AC0353029F00004.JPEG.

[5] A. G. Hadd, D. E. Raymond, J. W. Halliwell, S. C. Jacobson, and J. M. Ramsey, "Microchip Device for Performing Enzyme Assays," *Anal. Chem.*, vol. 69, no. 17, pp. 3407–3412, Sep. 1997, doi: 10.1021/AC970192P/ASSET/IMAGES/LARGE/AC970192PF00008.JPEG.

[6] F. Nason *et al.*, "Design of microfluidic devices for drug screening on in-vitro cells for osteoporosis therapies," *Microelectron. Eng.*, vol. 88, no. 8, pp. 1801–1806, Aug. 2011, doi: 10.1016/J.MEE.2011.02.115.

[7] C. H. Hsu and A. Folch, "Spatio-temporally-complex concentration profiles using a tunable chaotic micromixer," *Appl. Phys. Lett.*, vol. 89, no. 14, Oct. 2006, doi: 10.1063/1.2358194/331944.

[8] H. Lu, M. A. Schmidt, and K. F. Jensen, "A microfluidic electroporation device for cell lysis," *Lab Chip*, vol. 5, no. 1, pp. 23–29, Dec. 2005, doi: 10.1039/B406205A.

[9] M. X. Lin *et al.*, “Continuous labeling of circulating tumor cells with microbeads using a vortex micromixer for highly selective isolation,” *Biosens. Bioelectron.*, vol. 40, no. 1, pp. 63–67, Feb. 2013, doi: 10.1016/J.BIOS.2012.06.016.

[10] X. H. Yan, L. Hu, Y. Li, X. J. Feng, and B. F. Liu, “Microfluidic Slipchip-based Reaction Microarray with Dual Concentration Gradient,” *Chinese J. Anal. Chem.*, vol. 43, no. 10, pp. 1520–1525, Oct. 2015, doi: 10.1016/S1872-2040(15)60868-4.

[11] K. Petkovic *et al.*, “Rapid detection of Hendra virus antibodies: an integrated device with nanoparticle assay and chaotic micromixing,” *Lab Chip*, vol. 17, no. 1, pp. 169–177, Dec. 2016, doi: 10.1039/C6LC01263A.

[12] V. Hessel and H. Löwe, “Organic Synthesis with Microstructured Reactors,” *Chem. Eng. Technol.*, vol. 28, no. 3, pp. 267–284, Mar. 2005, doi: 10.1002/CEAT.200407167.

[13] F. Haselhuhn and M. Kind, “Pseudo-polymorphic Behavior of Precipitated Calcium Oxalate,” *Chem. Eng. Technol.*, vol. 26, no. 3, pp. 347–353, Mar. 2003, doi: 10.1002/CEAT.200390053.

[14] C. Rosenfeld, C. Serra, C. Brochon, V. Hessel, and G. Hadziioannou, “Use of micromixers to control the molecular weight distribution in continuous two-stage nitroxide-mediated copolymerizations,” *Chem. Eng. J.*, vol. 135, no. SUPPL. 1, pp. S242–S246, Jan. 2008, doi: 10.1016/J.CEJ.2007.07.038.

[15] M. Ma, J. Lu, and G. Tryggvason, “Using statistical learning to close two-fluid multiphase flow equations for bubbly flows in vertical channels,” *Int. J. Multiph. Flow*, vol. 85, pp. 336–347, Oct. 2016, doi: 10.1016/j.ijmultiphaseflow.2016.06.021.

[16] S. H. Wong, P. Bryant, M. Ward, and C. Wharton, “Investigation of mixing in a cross-shaped micromixer with static mixing elements for reaction kinetics studies,” *Sensors Actuators B Chem.*, vol. 95, no. 1–3, pp. 414–424, Oct. 2003, doi: 10.1016/S0925-4005(03)00447-7.

[17] A. Tiwari, V. M. Rajesh, and S. Yadav, “Biodiesel production in micro-reactors: A review,” *Energy Sustain. Dev.*, vol. 43, pp. 143–161, Apr. 2018, doi: 10.1016/J.ESD.2018.01.002.

[18] N. L. Jeon, S. K. W. Dertinger, D. T. Chiu, I. S. Choi, A. D. Stroock, and G. M.

Whitesides, “Generation of solution and surface gradients using microfluidic systems,” *Langmuir*, vol. 16, no. 22, pp. 8311–8316, Oct. 2000, doi: 10.1021/LA000600B/ASSET/IMAGES/LARGE/LA000600BF00004.JPEG.

[19] K. Anwar, T. Han, S. Yu, and S. M. Kim, “Integrated micro/nano-fluidic system for mixing and preconcentration of dissolved proteins,” *Microchim. Acta*, vol. 173, no. 3–4, pp. 331–335, Jun. 2011, doi: 10.1007/S00604-011-0567-6/FIGURES/6.

[20] C. H. Yeh, C. H. Chen, and Y. C. Lin, “Use of a gradient-generating microfluidic device to rapidly determine a suitable glucose concentration for cell viability test,” *Microfluid. Nanofluidics*, vol. 10, no. 5, pp. 1011–1018, May 2011, doi: 10.1007/S10404-010-0730-0/FIGURES/6.

[21] D. Friedrich, C. P. Please, and T. Melvin, “Design of novel microfluidic concentration gradient generators suitable for linear and exponential concentration ranges,” *Chem. Eng. J.*, vol. 193–194, pp. 296–303, Jun. 2012, doi: 10.1016/J.CEJ.2012.04.041.

[22] S. Wang *et al.*, “Highly Efficient Capture of Circulating Tumor Cells by Using Nanostructured Silicon Substrates with Integrated Chaotic Micromixers,” *Angew. Chemie*, vol. 123, no. 13, pp. 3140–3144, Mar. 2011, doi: 10.1002/ANGE.201005853.

[23] W. Sheng *et al.*, “Capture, release and culture of circulating tumor cells from pancreatic cancer patients using an enhanced mixing chip,” *Lab Chip*, vol. 14, no. 1, pp. 89–98, Nov. 2013, doi: 10.1039/C3LC51017D.

[24] M. Cho, S. Chung, Y. T. Kim, J. H. Jung, D. H. Kim, and T. S. Seo, “A fully integrated microdevice for biobarcode assay based biological agent detection,” *Lab Chip*, vol. 15, no. 13, pp. 2744–2748, Jun. 2015, doi: 10.1039/C5LC00355E.

[25] Y. F. Lee, K. Y. Lien, H. Y. Lei, and G. Bin Lee, “An integrated microfluidic system for rapid diagnosis of dengue virus infection,” *Biosens. Bioelectron.*, vol. 25, no. 4, pp. 745–752, Dec. 2009, doi: 10.1016/J.BIOS.2009.08.020.

[26] B. Zhang, Y. Luo, B. Zhou, Q. Wang, and P. D. Millner, “A novel microfluidic mixer-based approach for determining inactivation kinetics of Escherichia coli O157:H7 in chlorine solutions,” *Food Microbiol.*, vol. 49, pp. 152–160, Aug. 2015, doi: 10.1016/J.FM.2015.01.013.

[27] S. Bensaid, F. A. Deorsola, D. L. Marchisio, N. Russo, and D. Fino, “Flow field

simulation and mixing efficiency assessment of the multi-inlet vortex mixer for molybdenum sulfide nanoparticle precipitation," *Chem. Eng. J.*, vol. 238, pp. 66–77, Feb. 2014, doi: 10.1016/J.CEJ.2013.09.065.

[28] S. Li, S. Meierott, and J. M. Köhler, "Effect of water content on growth and optical properties of ZnO nanoparticles generated in binary solvent mixtures by micro-continuous flow synthesis," *Chem. Eng. J.*, vol. 165, no. 3, pp. 958–965, Dec. 2010, doi: 10.1016/J.CEJ.2010.08.033.

[29] S. I. Kawasaki *et al.*, "Engineering study of continuous supercritical hydrothermal method using a T-shaped mixer: Experimental synthesis of NiO nanoparticles and CFD simulation," *J. Supercrit. Fluids*, vol. 54, no. 1, pp. 96–102, Jul. 2010, doi: 10.1016/J.SUPFLU.2010.03.001.

[30] T. Honda, M. Miyazaki, H. Nakamura, and H. Maeda, "Controllable polymerization of N -carboxy anhydrides in a microreaction system," *Lab Chip*, vol. 5, no. 8, pp. 812–818, Jul. 2005, doi: 10.1039/B505137A.

[31] D. Kessler, H. Lowe, and P. Theato, "Synthesis of Defined Poly(silsesquioxane)s: Fast Polycondensation of Trialkoxysilanes in a Continuous-Flow Microreactor," *Macromol. Chem. Phys.*, vol. 210, no. 10, pp. 807–813, May 2009, doi: 10.1002/MACP.200800611.

[32] C. Tonhauser *et al.*, "Multihydroxyl-functional polystyrenes in continuous flow," *Macromolecules*, vol. 43, no. 13, pp. 5582–5588, Jul. 2010, doi: 10.1021/MA902849R/SUPPL_FILE/MA902849R_SI_001.PDF.

[33] C. H. Lin, Y. N. Wang, and L. M. Fu, "Integrated microfluidic chip for rapid DNA digestion and time-resolved capillary electrophoresis analysis," *Biomicrofluidics*, vol. 6, no. 1, Mar. 2012, doi: 10.1063/1.3654950/923114.

[34] I. N. Kefala, V. E. Papadopoulos, G. Karpou, G. Kokkoris, G. Papadakis, and A. Tserepi, "A labyrinth split and merge micromixer for bioanalytical applications," *Microfluid. Nanofluidics*, vol. 19, no. 5, pp. 1047–1059, Nov. 2015, doi: 10.1007/S10404-015-1610-4/FIGURES/13.

[35] V. E. Papadopoulos *et al.*, "A passive micromixer for enzymatic digestion of DNA," *Microelectron. Eng.*, vol. 124, pp. 42–46, Jul. 2014, doi: 10.1016/J.MEE.2014.04.011.

[36] A. S. Kastania *et al.*, “Plasma micro-nanotextured polymeric micromixer for DNA purification with high efficiency and dynamic range,” *Anal. Chim. Acta*, vol. 942, pp. 58–67, Oct. 2016, doi: 10.1016/J.ACA.2016.09.007.

[37] “Micromixers: Fundamentals, Design and Fabrication - Nam-Trung Nguyen - Google Books.” https://books.google.co.in/books?hl=en&lr=&id=BHB0fBQuifkC&oi=fnd&pg=PP1&dq=Nguyen,+N.+T.+(2011).+Micromixers:+fundamentals,+design+and+fabrication.+William+Andrew.&ots=cSeuU4tuLK&sig=O3OncfnnYGdZEokYgmkO6OV8S2A&redir_esc=y#v=onepage&q=Nguyen%2C N. T. (2011). Micromixers%3A fundamentals%2C design and fabrication. William Andrew.&f=false (accessed Aug. 06, 2023).

[38] D. Qin, Y. Xia, J. A. Rogers, R. J. Jackman, X.-M. Zhao, and G. M. Whitesides, “Microfabrication, Microstructures and Microsystems,” pp. 1–20, 1998, doi: 10.1007/3-540-69544-3_1.

[39] S. Hardt, K. Drese, V. Hessel, and F. Schönfeld, “Passive Micro Mixers for Applications in the Micro Reactor and μTAS Field,” *Proc. Second Int. Conf. Microchannels Minichannels*, pp. 45–55, Dec. 2008, doi: 10.1115/ICMM2004-2319.

[40] “Micro- and Nanoscale Fluid Mechanics: Transport in Microfluidic Devices - Brian J. Kirby - Google Books.” https://books.google.co.in/books?hl=en&lr=&id=y7PB9f5zmU4C&oi=fnd&pg=PR15&dq=Kirby,+B.+J.+(2010).+Micro-and+nanoscale+fluid+mechanics:+transport+in+microfluidic+devices.+Cambridge+university+press.&ots=dslw55Z4Ny&sig=XaXu0qwqKRP_WjxcEt1MWnIh_nU&redir_esc=y#v=onepage&q=Kirby%2C B. J. (2010). Micro-and nanoscale fluid mechanics%3A transport in microfluidic devices. Cambridge university press.&f=false (accessed Aug. 06, 2023).

[41] A. E. Kamholz, B. H. Weigl, B. A. Finlayson, and P. Yager, “Quantitative analysis of molecular interaction in a microfluidic channel: The T-sensor,” *Anal. Chem.*, vol. 71, no. 23, pp. 5340–5347, Dec. 1999, doi: 10.1021/AC990504J/ASSET/IMAGES/LARGE/AC990504JF00007.JPEG.

[42] Z. Wu, N. T. Nguyen, and X. Huang, “Nonlinear diffusive mixing in microchannels:

theory and experiments," *J. Micromechanics Microengineering*, vol. 14, no. 4, p. 604, Feb. 2004, doi: 10.1088/0960-1317/14/4/022.

[43] J. P. Brody and P. Yager, "Diffusion-based extraction in a microfabricated device," *Sensors Actuators A Phys.*, vol. 58, no. 1, pp. 13–18, Jan. 1997, doi: 10.1016/S0924-4247(97)80219-1.

[44] S. Hossain, M. A. Ansari, and K. Y. Kim, "Evaluation of the mixing performance of three passive micromixers," *Chem. Eng. J.*, vol. 150, no. 2–3, pp. 492–501, Aug. 2009, doi: 10.1016/J.CEJ.2009.02.033.

[45] C. Nonino, S. Savino, and S. Del Giudice, "Numerical Assessment of the Mixing Performance of Different Serpentine Microchannels," *https://doi.org/10.1080/01457630802293506*, vol. 30, no. 1–2, pp. 101–112, 2010, doi: 10.1080/01457630802293506.

[46] J. N. Kuo, H. S. Liao, and X. M. Li, "Design optimization of capillary-driven micromixer with square-wave microchannel for blood plasma mixing," *Microsyst. Technol.*, vol. 23, no. 3, pp. 721–730, 2017, doi: 10.1007/s00542-015-2722-1.

[47] M. Khosravi Parsa, F. Hormozi, and D. Jafari, "Mixing enhancement in a passive micromixer with convergent–divergent sinusoidal microchannels and different ratio of amplitude to wave length," *Comput. Fluids*, vol. 105, pp. 82–90, Dec. 2014, doi: 10.1016/J.COMPFLUID.2014.09.024.

[48] C. Y. Wu and R. T. Tsai, "Fluid mixing via multidirectional vortices in converging–diverging meandering microchannels with semi-elliptical side walls," *Chem. Eng. J.*, vol. 217, pp. 320–328, Feb. 2013, doi: 10.1016/J.CEJ.2012.12.016.

[49] A. Afzal and K. Y. Kim, "PERFORMANCE EVALUATION OF THREE TYPES OF PASSIVE MICROMIXER WITH CONVERGENT-DIVERGENT SINUSOIDAL WALLS," *J. Mar. Sci. Technol.*, vol. 22, no. 6, p. 3, Dec. 2014, doi: 10.6119/JMST-014-0321-2.

[50] L. Chen *et al.*, "Evaluation of passive mixing behaviors in a pillar obstruction poly(dimethylsiloxane) microfluidic mixer using fluorescence microscopy," *Microfluid. Nanofluidics*, vol. 7, no. 2, pp. 267–273, 2009, doi: 10.1007/S10404-008-0386-1.

[51] L. Y. Tseng, A. S. Yang, C. Y. Lee, and C. Y. Hsieh, “CFD-based optimization of a diamond-obstacles inserted micromixer with boundary protrusions,” *Eng. Appl. Comput. Fluid Mech.*, vol. 5, no. 2, pp. 210–222, 2011, doi: 10.1080/19942060.2011.11015365.

[52] Y. Fang *et al.*, “Mixing enhancement by simple periodic geometric features in microchannels,” *Chem. Eng. J.*, vol. 187, pp. 306–310, Apr. 2012, doi: 10.1016/J.CEJ.2012.01.130.

[53] A. Alam, A. Afzal, and K. Y. Kim, “Mixing performance of a planar micromixer with circular obstructions in a curved microchannel,” *Chem. Eng. Res. Des.*, vol. 92, no. 3, pp. 423–434, Mar. 2014, doi: 10.1016/j.cherd.2013.09.008.

[54] H. S. Santana, J. L. Silva, D. S. Tortola, and O. P. Taranto, “Transesterification of sunflower oil in microchannels with circular obstructions,” *Chinese J. Chem. Eng.*, vol. 26, no. 4, pp. 852–863, Apr. 2018, doi: 10.1016/j.cjche.2017.08.018.

[55] S. Hossain and K. Y. Kim, “Mixing analysis in a three-dimensional serpentine split-and-recombine micromixer,” *Chem. Eng. Res. Des.*, vol. 100, pp. 95–103, Aug. 2015, doi: 10.1016/J.CHERD.2015.05.011.

[56] W. Raza, S. Hossain, and K. Y. Kim, “Effective mixing in a short serpentine split-and-recombination micromixer,” *Sensors Actuators B Chem.*, vol. 258, pp. 381–392, Apr. 2018, doi: 10.1016/J.SNB.2017.11.135.

[57] P. Hermann *et al.*, “Optimization of a split and recombine micromixer by improved exploitation of secondary flows,” *Chem. Eng. J.*, vol. 334, pp. 1996–2003, Feb. 2018, doi: 10.1016/J.CEJ.2017.11.131.

[58] M. Nimafar, V. Viktorov, and M. Martinelli, “Experimental comparative mixing performance of passive micromixers with H-shaped sub-channels,” *Chem. Eng. Sci.*, vol. 76, pp. 37–44, Jul. 2012, doi: 10.1016/J.CES.2012.03.036.

[59] N. Kockmann, T. Kiefer, M. Engler, and P. Woias, “Convective mixing and chemical reactions in microchannels with high flow rates,” *Sensors Actuators, B Chem.*, vol. 117, no. 2, pp. 495–508, Oct. 2006, doi: 10.1016/j.snb.2006.01.004.

[60] C. A. Cortes-Quiroz, A. Azarbadegan, and M. Zangeneh, “Evaluation of flow characteristics that give higher mixing performance in the 3-D T-mixer versus the

typical T-mixer," *Sensors Actuators B Chem.*, vol. 202, pp. 1209–1219, Oct. 2014, doi: 10.1016/J.SNB.2014.06.042.

[61] M. A. Ansari, K. Y. Kim, K. Anwar, and S. M. Kim, "Vortex micro T-mixer with non-aligned inputs," *Chem. Eng. J.*, vol. 181–182, pp. 846–850, Feb. 2012, doi: 10.1016/J.CEJ.2011.11.113.

[62] A. D. Stroock, S. K. W. Dertinger, A. Ajdari, I. Mezić, H. A. Stone, and G. M. Whitesides, "Chaotic Mixer for Microchannels," *Science (80-.).*, vol. 295, no. 5555, pp. 647–651, Jan. 2002, doi: 10.1126/SCIENCE.1066238.

[63] X. Chen and X. Wang, "Optimized Modular Design and Experiment for Staggered Herringbone Chaotic Micromixer," *Int. J. Chem. React. Eng.*, vol. 13, no. 3, pp. 305–309, Sep. 2015, doi: 10.1515/IJCRE-2014-0123/MACHINEREADABLECITATION/RIS.

[64] Y. Du, Z. Zhang, C. H. Yim, M. Lin, and X. Cao, "Evaluation of Floor-grooved Micromixers using Concentration-channel Length Profiles," *Micromachines 2010, Vol. 1, Pages 19-33*, vol. 1, no. 1, pp. 19–33, May 2010, doi: 10.3390/MI1010019.

[65] C. C. Hong, J. W. Choi, and C. H. Ahn, "A novel in-plane passive microfluidic mixer with modified Tesla structures," *Lab Chip*, vol. 4, no. 2, pp. 109–113, Mar. 2004, doi: 10.1039/B305892A.

[66] S. Hossain, M. A. Ansari, A. Husain, and K. Y. Kim, "Analysis and optimization of a micromixer with a modified Tesla structure," *Chem. Eng. J.*, vol. 158, no. 2, pp. 305–314, Apr. 2010, doi: 10.1016/J.CEJ.2010.02.002.

[67] A. Yang, F. Chuang, C. Chen, … M. L.-C. E., and undefined 2015, "A high-performance micromixer using three-dimensional Tesla structures for bio-applications," *Elsevier*, Accessed: Feb. 21, 2023. [Online]. Available: https://www.sciencedirect.com/science/article/pii/S1385894714014892.

[68] Y. Zhang, Y. Hu, and H. Wu, "Design and simulation of passive micromixers based on capillary," *Microfluid. Nanofluidics*, vol. 13, no. 5, pp. 809–818, Nov. 2012, doi: 10.1007/S10404-012-1002-Y/FIGURES/12.

[69] M. Bahiraei and N. Mazaheri, "Application of a novel hybrid nanofluid containing graphene–platinum nanoparticles in a chaotic twisted geometry for utilization in

miniature devices: Thermal and energy efficiency considerations," *Int. J. Mech. Sci.*, vol. 138–139, pp. 337–349, Apr. 2018, doi: 10.1016/J.IJMECSCI.2018.02.030.

[70] M. Bahiraei, K. Gharagozloo, M. Alighardashi, and N. Mazaheri, "CFD simulation of irreversibilities for laminar flow of a power-law nanofluid within a minichannel with chaotic perturbations: An innovative energy-efficient approach," *Energy Convers. Manag.*, vol. 144, pp. 374–387, Jul. 2017, doi: 10.1016/J.ENCONMAN.2017.04.068.

[71] M. Bahiraei, N. Mazaheri, and F. Aliee, "Second law analysis of a hybrid nanofluid in tubes equipped with double twisted tape inserts," *Powder Technol.*, vol. 345, pp. 692–703, Mar. 2019, doi: 10.1016/J.POWTEC.2019.01.060.

[72] M. Engler, N. Kockmann, T. Kiefer, and P. Woias, "Numerical and experimental investigations on liquid mixing in static micromixers," *Chem. Eng. J.*, vol. 101, no. 1–3, pp. 315–322, Aug. 2004, doi: 10.1016/J.CEJ.2003.10.017.

[73] S. H. Wong, M. C. L. Ward, and C. W. Wharton, "Micro T-mixer as a rapid mixing micromixer," *Sensors Actuators, B Chem.*, vol. 100, no. 3, pp. 359–379, May 2004, doi: 10.1016/j.snb.2004.02.008.

[74] A. Soleymani, E. Kolehmainen, and I. Turunen, "Numerical and experimental investigations of liquid mixing in T-type micromixers," *Chem. Eng. J.*, vol. 135, no. SUPPL. 1, pp. S219–S228, Jan. 2008, doi: 10.1016/J.CEJ.2007.07.048.

[75] M. Hoffmann, M. Schlüter, and N. Räbiger, "Experimental investigation of liquid-liquid mixing in T-shaped micro-mixers using μ-LIF and μ-PIV," *Chem. Eng. Sci.*, vol. 61, no. 9, pp. 2968–2976, May 2006, doi: 10.1016/j.ces.2005.11.029.

[76] D. Bothe, A. Lojewski, and H. J. Warnecke, "Fully resolved numerical simulation of reactive mixing in a T-shaped micromixer using parabolized species equations," *Chem. Eng. Sci.*, vol. 66, no. 24, pp. 6424–6440, Dec. 2011, doi: 10.1016/J.CES.2011.08.045.

[77] S. Dreher, N. Kockmann, and P. Woias, "Characterization of laminar transient flow regimes and mixing in t-shaped micromixers," *Heat Transf. Eng.*, vol. 30, no. 1–2, pp. 91–100, Jan. 2009, doi: 10.1080/01457630802293480.

[78] A. Fani, S. Camarri, and M. V. Salvetti, "Investigation of the steady engulfment regime in a three-dimensional T-mixer," *Phys. Fluids*, vol. 25, no. 6, p. 64102, Jun. 2013, doi: 10.1063/1.4809591/257935.

[79] S. K. Reddy Cherlo and S. Pushpavanam, “Effect of depth on onset of engulfment in rectangular micro-channels,” *Chem. Eng. Sci.*, vol. 65, no. 24, pp. 6486–6490, Dec. 2010, doi: 10.1016/J.CES.2010.08.025.

[80] B. Calado, A. dos Santos, V. S.-E. T. and Fluid, and undefined 2016, “Characterization of the mixing regimes of Newtonian fluid flows in asymmetrical T-shaped micromixers,” *Elsevier*, Accessed: Feb. 21, 2023. [Online]. Available: https://www.sciencedirect.com/science/article/pii/S0894177715003337.

[81] J. P. Silva, A. dos Santos, and V. Semiao, “Experimental characterization of pulsed Newtonian fluid flows inside T-shaped micromixers with variable inlets widths,” *Exp. Therm. Fluid Sci.*, vol. 89, pp. 249–258, Dec. 2017, doi: 10.1016/J.EXPTHERMFLUSCI.2017.08.018.

[82] L. Siconolfi, A. Fani, S. Camarri, and M. V. Salvetti, “Effect of geometry modifications on the engulfment in micromixers: Numerical simulations and stability analysis,” *Eur. J. Mech. - B/Fluids*, vol. 55, pp. 360–366, Jan. 2016, doi: 10.1016/J.EUROMECHFLU.2015.08.008.

[83] D. Bökenkamp, A. Desai, X. Yang, Y. C. Tai, E. M. Marzluff, and S. L. Mayo, “Microfabricated Silicon Mixers for Submillisecond Quench-Flow Analysis,” *Anal. Chem.*, vol. 70, no. 2, pp. 232–236, Jan. 1998, doi: 10.1021/AC9708250.

[84] M. Ståhl, B. L. Åslund, and Å. C. Rasmuson, “Reaction crystallization kinetics of benzoic acid,” *AIChE J.*, vol. 47, no. 7, pp. 1544–1560, Jul. 2001, doi: 10.1002/AIC.690470708.

[85] T. Iwasaki and J. I. Yoshida, “Free radical polymerization in microreactors. Significant improvement in molecular weight distribution control,” *Macromolecules*, vol. 38, no. 4, pp. 1159–1163, Feb. 2005, doi: 10.1021/MA048369M/ASSET/IMAGES/LARGE/MA048369MF00005.JPEG.

[86] D. Yamamoto, T. Maki, S. Watanabe, H. Tanaka, M. T. Miyahara, and K. Mae, “Synthesis and adsorption properties of ZIF-8 nanoparticles using a micromixer,” *Chem. Eng. J.*, vol. 227, pp. 145–150, Jul. 2013, doi: 10.1016/J.CEJ.2012.08.065.

[87] H. S. Santana, D. S. Tortola, J. L. Silva, and O. P. Taranto, “Biodiesel synthesis in micromixer with static elements,” *Energy Convers. Manag.*, vol. 141, pp. 28–39, Jun.

2017, doi: 10.1016/J.ENCONMAN.2016.03.089.

[88] T. Yasukawa, W. Ninomiya, K. Ooyachi, N. Aoki, and K. Mae, “Enhanced production of ethyl pyruvate using gas–liquid slug flow in microchannel,” *Chem. Eng. J.*, vol. 167, no. 2–3, pp. 527–530, Mar. 2011, doi: 10.1016/J.CEJ.2010.08.077.

[89] A. Montillet, S. Nedjar, and M. Tazerout, “Continuous production of water-in-oil emulsion using micromixers,” *Fuel*, vol. 106, pp. 410–416, Apr. 2013, doi: 10.1016/J.FUEL.2012.11.018.

[90] J. Jeßberger, J. E. Marquardt, L. Heim, J. Mangold, F. Bukreev, and M. J. Krause, “Optimization of a Micromixer with Automatic Differentiation,” 2022, doi: 10.3390/fluids7050144.

[91] C. K. Chan, Y. Hu, S. Takahashi, D. L. Rousseau, W. A. Eaton, and J. Hofrichter, “Submillisecond protein folding kinetics studied by ultrarapid mixing.,” *Proc. Natl. Acad. Sci. U. S. A.*, vol. 94, no. 5, pp. 1779–84, Mar. 1997, doi: 10.1073/pnas.94.5.1779.

[92] C. Zhang, D. Xing, and Y. Li, “Micropumps, microvalves, and micromixers within PCR microfluidic chips: Advances and trends,” *Biotechnol. Adv.*, vol. 25, no. 5, pp. 483–514, Sep. 2007, doi: 10.1016/J.BIOTECHADV.2007.05.003.

[93] K. Y. Lu, A. M. Wo, Y. J. Lo, K. C. Chen, C. M. Lin, and C. R. Yang, “Three dimensional electrode array for cell lysis via electroporation,” *Biosens. Bioelectron.*, vol. 22, no. 4, pp. 568–574, Oct. 2006, doi: 10.1016/J.BIOS.2006.08.009.

[94] S. Suga, A. Nagaki, and J.-I. Yoshida, “Highly selective Friedel-Crafts monoalkylation using micromixing †,” vol. 5, pp. 5–22, 2002, doi: 10.1039/b211433j.

[95] S. Freitas, B. Rudolf, H. P. Merkle, and B. Gander, “Flow-through ultrasonic emulsification combined with static micromixing for aseptic production of microspheres by solvent extraction,” *Eur. J. Pharm. Biopharm.*, vol. 61, no. 3, pp. 181–187, Oct. 2005, doi: 10.1016/J.EJPB.2005.05.004.

[96] H. H. Bau, J. Zhong, and M. Yi, “A minute magneto hydro dynamic (MHD) mixer,” *Sensors Actuators B Chem.*, vol. 79, no. 2–3, pp. 207–215, Oct. 2001, doi: 10.1016/S0925-4005(01)00851-6.

[97] G. G. Yaralioglu, I. O. Wygant, T. C. Marentis, and B. T. Khuri-Yakub, “Ultrasonic

mixing in microfluidic channels using integrated transducers," *Anal. Chem.*, vol. 76, no. 13, pp. 3694–3698, Jul. 2004, doi: 10.1021/ac035220k.

[98] o-K. A. Chen Ching-Chang Cho, "Electrokinetically driven flow mixing utilizing chaotic electric fields," doi: 10.1007/s10404-008-0286-4.

[99] C. K. Chung, • T R Shih, • B H Wu, and • C K Chang, "Design and mixing efficiency of rhombic micromixer with flat angles," doi: 10.1007/s00542-009-0980-5.

[100] W. Buchegger, C. Wagner, B. Lendl, M. Kraft, and M. J. Vellekoop, "A highly uniform lamination micromixer with wedge shaped inlet channels for time resolved infrared spectroscopy," *Microfluid. Nanofluidics*, vol. 10, no. 4, pp. 889–897, Apr. 2011, doi: 10.1007/s10404-010-0722-0.

[101] K. Y. Hsiao, C. Y. Wu, and Y. T. Huang, "Fluid mixing in a microchannel with longitudinal vortex generators," *Chem. Eng. J.*, vol. 235, pp. 27–36, Jan. 2014, doi: 10.1016/J.CEJ.2013.09.010.

[102] X. Chen and J. Shen, "Numerical analysis of mixing behaviors of two types of E-shape micromixers," *Int. J. Heat Mass Transf.*, vol. 106, pp. 593–600, Mar. 2017, doi: 10.1016/J.IJHEATMASSTRANSFER.2016.09.034.

[103] J. Yang, L. Qi, Y. Chen, and H. Ma, "Design and Fabrication of a Three Dimensional Spiral Micromixer," *Chinese J. Chem.*, vol. 31, no. 2, pp. 209–214, Feb. 2013, doi: 10.1002/CJOC.201200922.

[104] S. J. Park, J. K. Kim, J. Park, S. Chung, C. Chung, and J. K. Chang, "Rapid three-dimensional passive rotation micromixer using the breakup process," *J. Micromechanics Microengineering*, vol. 14, no. 1, p. 6, Aug. 2003, doi: 10.1088/0960-1317/14/1/302.

[105] D. Bothe, C. Stemich, and H. J. Warnecke, "Fluid mixing in a T-shaped micro-mixer," *Chem. Eng. Sci.*, vol. 61, no. 9, pp. 2950–2958, 2006, doi: 10.1016/j.ces.2005.10.060.

[106] J. N. Kuo, H. S. Liao, and X. M. Li, "Design optimization of capillary-driven micromixer with square-wave microchannel for blood plasma mixing," *Microsyst. Technol.*, vol. 23, no. 3, pp. 721–730, Mar. 2017, doi: 10.1007/s00542-015-2722-1.

[107] K. Y. Lu, A. M. Wo, Y. J. Lo, K. C. Chen, C. M. Lin, and C. R. Yang, "Three dimensional electrode array for cell lysis via electroporation," *Biosens. Bioelectron.*,

vol. 22, no. 4, pp. 568–574, Oct. 2006, doi: 10.1016/J.BIOS.2006.08.009.

[108] J. M. Ottino, “The kinematics of mixing: stretching, chaos, and transport,” 1989. https://books.google.co.in/books?hl=en&lr=&id=8OLVcbRoNSgC&oi=fnd&pg=PR9&dq=Ottino+JM+(1989)+The+kinematics+of+mixing:+stretching,+chaos,+and+transport.+Cambridge+University+Press,+Cambridge&ots=uqRzexjTL0&sig=Ib6xGWyHugN7Zk-TMcqcH0oOE0U&redir_esc=y#v=one (accessed Aug. 09, 2021).

[109] E. Tripathi, P. K. Patowari, and S. Pati, “Mixing characteristics and pressure drop analysis in a spiral micromixer,” *Proc. Inst. Mech. Eng. Part E J. Process Mech. Eng.*, 2022, doi: 10.1177/09544089221095636.

[110] M. Dundi, R. V.R.K, and C. V.P, “Characterization of enhanced liquid mixing in T-T mixer at various Reynolds numbers,” *Asia-Pacific J. Chem. Eng.*, vol. 14, no. 2, p. e2298, Mar. 2019, doi: 10.1002/APJ.2298.

[111] M. Irfan *et al.*, “Numerical analysis of non-aligned inputs M-type micromixers with different shaped obstacles for biomedical applications,” *Proc. Inst. Mech. Eng. Part E J. Process Mech. Eng.*, vol. 236, no. 3, pp. 870–880, 2021, doi: 10.1177/09544089211051630.

[112] M. Rahimi, M. Akbari, M. A. Parsamoghadam, and A. A. Alsairafi, “CFD study on effect of channel confluence angle on fluid flow pattern in asymmetrical shaped microchannels,” *Comput. Chem. Eng.*, vol. 73, pp. 172–182, Feb. 2015, doi: 10.1016/J.COMPCHEMENG.2014.12.007.

[113] M. Jain and K. Nandakumar, “Optimal patterning of heterogeneous surface charge for improved electrokinetic micromixing,” *Comput. Chem. Eng.*, vol. 49, pp. 18–24, Feb. 2013, doi: 10.1016/J.COMPCHEMENG.2012.09.004.

[114] F. Jiang, K. S. Drese, S. Hardt, M. Küpper, and F. Schönfeld, “Helical flows and chaotic mixing in curved micro channels,” *AIChE J.*, vol. 50, no. 9, pp. 2297–2305, Sep. 2004, doi: 10.1002/AIC.10188.

[115] Virginie Mengeaud, and Jacques Josserand, and H. H. Girault*, “Mixing Processes in a Zigzag Microchannel: Finite Element Simulations and Optical Study,” *Anal. Chem.*, vol. 74, no. 16, pp. 4279–4286, Aug. 2002, doi: 10.1021/AC025642E.

[116] R. H. Liu *et al.*, “Passive mixing in a three-dimensional serpentine microchannel,” *J.*

Microelectromechanical Syst., vol. 9, no. 2, pp. 190–197, Jun. 2000, doi: 10.1109/84.846699.

[117] M. Jain, A. Rao, and • K Nandakumar, "Numerical study on shape optimization of groove micromixers," doi: 10.1007/s10404-013-1169-x.

[118] S. Hossain, M. A. Ansari, and K. Y. Kim, "Evaluation of the mixing performance of three passive micromixers," *Chem. Eng. J.*, vol. 150, no. 2–3, pp. 492–501, 2009, doi: 10.1016/j.cej.2009.02.033.

[119] E. Perry, R. Balling, M. Landon, and R. Johnson, "Aerodynamic shape optimization of internal fluid flow systems," *29th AIAA Fluid Dyn. Conf.*, pp. 1–8, 1998, doi: 10.2514/6.1998-2896.

[120] A. haghighinia and S. Movahedirad, "Fluid micro-mixing in a passive microchannel: Comparison of 2D and 3D numerical simulations," *Int. J. Heat Mass Transf.*, vol. 139, pp. 907–916, Aug. 2019, doi: 10.1016/J.IJHEATMASSTRANSFER.2019.05.084.

[121] K. Ho-Le, "Finite element mesh generation methods: a review and classification," *Comput. Des.*, vol. 20, no. 1, pp. 27–38, 1988, doi: 10.1016/0010-4485(88)90138-8.

[122] W. K. Anderson and V. Venkatakrishnan, "Aerodynamic design optimization on unstructured grids with a continuous adjoint formulation," *Comput. Fluids*, vol. 28, no. 4–5, pp. 443–480, May 1999, doi: 10.1016/S0045-7930(98)00041-3.

[123] M. F. Eggl and P. J. Schmid, "Shape optimization of stirring rods for mixing binary fluids," *IMA J. Appl. Math. (Institute Math. Its Appl.*, vol. 85, no. 5, pp. 762–789, 2020, doi: 10.1093/imamat/hxaa012.

[124] V. Hessel, H. Löwe, and F. Schönfeld, "Micromixers—a review on passive and active mixing principles," *Chem. Eng. Sci.*, vol. 60, no. 8–9, pp. 2479–2501, Apr. 2005, doi: 10.1016/J.CES.2004.11.033.

[125] Y. K. Suh and S. Kang, "A review on mixing in microfluidics," *Micromachines*, vol. 1, no. 3, pp. 82–111, 2010, doi: 10.3390/MI1030082.

[126] N. T. Nguyen and Z. Wu, "Micromixers—a review," *J. Micromechanics Microengineering*, vol. 15, no. 2, p. R1, Dec. 2004, doi: 10.1088/0960-1317/15/2/R01.

[127] G. S. Jeong, S. Chung, C. B. Kim, and S. H. Lee, "Applications of micromixing

technology," *Analyst*, vol. 135, no. 3, pp. 460–473, 2010, doi: 10.1039/b921430e.

[128] D. Gobby, P. Angeli, and A. Gavriilidis, "Mixing characteristics of T-type microfluidic mixers," *J. Micromechanics Microengineering*, vol. 11, no. 2, p. 126, Mar. 2001, doi: 10.1088/0960-1317/11/2/307.

[129] G. Deerberg, J. Grän-Heedfeld, T. Hennig, and E. Weidner, "Mikrofluidisches Mischen als Bestandteil mikroreaktions-technischer Modellierung," *Chemie-Ingenieur-Technik*, vol. 77, no. 10, pp. 1501–1511, 2005, doi: 10.1002/cite.200500095.

[130] V. Hessel, S. Hardt, H. Löwe, and F. Schönfeld, "Laminar mixing in different interdigital micromixers: I. Experimental characterization," *AIChE J.*, vol. 49, no. 3, pp. 566–577, Mar. 2003, doi: 10.1002/AIC.690490304.

[131] Y. Z. Liu, B. J. Kim, and H. J. Sung, "Two-fluid mixing in a microchannel," *Int. J. Heat Fluid Flow*, vol. 25, no. 6, pp. 986–995, Dec. 2004, doi: 10.1016/J.IJHEATFLUIDFLOW.2004.03.006.

[132] B. H. Jo, L. M. Van Lerberghe, K. M. Motsegood, and D. J. Beebe, "Three-dimensional micro-channel fabrication in polydimethylsiloxane (PDMS) elastomer," *J. Microelectromechanical Syst.*, vol. 9, no. 1, pp. 76–81, Mar. 2000, doi: 10.1109/84.825780.

[133] C. H. Lin, C. H. Tsai, and L. M. Fu, "A rapid three-dimensional vortex micromixer utilizing self-rotation effects under low Reynolds number conditions," *J. Micromechanics Microengineering*, vol. 15, no. 5, pp. 935–943, May 2005, doi: 10.1088/0960-1317/15/5/006.

[134] X. Chen and Z. Zhao, "Numerical investigation on layout optimization of obstacles in a three-dimensional passive micromixer," *Anal. Chim. Acta*, vol. 964, pp. 142–149, Apr. 2017, doi: 10.1016/j.aca.2017.01.066.

[135] "Characterization of mixing in an optimized designed T–T mixer with cylindrical elements - ScienceDirect." https://www.sciencedirect.com/science/article/pii/S1004954118313557 (accessed Feb. 21, 2023).

[136] J. L. Thiffeault, "Using multiscale norms to quantify mixing and transport," *Nonlinearity*, vol. 25, no. 2, 2012, doi: 10.1088/0951-7715/25/2/R1.

[137] A. A. S. Bhagat, E. T. K. Peterson, and I. Papautsky, “A passive planar micromixer with obstructions for mixing at low Reynolds numbers,” *J. Micromechanics Microengineering*, vol. 17, no. 5, p. 1017, Apr. 2007, doi: 10.1088/0960-1317/17/5/023.

[138] I. Shah, S. W. Kim, K. Kim, Y. H. Doh, and K. H. Choi, “Experimental and numerical analysis of Y-shaped split and recombination micro-mixer with different mixing units,” *Chem. Eng. J.*, vol. 358, pp. 691–706, Feb. 2019, doi: 10.1016/J.CEJ.2018.09.045.

PUBLICATIONS

Publications in International/National Journals

1. Shasidar Rampalli, T Manoj Dundi, V.R.K. Raju, VP. Chandramohan, "Numerical evaluation of liquid mixing in a serpentine square convergent-divergent passive micromixer". Chemical Product and Process Modelling. DOI: https://doi.org/10.1515/cppm-2019-0071| Published , Online 23 jan 2020 **(**ESCI**).**

2. Shasidhar Rampalli, Raju VRK, Das S. Mixing enhancement of passive type T-mixer through shape optimization. Proceedings of the Institution of Mechanical Engineers, Part E:Journal of Process Mechanical Engineering. 2022;0(0). doi:10.1177/09544089221143892, Published, Online 12 dec 2022 (SCI).

3. Shasidhar Rampalli, V. R. K. Raju, Optimization study of obstacles in T-T mixing channel at low Reynolds numbers." *Canadian journal of chemical engineering"* (2023): CJCE-23-0269 (SCI): UNDER REVIEW

4. Shasidhar Rampalli, V. R. K. Raju, Simple structured passive T-type micromixers with an optimized circumferential in-step in main channel. (Yet to communicate)